ELECTROWEAK CORRECTIONS : TECHNIQUES AND APPLICATIONS

W.J.P. Beenakker

ELECTROWEAK CORRECTIONS : TECHNIQUES AND APPLICATIONS

ELECTROWEAK CORRECTIONS : TECHNIQUES AND APPLICATIONS

PROEFSCHRIFT

TER VERKRIJGING VAN DE GRAAD VAN DOCTOR AAN DE RIJKSUNIVERSITEIT TE LEIDEN, OP GEZAG VAN DE RECTOR MAGNIFICUS DR. J.J.M. BEENAKKER, HOOGLERAAR IN DE FACULTEIT DER WISKUNDE EN NATUURWETENSCHAPPEN, VOLGENS BESLUIT VAN HET COLLEGE VAN DEKANEN TE VERDEDIGEN OP DONDERDAG 19 OKTOBER 1989 TE KLOKKE 15.15 UUR

DOOR

Wilhelmus Johannes Petrus Beenakker

GEBOREN TE EINDHOVEN IN 1962

Promotie-commissie:

Promotor	: Prof. Dr. F.A. Berends
Referent	: Dr. W.L.G.A.M. van Neerven
Overige leden	: Prof. Dr. K.J.F. Gaemers
	Prof. Dr. J.M.J. van Leeuwen
	Prof. Dr. C.J.N. van den Meijdenberg

This investigation is part of the research program of the Stichting voor Fundamenteel Onderzoek der Materie (FOM) which is financially supported by the Nederlandse Organisatie voor Wetenschappelijk Onderzoek (NWO).

Contents

Chapter I

Outline

In calculations within the framework of the electroweak standard model more and more the interest is shifting towards the radiative corrections. This shift is a result of the prospect of high accuracy measurements investigating the weak interactions which are expected to take place from 1989 onward at the e^+e^- storage ring LEP at CERN and the linear collider SLC at SLAC.

Up to now the investigation of the weak interactions has been in its childhood years although a lot of progress has been made since nuclear decay experiments gave a first indication of its existence. As the years went by more and more of the rich structure of weak interactions was revealed, like for instance the discovery of charged and neutral currents, the existence of CP violating interactions and the ordering of the fermions into families. A first climax was reached in 1983 with the discovery of the heavy gauge bosons $W^{\pm}$,Z at the proton-antiproton collider S$p\bar{p}$S at CERN. This was the experimental verification of a prediction made by the Glashow-Salam-Weinberg (GSW) model for electroweak interactions [1] and consequently meant the breakthrough for this model, establishing itself as what is often referred to as the electroweak standard model. Subsequent experiments at PEP and PETRA (with energies up to 40 GeV) did not change this picture of the GSW model being at present the most successful theoretical concept to describe electroweak phenomena [2].

But it should be kept in mind that at present weak experiments can only give insight in the lowest order (classical) content of any theory describing weak interactions. This feature causes the investigation of the weak interactions to trail, at the moment, a long way behind that of QED, the tremendously successful quantum field theory describing pure electromagnetic forces. The presence of very high accuracy experiments, involving the measurements of the anomalous magnetic moment $g-2$ of the electron as well as muon [3], have made it possible to verify theoretical QED predictions with unmatched precision. In this way one has been able to probe the theory of electromagnetic interactions beyond the classical level entering its very heart as a quantum mechanical perturbation theory in the form of the higher

order (radiative) corrections which constitute the quantum effects. So, in order to have access to the quantum mechanical content of the electroweak standard model, bearing in mind that its renormalizability as proved by 't Hooft in 1971 [4] assures its predictive power as a perturbation theory, experiments are required which are accurate enough to be sensitive to the small weak quantum effects.

In the near future this requirement will be satisfied by the experiments taking place at SLC and the first stage of LEP (commonly referred to as LEP 1). These two colliders will reach center of mass energies up to about 100 GeV, which lies beyond the energy necessary to produce a real Z gauge boson ($M_Z \approx 91$ GeV). This allows for an expected LEP yearly production rate of $\mathcal{O}(10^6)$ near resonance Z events in fermion pair production experiments of the form $e^+e^- \to f\bar{f}$. The fact that the background will be negligible in this energy region will enable us to perform high precision measurements. This involves the determination of the mass of the Z gauge boson and its width, two important parameters of the electroweak standard model. The expected experimental uncertainties are predicted to be [5,6] :

- $\Delta M_Z = 20 - 50$ MeV from the determination of the peak position of the Z resonance, which corresponds to uncertainties smaller than 0.1%
- $\Delta \Gamma_Z = 20$ MeV from an examination of the form of the Z resonance, which corresponds to uncertainties smaller than 1%.

Measurements of on-resonance asymmetries, like the left-right asymmetry A_{LR} in case of longitudinal beam polarization [6,7] or the forward-backward asymmetry A_{FB} [7,8], supply us with a supplementary set of high precision quantities. Especially A_{LR} is well suited to fulfil the high standards set in order to be sensitive to the weak quantum effects.

At stage two of LEP (commonly referred to as LEP 200) the aim is to increase the center of mass energy to about 200 GeV by means of superconducting techniques. This means that another interesting aspect of the electroweak standard model comes into our reach : its non-abelian character. This is caused by the fact that center of mass energies above the W-pair production threshold will be reached, allowing us to investigate the reaction $e^+e^- \to W^+W^-$ to its full extent. At a production rate of $\mathcal{O}(10^4)$ W-pair events per year it is expected that the W mass can be determined with an accuracy of about 0.1% ($\Delta M_W \approx 100$ MeV) from threshold analysis [9]. Moreover it will allow for the first time a look into the kitchen of non-abelian couplings entering via the 3-gauge boson interactions γW^+W^- and ZW^+W^- as appearing at the classical level of the theory.

Besides being a necessity for probing the consistency of theories at the quantum level, electroweak radiative corrections (EWRC) can also offer us the possibility of getting information about objects that escape observation (even at SLC and LEP energies). Within the framework of the standard model there are still two pieces of the puzzle missing :

- the top quark as the missing constituent of the third fermion generation
- the Higgs boson as the physically accessible remnant of the Higgs - Kibble mechanism of spontaneous symmetry breaking [10].

Both particles might just be too massive to be detected directly by the above mentioned e^+e^- colliders. In that case an indirect investigation would be appropriate, involving high precision experimental quantities sensitive to EWRC effects depending on the unknown parameters M_H (Higgs boson mass) and m_t (top quark mass). In view of this the on-resonance asymmetries play an essential role.

This is however not the whole story. It might be possible that the experimental outcome opens the way to a whole scope of theoretical concepts which lie beyond the restricted area of the standard model, indicated by the term new physics [11,12]. To this end a precise knowledge of the EWRC effects is crucial for setting the margins of the standard model predictions. The present experimental status is such that any glimpses of new physics is expected to be found via indirect detection rather than via direct production, stressing once again the importance of a profound understanding of the very limits set by the standard model. As an example the 3-gauge boson vertices, as appearing at the classical level of the process $e^+e^- \rightarrow W^+W^-$, could be mentioned. Alternative models [13,14,15], allowing for a much broader spectrum of 3-gauge boson couplings, in general introduce small deviations from the standard model predictions. So, in order to distinguish between results lying within the margins set by the standard model and those bearing traces of new physics, one has to go beyond the lowest order and also include EWRC effects as an indispensable ingredient.

When dealing with the actual calculation of those on many occasions complicated EWRC effects, one is bound to encounter divergent loop integrals. These divergences are twofold :

- ultraviolet (UV) divergences, originating from the large integration momentum region
- infrared (IR) divergences, appearing when virtual photons are attached to two external particles or when real photons are radiated off external particles (bremsstrahlung). These divergences have their origin in that part of the integration region or real photon phase space where the 4-momentum of the photon becomes zero.

The first source of divergences will be handled by means of n-dimensional regularization [16] and an 'on-shell' renormalization scheme [17,18,19]. In the case of IR divergences, regularized by giving the photon a small fictitious mass indicated by λ, the combination of virtual and real photonic corrections will render finite results [20]. This leads to strong internal cancellations enhanced by the possible presence

of so-called 'mass singularities' [21], large contributions originating from the couplings of light particles (e.g. compared with the center of mass energy) to a photon, as the 'mass singular' double poles will cancel in analogy to the IR divergences when the virtual and real photonic corections are combined. In calculations within the framework of massless theories (like QCD) this is related to the cancellations of double poles. In order to remain in control in spite of all these cancellations some special techniques are required enabling us to have analytical access to the very terms responsible for this discomfort. Especially when many contributions come into play the presence of special techniques, resulting in some shade in the blazing sun of numerical instabilities inherent to any model containing large gauge cancellations, might be appreciated.

This thesis is organized as follows. In chapter II the GSW standard model of electroweak interactions will be described briefly. Its classical as well as quantized aspects will be discussed and some specifications will be made as to settle the question concerning the at the moment preferred input parameter set. Chapter III will contain a description of the special techniques as there are :

- the combined use of the Cutkosky cutting rule and dispersion integral techniques in order to calculate some specific scalar 3- and 4-point integrals containing the above mentioned contributions responsible for the large cancellations
- projection methods necessary to get hold of the extensive algebra typical for electroweak radiative corrections.

Discussions of the various aspects of EWRC effects in specific processes which are in the limelight at the moment can be found in chapter IV. We will focus on some important features of the production of light as well as heavy fermions from e^+e^- collisions. Furthermore explicit expressions will be presented for the $\mathcal{O}(\alpha)$ corrected fermionic decay width Γ_Z of the Z gauge boson.

References

[1] S.L. Glashow, Nucl. Phys. **B22** (1961) 579;
S. Weinberg, Phys. Rev. Lett. **19** (1967) 19;
A. Salam, in: "Elementary Particle Theory", p. 367, ed. N. Svartholm (Stockholm 1968).

[2] P. Langacker, Talk at the XXIV International Conference on High Energy Physics, München 1988.

[3] T. Kinoshita, "Recent Developments of QED", in: Proceedings of the 19th International Conference on High Energy Physics, Tokyo 1978,

eds. S. Homma et al. (Tokyo 1979);
J. Bailey et al., Nucl. Phys. **B150** (1979) 1.

[4] G. 't Hooft, Nucl. Phys. **B33** (1971) 173; Nucl. Phys. **B35** (1971) 167.

[5] Yellow CERN Report: "Physics at LEP", eds. J. Ellis and R.D. Peccei, CERN 86-02 (1986).

[6] Yellow CERN Report: "Polarization at LEP", eds. G. Alexander et al., CERN 88-06 (1988).

[7] G. Altarelli, in [6].

[8] G. Altarelli, in [5].

[9] Proceedings of the ECFA Workshop on LEP 200, Aachen 1986, eds. A. Böhm and W. Hoogland, CERN 87-08, ECFA 87/108 (1987).

[10] P.W. Higgs, Phys. Lett. **12B** (1964) 132; Phys. Rev. Lett. **13** (1964) 508; Phys. Rev. **145** (1966) 1156;
T. Kibble, Phys. Rev. **155** (1967) 1554;
R. Brout and F. Englert, Phys. Rev. Lett. **13** (1964) 321.

[11] B.W. Lynn, M. Peskin and R.G. Stuart, in [5];
B.W. Lynn, in [6].

[12] W. Hollik, in [6], and DESY 88-106 (1988).

[13] H. Neufeld, J.D. Stroughair and D. Schildknecht, Phys. Lett. **198B** (1987) 563.

[14] K. Hagiwara, R.D. Peccei, D. Zeppenfeld and K. Hikasa, Nucl. Phys. **B282** (1987) 253.

[15] P. Mery, M. Perottet and F. Renard, Z. Phys. **C36** (1987) 259.

[16] C.G. Bollini and J.J. Giambiagi, Phys. Lett. **40B** (1972) 566;
Nuovo Cim. **12B** (1972) 20;
G. 't Hooft and M. Veltman, Nucl. Phys. **B44** (1972) 189;
W.J. Marciano, Phys. Rev. **D12** (1975) 3861.

[17] M. Böhm, W. Hollik, and H. Spiesberger, Fortschr. Phys. **34** (1986) 687.

[18] K.I. Aoki, Z. Hioki, R. Kawabe, M. Konuma and T. Muta, Suppl. Progr. Theor. Phys. **73** (1982) 1.

[19] W. Hollik, DESY 88-188, to be published in Fortschritte der Physik.

[20] D.R. Yennie, S.C. Frautschi and H. Suura, Ann. of Phys. **13** (1961) 379;
F. Bloch and A. Nordsieck, Phys. Rev. **52** (1937) 54.

[21] T. Kinoshita, J. Math. Phys. **3** (1962) 650;
T.D. Lee and M. Nauenberg, Phys. Rev. **133** (1964) 1549;
N. Nakanishi, Progr. Theor. Phys. **19** (1958) 159.

Chapter II

The GSW model

1 Introduction

In this chapter some attention will be paid to the classical as well as quantized aspects of the Glashow-Salam-Weinberg model of electroweak interactions [1]. It is considered to be the best minimal model, incorporating the well established features of the low energy behaviour of the interactions and at the same time fulfilling the requirements of a consistent quantum field theory : renormalizability and absence of anomalies.

In order to tune theoretical predictions and experimental outcomes as much as possible, the question of the best input parameter set for actual calculations at LEP/SLC energies will be discussed. In this light improvements on existing parameters at SLC and the LEP 1 stage have to be taken into account.

Led by experimental findings the GSW model is described by a Lagrangian containing doublet as well as singlet structures for the fermions, which is realized by a gauge field theory based on the non-abelian gauge group $SU(2)_L \times U(1)_Y$. Incorporation of the Higgs - Kibble mechanism of spontaneous symmetry breaking [2] provides in a gauge invariant way for the, experimentally backed, presence of massive gauge fields. The classical Lagrangian constitutes of a gauge field, a Higgs and a fermion part :

$$\mathcal{L}_{cl} = \mathcal{L}_G + \mathcal{L}_H + \mathcal{L}_F \ . \tag{1.1}$$

2 Gauge field part

Adopting the metric and summation convention of appendix A the pure gauge field part of the classical Lagrangian, describing massless gauge fields $W^a_\mu(x)$ (a=1,2,3) and $B_\mu(x)$, is given by a Yang-Mills Lagrangian

$$\mathcal{L}_G = -\frac{1}{4} W^a_{\mu\nu} W^{\mu\nu,a} - \frac{1}{4} B_{\mu\nu} B^{\mu\nu} \tag{2.1}$$

containing the field strength tensors

$$\begin{aligned} W^a_{\mu\nu} &= \partial_\mu W^a_\nu - \partial_\nu W^a_\mu + g_2 \epsilon_{abc} W^b_\mu W^c_\nu \\ B_{\mu\nu} &= \partial_\mu B_\nu - \partial_\nu B_\mu \ , \end{aligned} \tag{2.2}$$

where ϵ_{abc} denote the structure constants of the $SU(2)$ subgroup and g_1, g_2 the abelian $U(1)$ resp. non-abelian $SU(2)$ coupling constants. The vector fields $W^a_\mu(x)$ (a=1,2,3) corresponding to the generators I_a of the isospin group $SU(2)$ form an isotriplet belonging to the adjoint representation of $SU(2)$, whereas the vector field $B_\mu(x)$ is a singlet corresponding to the hypercharge generator -Y/2 of $U(1)_Y$. The fact that we are dealing with a non-abelian gauge group is displayed by the presence of 3- and 4-point gauge field self interactions in the first term of (2.1), entering via the term quadratic in the gauge fields in (2.2).

3 Higgs fields and symmetry breaking

In order to explain the experimental findings of short range weak interactions theorists suggested that those weak interactions were mediated by massive vector bosons [3]. When trying to incorporate this suggestion in a gauge theory description of the electroweak interactions it proved necessary to implement a special mechanism for introducing those masses without the loss of gauge invariance as a tool of describing interactions. This mechanism, referred to as the Higgs - Kibble mechanism [2], involves a spontaneous symmetry breaking of the original $SU(2)_L \times U(1)_Y$ symmetry via the introduction of scalar fields which leads to a non-vanishing vacuum expectation value, leaving behind an unbroken $U(1)$ gauge subgroup to be identified with the electromagnetic gauge group $U(1)_{em}$. The generator Q of the $U(1)_{em}$ gauge group obeys the Gell-Mann - Nishijima relation

$$Q = I_3 + \frac{Y}{2} \ . \tag{3.1}$$

In this sense, the electromagnetic gauge group being the constituent that survives the symmetry breaking, we are dealing with a 'unification' of the weak and electromagnetic forces. The fact that each have their own independent coupling constant makes that this is not a unification in the true sense of the word.

The minimal Higgs - Kibble mechanism proceeds via the introduction of a complex scalar doublet field with hypercharge Y=1 :

$$\Phi(x) = \begin{pmatrix} \phi^+(x) \\ \phi^0(x) \end{pmatrix} \ . \tag{3.2}$$

The gauge invariant Lagrangian describing propagation of the Higgs fields, selfinteractions and couplings to the gauge fields is given by

$$\mathcal{L}_H = (D_\mu \Phi)^\dagger (D^\mu \Phi) - V(\Phi) \ , \tag{3.3}$$

with the Higgs potential

$$V(\Phi) = -\mu^2(\Phi^\dagger\Phi) + \frac{\lambda}{4}(\Phi^\dagger\Phi)^2 \tag{3.4}$$

and the covariant derivative

$$D_\mu = \partial_\mu - ig_2 I_a W_\mu^a + ig_1 \frac{Y}{2} B_\mu \ . \tag{3.5}$$

The essential concept is now to realise that the real ground state of the quantum system including Higgs fields corresponds to the minimum of the classical potential $V(\Phi)$, resulting in a non-vanishing expectation value of the quantum field operator $|\Phi| = \sqrt{\Phi^\dagger\Phi}$ with respect to this ground state :

$$< |\Phi| >_0 = \frac{\sqrt{2}\,\mu}{\sqrt{\lambda}} \equiv \frac{v}{\sqrt{2}} \ . \tag{3.6}$$

The choice

$$< \Phi >_0 = \begin{pmatrix} 0 \\ \frac{v}{\sqrt{2}} \end{pmatrix} \ , \tag{3.7}$$

a particular ground state obeying (3.6) with respect to which all other fields will be defined, leads to a reduction of the manifest symmetry of that very ground state from the full $SU(2)_L$ to the mere $U(1)_{em}$ subgroup. The Higgs doublet consequently takes on the form :

$$\Phi(x) = \begin{pmatrix} \phi^+(x) \\ \frac{1}{\sqrt{2}}(v + H(x) + i\chi(x)) \end{pmatrix} \ , \tag{3.8}$$

where the fields ϕ^+, H and χ now have zero vacuum expectation values, meaning that we have expanded Φ around its vacuum expectation value, in this way separating it into classical and quantum fluctuation parts.

Because of the presence of the quartic self couplings of the Higgs fields, as given by (3.4), the real field $H(x)$ acquires a mass

$$M_H = \sqrt{2}\,\mu \tag{3.9}$$

and describes neutral physical scalar particles. The fields $\phi^+(x)$ and $\chi(x)$ do not correspond to physical particles as they can be removed by choosing an appropriate (unitary) gauge as will be discussed in section 6.

Due to the Higgs field - gauge field interactions entering via the kinetic term of (3.3) three of the four gauge bosons will acquire a mass, leaving behind one massless gauge field corresponding to the remaining unbroken gauge group $U(1)_{em}$. This massless gauge boson will be identified with the photon.

4 Fermion fields and Yukawa couplings

The fermion fields are grouped into a singlet-doublet structure as follows (suppressing colour indices for the quarks and neglecting any quark mixing) :

- the left handed fermion fields are grouped into $SU(2)$ doublets with hypercharge Y_j^L. They are of the form

$$\psi_j^L = \begin{pmatrix} \psi_{j+}^L \\ \psi_{j-}^L \end{pmatrix} \quad : \textit{isospin } \frac{1}{2} \textit{ fermionic fields} . \tag{4.1}$$

  Here j denotes the family index (numbering the doublets) whereas the component index $\sigma = \pm$ corresponds to the weak isospin

- the right handed fermion fields are represented by $SU(2)$ singlets with hypercharge $Y_{j\sigma}^R$ denoted by

$$\psi_{j\sigma}^R \quad : \textit{isospin } 0 \textit{ fermionic fields} . \tag{4.2}$$

The various fermion doublets appearing in the standard model are :

$$\text{the lepton doublets : } \begin{pmatrix} \nu_e \\ e \end{pmatrix} , \begin{pmatrix} \nu_\mu \\ \mu \end{pmatrix} , \begin{pmatrix} \nu_\tau \\ \tau \end{pmatrix} \quad \begin{matrix} \leftarrow \sigma = + \\ \leftarrow \sigma = - \end{matrix}$$

$$\text{the quark doublets : } \begin{pmatrix} u \\ d \end{pmatrix} , \begin{pmatrix} c \\ s \end{pmatrix} , \begin{pmatrix} t \\ b \end{pmatrix} \quad \begin{matrix} \leftarrow \sigma = + \\ \leftarrow \sigma = - \end{matrix}$$

It should be noted that the quark doublets have a threefold degeneracy corresponding to their colour content. The doublet structure for the left handed fermion fields eliminates the possibility of generating by hand different fermion masses in a gauge invariant way. To avoid this problem couplings between the Higgs fields and the fermion fields, called Yukawa couplings, can be introduced, using the symmetry breaking mechanism to generate the necessary mass terms. The fermionic Lagrangian takes on the following form :

$$\mathcal{L}_F = \sum_j \bar{\psi}_j^L i\gamma^\mu D_\mu \psi_j^L + \sum_{j,\sigma} \bar{\psi}_{j\sigma}^R i\gamma^\mu D_\mu \psi_{j\sigma}^R + \mathcal{L}_{Yukawa} \tag{4.3}$$

$$\mathcal{L}_{Yukawa} = -\sum_j \Big\{ g_{j+} [\, \bar{\psi}_{j+}^L (\phi^0)^\dagger \psi_{j+}^R - \bar{\psi}_{j-}^L \phi^- \psi_{j+}^R \,] + g_{j-} [\, \bar{\psi}_{j+}^L \phi^+ \psi_{j-}^R + \bar{\psi}_{j-}^L \phi^0 \psi_{j-}^R \,] + h.c. \Big\} , \tag{4.4}$$

where ϕ^- stands for $(\phi^+)^\dagger$. The fermion masses are related to the Yukawa coupling constants $g_{j\sigma}$ through the presence of the non-vanishing vacuum expectation value of the Higgs field operator.

5 Physical fields and parameters

The mass terms for the gauge boson fields , as obtained from the Higgs field - gauge boson field interactions described in section 3, take on the following matrix form :

$$\frac{v^2}{8}(W_\mu^1, W_\mu^2, W_\mu^3, B_\mu)\begin{pmatrix} g_2^2 & 0 & 0 & 0 \\ 0 & g_2^2 & 0 & 0 \\ 0 & 0 & g_2^2 & g_1 g_2 \\ 0 & 0 & g_1 g_2 & g_1^2 \end{pmatrix}\begin{pmatrix} W^{\mu,1} \\ W^{\mu,2} \\ W^{\mu,3} \\ B^\mu \end{pmatrix} . \tag{5.1}$$

By performing a diagonalization procedure this can be casted in a diagonal form in terms of 'physical' parameters and fields, which are just the eigenvalues and corresponding eigenvectors of the above mass matrix. The term physical parameters refers to the fact that these parameters are directly accessible via experimental measurements if the suitable experiments become feasible. The application of the diagonalization procedure yields :

$$M_W^2\, W_\mu^+ W^{\mu,-} + \frac{1}{2}(A_\mu, Z_\mu)\begin{pmatrix} 0 & 0 \\ 0 & M_Z^2 \end{pmatrix}\begin{pmatrix} A^\mu \\ Z^\mu \end{pmatrix} , \tag{5.2}$$

consisting of the mass eigenvalues

$$M_W = \frac{1}{2}v g_2 \quad , \quad M_Z = \frac{1}{2}v\sqrt{g_1^2 + g_2^2} \quad , \quad M_\gamma = 0 \tag{5.3}$$

and the corresponding eigenvectors

$$\begin{aligned} W_\mu^\pm &= \frac{1}{\sqrt{2}}(W_\mu^1 \mp i W_\mu^2) \\ Z_\mu &= \cos\theta_w\, W_\mu^3 + \sin\theta_w\, B_\mu \\ A_\mu &= -\sin\theta_w\, W_\mu^3 + \cos\theta_w\, B_\mu , \end{aligned} \tag{5.4}$$

with the weak mixing angle θ_w, appearing in the rotation connecting the set (W^3, B) with (Z, A), defined by

$$\begin{aligned} c_w = \cos\theta_w &\equiv \frac{M_W}{M_Z} = \frac{g_2}{\sqrt{g_1^2 + g_2^2}} \\ s_w = \sin\theta_w &\equiv \sqrt{1 - \cos^2\theta_w} . \end{aligned} \tag{5.5}$$

The masses generated in the fermion sector as a consequence of the Yukawa couplings between the Higgs fields and the left and right handed fermion fields are given by

$$m_{j\sigma} = g_{j\sigma}\frac{v}{\sqrt{2}} . \tag{5.6}$$

The fact that we have identified the field A_μ with the photon field forces us to relate the coupling constants g_1 and g_2 to the electromagnetic coupling constant e as a measure of the interaction between the photon and the electron :

$$g_1 = \frac{e}{c_w} \quad , \quad g_2 = \frac{e}{s_w} \, . \tag{5.7}$$

6 Quantization of the classical Lagrangian

The presence of the massless gauge field $A_\mu(x)$ describing photons makes it mandatory to apply the gauge fixing principle. Because of a surplus of gauge freedom in the part of the classical Lagrangian containing the pure photon field propagation any successful attempt to quantize this part requires a reduction of this very gauge freedom beforehand. This reduction is commonly called gauge fixing. Because of practical reasons regarding the form of the free gauge boson propagators we will also apply this gauge fixing principle to the gauge fields describing massive gauge bosons. In this section we will mention the class of covariant 't Hooft gauges. This involves the addition of the following gauge fixing Lagrangian :

$$\mathcal{L}_{GF} = -\frac{1}{2}[(F_\gamma)^2 + (F_Z)^2 + 2F_+F_-] \, , \tag{6.1}$$

containing the linear gauge fixing functions

$$\begin{aligned} F_\pm &= \frac{1}{\sqrt{\xi_1^W}} \partial^\mu W_\mu^\pm \mp iM_W\sqrt{\xi_2^W}\,\phi^\pm \\ F_Z &= \frac{1}{\sqrt{\xi_1^Z}} \partial^\mu Z_\mu - M_Z\sqrt{\xi_2^Z}\,\chi \\ F_\gamma &= \frac{1}{\sqrt{\xi_1^\gamma}} \partial^\mu A_\mu \, . \end{aligned} \tag{6.2}$$

The pure photonic term $-\frac{1}{2}(F_\gamma)^2$ is equivalent to the gauge fixing term commonly used in QED.

Because of the non-abelian character of the $SU(2)_L$ subgroup compensation for the unphysical content of $\mathcal{L}_{GF}$ is necessary via the introduction of the Faddeev-Popov ghost term [4]. By replacing the group indices a by the indices $\alpha = \pm, Z, \gamma$, related to the physical gauge fields introduced in the last section, this Faddeev-Popov ghost term takes the form

$$\mathcal{L}_{FP} = \bar{u}^\alpha(x) \frac{\delta F^\alpha}{\delta\theta^\beta(x)} u^\beta(x) \, , \tag{6.3}$$

containing the independent anticommuting scalar fields u^α and $\bar{u}^\alpha$, obeying a Grassmann algebra, and the change of the gauge fixing functions under infinitesimal gauge transformations $\frac{\delta F^\alpha}{\delta\theta^\beta}$ (as related to the physical fields).

The choice $\xi_i^V \to \infty$ ($i = 1, 2$ and $V = W, Z, \gamma$), called the unitary gauge, has become very popular because it has the nice feature that no unphysical states enter the actual calculations. When dealing with calculations beyond the lowest order in α, however, one has to be careful to avoid violating unitarity or renormalizability. In contrast to what is often believed this can be achieved [5]. Another gauge choice well suited for performing higher order calculations is given by $\xi_i^V = 1$ ('t Hooft-Feynman gauge). The advantages of this gauge, to be adopted in the following chapters, are twofold :

- the free vector boson propagators take on the particularly pleasant form

$$D_{\mu\nu} = \frac{-ig_{\mu\nu}}{k^2 - M_V^2} \qquad (V = W, Z, \gamma) \tag{6.4}$$

in contrast to the more general form for $\xi_1^V = \xi_2^V \equiv \xi^V$

$$D_{\mu\nu} = \frac{i}{k^2 - M_V^2}\left(-g_{\mu\nu} + \frac{(1-\xi^V)k_\mu k_\nu}{k^2 - \xi^V M_V^2}\right) \tag{6.5}$$

- the other propagators in the unphysical sector corresponding to $\phi^\pm, \chi$ and $u^\pm, \bar{u}^\pm, u^Z, \bar{u}^Z$ have poles coinciding with those in the physical sector, located at M_W^2, M_Z^2.

Powerful checks on calculations and renormalization are provided for by the residual gauge invariance, which requires that any measurable quantity should not depend on the choice of a particular gauge. This means that measurable quantities should be free of ξ_i^V dependence. In case a particular gauge has been chosen for the sake of having a workable form for the Feynman rules, this feature takes on the form of the Slavnov-Taylor identities [6]. These identities are the generalized Ward identities corresponding to the so-called BRS symmetry [7], which includes besides the gauge transformations also transformations of the ghost fields in order to compensate for the fact that $\mathcal{L}_{GF} + \mathcal{L}_{FP}$ breaks the original gauge invariance. The complete quantized Lagrangian of the GSW model, reflecting this BRS invariance, is given by

$$\mathcal{L}_{GSW} = \mathcal{L}_{cl} + \mathcal{L}_{GF} + \mathcal{L}_{FP} \,. \tag{6.6}$$

7 Input parameters and renormalization

The most natural input parameter set, to be used for calculating EWRC effects, would only consist of the physical parameters

$$e, M_W, M_Z, M_H, m_{j\sigma} \quad , \tag{7.1}$$

replacing the original parameter set

$$g_1, g_2, \lambda, \mu^2, g_{j\sigma} \quad , \tag{7.2}$$

as they can be directly accessed in suitable experiments. At the LEP 1 stage the favoured parameter set should include those parameters which have the highest reliability. Besides the masses of the fermions and the physical Higgs, where M_H and m_t will play the role of free parameters, the following three parameters survive this criterion :

- the fine structure constant $\alpha = 1/137.03604(11)$, obtained from the Thomson limit of Compton scattering referred to as Thomson scattering, leading to a result which is free of radiative corrections [8] (so it corresponds to the classical electron charge e)

- the Fermi constant $G_\mu = 1.166344(11) \times 10^{-5}$ GeV^{-2}, obtained from the muon lifetime τ_μ, leading to a result which is only sensitive to electromagnetic corrections [9]

- the mass of the Z gauge boson, extracted from the line shape of the Z resonance in $e^+e^- \to f\bar{f}$ as will be measured at LEP 1. Because the peak position turns out to be independent of the other mass parameters, including the unknown Higgs and top mass, the measurement of the Z mass fulfils the additional requirement of being model assumption independent [10,11,12].

For concrete calculations of electroweak radiative corrections the electroweak 'on-shell' multiplicative renormalization scheme, proposed by Ross and Taylor [13] and worked out in great detail in [12], is applied as a natural extension of the well established on-shell scheme of QED. It relates the 'bare' parameters of the classical Lagrangian to the physically measurable parameters of the quantized renormalized Lagrangian : $\alpha, M_W, M_Z, M_H, m_{j\sigma}$. By applying this renormalization prescription one can derive the following relations, linking the quantities M_W, M_Z and $\sin^2\theta_w$ [14,15,16] :

$$M_W^2 = \frac{\pi\alpha}{\sqrt{2}\,G_\mu}\,\frac{1}{(1-\Delta r)\sin^2\theta_w} \quad , \tag{7.3}$$

containing higher order effects via the quantity Δr, which is a function of all model parameters (including M_H and m_t), and

$$\sin^2\theta_w = 1 - \frac{M_W^2}{M_Z^2} \quad , \tag{7.4}$$

providing for a process independent definition of the weak mixing angle valid in all orders of perturbation theory. The presence of $\sin^2\theta_w$ in (7.3) makes it necessary

to use an iterative procedure to determine M_W in terms of the input parameters $\alpha, G_\mu, M_Z, M_H, m_{j\sigma}$.

Until recently $\sin^2\theta_w$ played the role of one of the measurable input parameters of the standard model, taken from for instance neutrino-quark scattering [17]. The precision with which $\sin^2\theta_w$ will be determined at the LEP 1 phase will be an improvement compared with earlier experiments [18,19,20,21], but it will not be able to compete with the $< 0.1\%$ uncertainties expected for the determination of the Z mass [22]. For this reason the role of $\sin^2\theta_w$ in the electroweak standard model has changed to that of a quantity well suited for probing the unknown model parameters M_H and m_t, the quantum content of the theory and the consistency of the model. This is achieved by the Δr dependence as appearing in relation (7.3). Especially the measurement of on-resonance asymmetries, like A_{LR} and A_{FB}, and some branching ratios from $e^+e^- \to f\bar{f}$ experiments will render valuable information about $\sin^2\theta_w$ and hence about the above mentioned various important aspects of the model.

For aesthetic reasons the W gauge boson mass M_W has always been one of the prime candidates for entering the input parameter set. The expected accuracy of its determination however, even at the LEP 200 phase, prevents it from actually doing so [23]. This reduces its role to that of a probing quantity, just as $\sin^2\theta_w$ to which it is directly related via (7.4).

The fact that G_μ is not one of the natural on-shell quantities like α, M_W, M_Z, M_H and $m_{j\sigma}$, to which the 'on-shell' renormalization scheme owes its transparancy, is not a real disadvantage. Because it is the only parameter deviating from this preferred behaviour it can uniquely be expressed in terms of the on-shell quantities as ruled by relations (7.3) and (7.4).

References

[1] S.L. Glashow, Nucl. Phys. **B22** (1961) 579;
S. Weinberg, Phys. Rev. Lett. **19** (1967) 19;
A. Salam, in: "Elementary Particle Theory", p. 367, ed. N. Svartholm (Stockholm 1968).

[2] P.W. Higgs, Phys. Lett. **12B** (1964) 132; Phys. Rev. Lett. **13** (1964) 508; Phys. Rev. **145** (1966) 1156;
T. Kibble, Phys. Rev. **155** (1967) 1554;
R. Brout and F. Englert, Phys. Rev. Lett. **13** (1964) 321.

[3] J. Schwinger, Ann. of Phys. **2** (1957) 407.

[4] L.D. Faddeev and V.N. Popov, Phys. Lett. **25B** (1967) 29.

[5] G. 't Hooft and M. Veltman, "Example of a gauge field theory", in: Proceedings of the Marseille conference, 1972.

[6] A.A. Slavnov, Theor. Math. Phys. **10** (1972) 99;
J.C. Taylor, Nucl. Phys. **B33** (1971) 436.

[7] C. Becchi, A. Rouet and R. Stora, Phys. Lett. **52B** (1974) 344;
Comm. Math. Phys. **42** (1975) 127.

[8] J.M. Jauch and F. Rohrlich, "The Theory of Photons and Electrons",
New York, Heidelberg, Berlin 1976.

[9] R.E. Behrends, R.J. Finkelnstein and A. Sirlin, Phys. Rev. 101 (1956) 866;
T. Kinoshita and A. Sirlin, Phys. Rev. **113** (1959) 1652.

[10] F.A. Berends, G. Burgers, W. Hollik and W.L. van Neerven,
Phys. Lett. **203B** (1988) 177.

[11] G. Burgers, in [19], and CERN-TH 5119/88 (1988).

[12] W. Hollik, DESY 88-188, to be published in Fortschritte der Physik.

[13] D.A. Ross and J.C. Taylor, Nucl. Phys. **B51** (1973) 25.

[14] W.J. Marciano, Phys. Rev. **D20** (1979) 274.

[15] A. Sirlin, Phys. Rev. **D22** (1980) 971.

[16] W.J. Marciano and A. Sirlin, Phys. Rev. **D22** (1980) 2695.

[17] G.L. Fogli and D. Haidt, Z. Phys. **C40** (1988) 379.

[18] CHARM II proposal, CERN/SPSC/83-24 and 83-37.

[19] Yellow CERN Report: "Polarization at LEP", eds. G. Alexander et al.,
CERN 88-06 (1988).

[20] G. Altarelli, in [19].

[21] G. Altarelli, in [22].

[22] Yellow CERN Report: "Physics at LEP", eds. J. Ellis and R.D. Peccei,
CERN 86-02 (1986).

[23] Proceedings of the ECFA Workshop on LEP 200, Aachen 1986,
eds. A. Böhm and W. Hoogland, CERN 87-08, ECFA 87/108 (1987).

Chapter III

Special techniques

1 Introduction

In this chapter some handy techniques will be discussed which can help to improve our ability to handle the large cancellations and extensive algebra inherent to any of the calculations involving electroweak radiative corrections. The first special technique involves the use of causality within Feynman diagrams, leading to the Cutkosky cutting rule, in order to derive their absorptive part. The calculation is completed by applying dispersion integral techniques as a result of the analytic nature of those Feynman diagrams. To extend the results to all possible regions (even unphysical ones) analytic continuation procedures have to be performed. Because of the way these techniques can be implemented in our specific calculations, applications will only involve scalar integrals of the 2-,3- and 4-point type.

Besides the scalar content of EWRC calculations we also have to deal with the unavoidable algebra originating from the Lorentz structure of Feynman diagrams. To this end some propositions will be made regarding the use of projective methods to derive general as well as special reduction schemes depending on the purpose for which they are going to be applied. In view of the applicability outside the restricted area of EWRC calculations somewhat more generality will be introduced on a few occasions.

2 Causality and the Cutkosky cutting rule

The use of causality to arrive at the Cutkosky cutting rule for Feynman diagrams involves the analysis of energy flow through those diagrams. To be able to do this we first have to discuss some aspects of energy flow in propagators. Because we are only interested in scalar quantities like 2-,3- and 4-point integrals we will restrict ourselves to propagators involving scalar fields, following the line of reasoning given in [1].

According to the Kallén-Lehmann representation [2] for bare as well as dressed propagators we can write :

$$< 0|\, T(\phi(x)\,\phi(x'))\,|0 > \equiv \Delta_F(x - x')\ , \tag{2.1}$$

where

$$\Delta_F(x - x') = \frac{i}{(2\pi)^4} \int_0^\infty ds\, \rho(s) \int d^4k\, \frac{e^{-ik.(x-x')}}{k^2 - s + i\epsilon}\ . \tag{2.2}$$

The integration variable k in the above expression corresponds to the 4-momentum mediated from x' to x. The positive infinitesimal imaginary part ϵ added to the denominator ensures a proper incorporation of causality as will become clear from the forthcoming discussion. It should be noted that we have adopted the Bjorken-Drell metric as described in appendix A, in contrast to the metric used in [1]. The general form of the spectral function $\rho(s)$ is given by :

$$\rho(s) = c\,\delta(s - m^2) + \sigma(s)\ \epsilon\ I\!R\ , \tag{2.3}$$

where the first contribution originates from the discrete 1-particle state spectrum (with corresponding mass m) and the second one from the continuous spectrum of intermediate states, like two- or three-particle states. In this sense the function $\sigma(s)$ represents the presence of interactions contributing to the above mentioned dressed propagator above a certain threshold value s_{th}, indicating the lowest mass intermediate state. In case of free fields with mass m the spectral function ρ takes on the form

$$\rho(s) = \delta(s - m^2)\ . \tag{2.4}$$

Now we can introduce a decomposition of the propagator function $\Delta_F(x)$ of (2.2) in terms of a contribution with $x_0 > 0$ and a contribution with $x_0 < 0$:

$$\Delta_F(x) = \theta(x_0)\,\Delta^+(x) + \theta(-x_0)\,\Delta^-(x)\ , \tag{2.5}$$

where $\theta(x)$ is defined by

$$\theta(x) = \begin{cases} 1 & x > 0 \\ 0 & x < 0 \end{cases} \quad , \quad \theta(x) + \theta(-x) = 1\ . \tag{2.6}$$

As ruled by causality $\Delta^{+/-}(x)$ corresponds to the positive/negative energy function (energy flowing towards/from x). This will become clear on the next page when the Fourier transforms of these functions are presented. Explicit expressions for these energy functions can be derived from (2.2) by performing the k_0 integration. By applying Jordans rule for complex integration the decomposition (2.5) will immediately become visible. Consider the integral

$$I \equiv \int_{-\infty}^{\infty} dk_0\, \frac{e^{-ik_0 x_0}}{k^2 - s + i\epsilon} = \int_{-\infty}^{\infty} dk_0\, \frac{e^{-ik_0 x_0}}{(\,k_0 - \sqrt{\omega^2 - i\epsilon}\,)(\,k_0 + \sqrt{\omega^2 - i\epsilon}\,)}\ , \tag{2.7}$$

with

$$\omega = \sqrt{\vec{k}^{\,2} + s}\ . \tag{2.8}$$

According to Jordans rule this integral can be written as

$$I = \theta(x_0) \oint_{C_{II}} dk_0 \frac{e^{-ik_0x_0}}{(k_0 - \sqrt{\omega^2 - i\epsilon})(k_0 + \sqrt{\omega^2 - i\epsilon})} + \theta(-x_0) \oint_{C_I} dk_0 \frac{e^{-ik_0x_0}}{(k_0 - \sqrt{\omega^2 - i\epsilon})(k_0 + \sqrt{\omega^2 - i\epsilon})}\ , \tag{2.9}$$

where the contours C_I and C_{II} are specified in fig. 1.

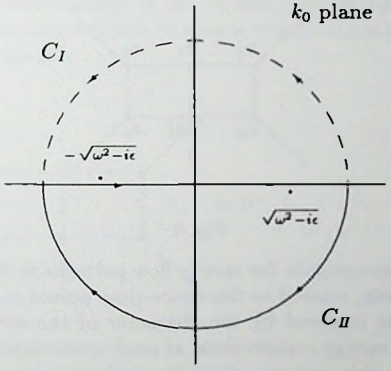

Fig. 1. Contours in the complex k_0 plane

Complex contour integration of meromorphic functions renders

$$I = -2\pi i \left\{ \theta(x_0) \frac{e^{-i\omega x_0}}{2\omega} + \theta(-x_0) \frac{e^{i\omega x_0}}{2\omega} \right\}\ . \tag{2.10}$$

Consequently the energy functions take on the form :

$$\Delta^{\pm}(x) = \frac{1}{(2\pi)^3} \int_0^\infty ds\, \rho(s) \int d^4k\, e^{-ik.x}\, \theta(\pm k_0)\, \delta(k^2 - s) \tag{2.11}$$

by making use of the integral identity

$$e^{\mp i\omega x_0} \int \frac{d\vec{k}}{2\omega} e^{i\vec{k}.\vec{x}} = \int d^4k\, e^{-ik.x}\, \theta(\pm k_0)\, \delta(k^2 - s)\ . \tag{2.12}$$

As $\rho(s) \epsilon \mathbb{R}$ the complex conjugate propagator function consequently has a reversed energy flow behaviour as visualized by the decompostion

$$\Delta_F^*(x) = \theta(x_0)\,\Delta^-(x) + \theta(-x_0)\,\Delta^+(x)\ . \tag{2.13}$$

The actual incorporation of the causality principle in scalar Feynman diagrams proceeds via the introduction of so-called skeleton functions $G(x_1,\ldots,x_n)$, which are constituents of a particular amputated Green's function. After it has been multiplied with the appropriate sources (not necessarily on mass-shell) and integrated over all x_i $(i = 1,\ldots,n)$, such a skeleton function corresponds to a particular diagram contributing to the S-matrix. As an example we show in fig. 2 a diagram corresponding to a skeleton function of the form $G(x_1,\ldots,x_6)$.

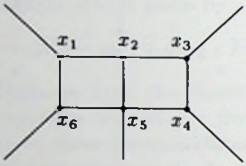

Fig. 2.

The aim is now to investigate the energy flow patterns in those skeleton functions led by the time ordering, related to the space-time points x_i, and restricted by the energy flow conditions imposed by the character of the external sources (energy input or output) and energy conservation at each space-time point regarding those external sources. To this end we study the influence on the skeleton functions caused by forcing the energy in certain propagators to flow in a particular direction. This can be represented diagrammatically by introducing for instance the diagram depicted in fig. 3. This diagram can be obtained from the diagram without the

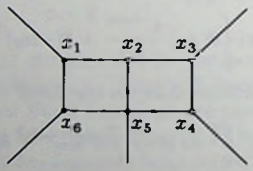

Fig. 3. Diagram with forced energy flow

circles by means of the following mechanism :

1 x_i ——— x_j : keep the original propagator $\Delta_F(x_i - x_j)$

2 x_i ———o x_j : replace the original propagator by $\Delta^-(x_i - x_j)$

3 x_i o——— x_j : replace the original propagator by $\Delta^+(x_i - x_j)$

4 x_i o———o x_j : replace the original propagator by $\Delta_F^*(x_i - x_j)$

5 any circled space-time point induces the replacement of one factor i by its complex conjugate -i.

So, the arrows appearing in the above depicted propagators denote the direction in which the energy is forced to flow. From energy conservation at each vertex (space time point) it is obvious that diagrams containing circled vertices can only give rise to non-zero contributions if the circled vertices form connected regions attached to at least one outgoing line (a source which causes the energy to flow out of the diagram). For example :

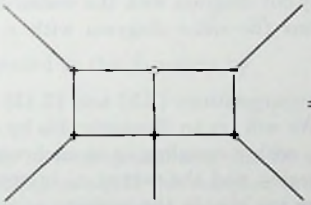

= 0

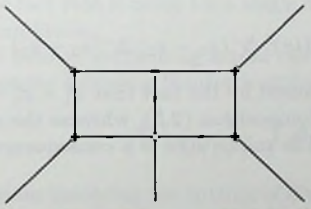

= not necessarily 0 .

Because of this feature we can skip circling the vertices and represent any contributing diagram by means of dividing it into regions of circled and uncircled vertices separated by so-called cutting lines as depicted in fig. 4.
The shaded region in the first diagram of fig. 4 is the one containing the circled vertices. So, the energy flows from the unshaded regions into the shaded regions. Now we can explicitly make use of causality to establish a relation between cut skeleton diagrams : the largest time equation. It states the following :

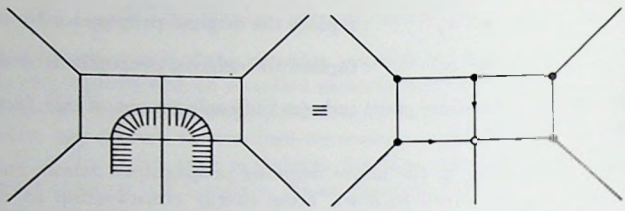

Fig. 4. Relation between cutting lines and circled ve

suppose $x_i^0 \geq x_j^0 \quad \forall_{j \neq i}$ in a particular diagram contai ertices indicated by $x_1, \ldots, x_n$. Then any cut diagram with the v inside the unshaded region equals minus the same diagram w in the shaded region.

This is a direct consequence of the decompositions (2.5) and (2.13) and the prescription 5 of the circling procedure. We will try to illustrate this by considering a string of 3 connected vertices x_1, x_2, x_3 with a coupling ig at each vertex. We will place the vertex x_1 in the unshaded region and the vertex x_3 in the shaded one. By assuming finally that $x_2^0 > x_1^0, x_3^0$ we are now in the position to investigate the origin of the largest time equation.

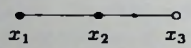

$$\rightarrow \quad -(ig)^3 \Delta^-(x_1 - x_2)\, \Delta^-(x_2 - x_3)\ .$$

The first negative energy function is caused by the fact that $x_1^0 - x_2^0 < 0$, selecting in this way the second term in the decomposition (2.5), whereas the second one is a result of the circling prescriptions. The minus sign is a consequence of applying once circling prescription 5.

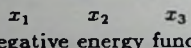

$$\rightarrow \quad +(ig)^3 \Delta^-(x_1 - x_2)\, \Delta^-(x_2 - x_3)\ .$$

The first negative energy function is a result of the circling prescriptions, whereas the second one is caused by the fact that $x_2^0 - x_3^0 > 0$, selecting in this way the first term in the decomposition (2.13). The plus sign is a consequence of applying twice circling prescription 5.

This immediately leads to the Cutkosky cutting rule, which states that the sum over all possible cuttings of a particular skeleton diagram equals zero. The sum over all possible cuttings consists of two separate contributions :

1. the contribution coming from those diagrams which do not contain any cuts at all. This means that all vertices of those diagrams lie completely in the shaded or unshaded region.

2. the contribution formed by the so-called cut graphs, consisting of all other cut diagrams which hence contain one or more internal cuts.

All this can be depicted by the Cutkosky cutting rule in diagram form :

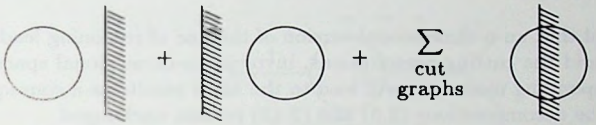

$$= 0 \,, \qquad (2.14)$$

where the blob stands for any skeleton diagram. Because we are only interested in the scalar content of the Cutkosky cutting rule and because we will only be dealing with hermitean Lagrangians, this cutting rule can be related directly to the unitarity equation

$$T - T^\dagger = iT^\dagger T \,, \qquad (2.15)$$

where T is related to the S-matrix by

$$S = 1 + iT \,. \qquad (2.16)$$

This can easily be seen by realizing that the above restrictions will cause the second diagram in (2.14) to equal the complex conjugate of the first diagram. It should be remarked that the cutting rule is more stringent than the unitarity equation because of the fact that it holds for a single diagram instead of a complete T-matrix probability amplitude.

As we are used to performing actual calculations in the momentum representation, we define the following Fourier transform :

$$f(x) = \frac{1}{(2\pi)^4} \int d^4k \, e^{-ik.x} \, F(k) \,. \qquad (2.17)$$

The prescriptions involving the cutting of diagrams take on the following form to be used in future specific applications (to this end we restrict ourselves to free scalar fields) :

1 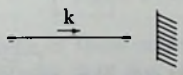

: free scalar propagator in unshaded region $\frac{i}{k^2-m^2+i\epsilon}$

2 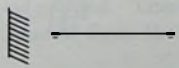
: free scalar propagator in shaded region $\frac{-i}{k^2-m^2-i\epsilon}$

3  : cut scalar free propagator $2\pi\,\theta(k_0)\,\delta(k^2 - m^2)$

4 vertex in shaded region means replacing a factor i by -i.

It should be noted that an n-dimensional version of the line of reasoning leading to the cutting rule and the cutting prescriptions, involving n-dimensional space-time points and corresponding momenta, will lead to the same results as a consequence of the fact that the decompositions (2.5) and (2.13) remain unchanged.

Let us now consider a diagram corresponding to a scalar 4-point integral :

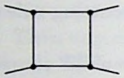 $\equiv \frac{i}{16\pi^2} D_0$, (2.18)

suppressing the parameter content of D_0 at the moment. The Cutkosky cutting rule takes in this case the form :

$$\frac{i}{16\pi^2}\,(D_0 - D_0^*) = -\frac{\mathrm{Im}\,D_0}{8\pi^2} = -\sum_{\substack{\text{cut}\\ \text{graphs}}}$$ 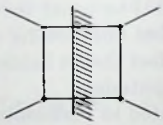 , (2.19)

where the sum over the cut graphs consists of the following different types of cut diagrams :

1. diagrams with opposite propagators cut, like 

2. diagrams with two neighbouring propagators cut, like 

3. diagrams with two sets of neighbouring propagators cut, like 

Which of these cut diagrams actually contribute to the imaginary part (absorptive part) of D_0 is ruled by the sources, indicating whether energy is being absorbed or emitted at a certain vertex connected to such a source, and momentum conservation at each vertex. It should be noted that the nature of the sources have not been specified at any stage of the above reasoning. So it is very well possible that the considered diagrams are even constituents of yet larger diagrams (see for example fig. 5).

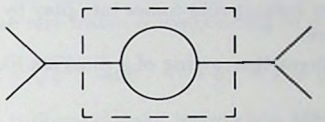

Fig. 5. Example of a diagram (inside the dashed box) within a larger diagram

3 Dispersion integrals

Now we can try to explore the consequences of the Cutkosky cutting rule (2.14). To do this the analyticity properties of Feynman diagrams and integrals will be applied. Consider a Feynman integral I depending on the external momenta $q_1, \ldots, q_n$ via all possible invariants $q_i.q_j$. Then the following has been shown in the literature [3] : I is analytic on the upper half of the complex plane corresponding to any of the invariants provided the other invariants are taken to be fixed. This means that I is an analytic function in all variables when their definition range is extended from being pure physical real quantities to complex quantities on the upper half plane. Let us now restrict ourselves for a moment to a Feynman integral depending on just one external momentum q (see fig. 6) in order to have a closer look at the

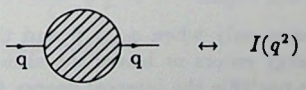

Fig. 6. Feynman diagram with one external momentum

implications of these analyticity properties. In case there exists a region of real q^2 values such that $I(q^2) \epsilon \mathbb{R}$ in that region, the reflection principle of Schwartz can be applied. This principle states that the function $I(q^2)$ can in that case be continuated from the upper to the lower half complex plane by the prescription

$I([q^2]^*) = I^*(q^2)$. In this way a holomorphic function is obtained with a possible cut on the real q^2 axis in the presence of real q^2 regions with non-zero imaginary parts for $I(q^2)$. The discontinuity across that cut is given by ($q^2 \epsilon \mathbb{R}$)

$$\begin{aligned} \text{disc}\, I(q^2) &= \lim_{\delta \downarrow 0} \left[I(q^2 + i\delta) - I(q^2 - i\delta) \right] \\ &= 2i \lim_{\delta \downarrow 0} \text{Im} \left[I(q^2 + i\delta) \right] \equiv 2i\, \text{Im}_+ I(q^2) \,. \end{aligned} \tag{3.1}$$

At this stage the Cutkosky cutting rule comes into play by giving information about $\text{Im}_+ I(q^2)$ for real q^2 values.

Let us now explicitly treat the cutting of a diagram like the one in fig. 6. Define to this end :

$$\frac{i}{16\pi^2} B_0(q^2) = \quad = \mu^{4-n} \int \frac{d^n l}{(2\pi)^n} \frac{1}{[l^2 - m_1^2 + i\epsilon][(l+q)^2 - m_2^2 + i\epsilon]} \,, \tag{3.2}$$

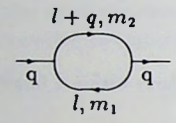

where the loop momentum l covers n degrees of freedom in order to handle the UV divergences present in this particular example. The causality related positive infinitesimal imaginary parts ϵ in the denominator are part of the Feynman rules leading to this scalar 2-point Feynman integral. They will ensure that the cutting rule (2.14) leads to an imaginary part of the form (3.1). When investigating the analyticity properties of $B_0(q^2)$, however, we will be dealing with (3.2) without these imaginary parts. They will only reappear when the Feynman integral (3.2) is considered or results thereof. Without loss of explanatory power we assume, for convenience, that $m_1 > 0$. The cutting rule yields according to (2.14) the following :

$$-\frac{\text{Im}_+ B_0(q^2)}{8\pi^2} = -$$

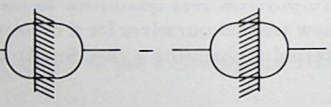

. (3.3)

The first diagram contributes only when $q_0 > 0$ and the second one only when $q_0 < 0$. At $q_0 = 0$ no energy enters or leaves the skeleton part of the diagram. So, the external sources do not rule the internal energy flow anymore. This is not a problem as we can make use of the Lorentz invariance of (3.2) by boosting in such a way that $q_0 > 0$. If this is not possible we can immediately conclude that $q = 0$, a situation which will not lead to imaginary parts. Hence the easiest way to incorporate the case $q_0 = 0$ using (3.3) is to regard it as $q_0 \downarrow 0$. Because of the symmetry of the integral (3.2) under the transformation $q \to -q$, it will be sufficient to consider only the case $q_0 \geq 0$, in this way selecting the first diagram (regarding $q_0 = 0$ as $q_0 \downarrow 0$). Now the cutting prescription can be applied, yielding :

$8\pi^2$ 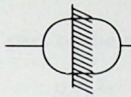 $= 2(2\pi\mu)^{4-n} \int d^n l\, \theta(-l_0)\, \delta(l^2 - m_1^2)\, \theta(l_0 + q_0)\, \delta([l+q]^2 - m_2^2)\,.$ (3.4)

The first thing to realize is that we are dealing with a Lorentz invariant integral, only depending on scalar invariants. As a result of that property the case $q^2 < 0$ will not lead to a non-zero result as can easily be seen by working in that inertial frame in which $q_0 = 0$, resulting in a conflict between the two θ-functions. Let us now restrict ourselves to the cases $q^2 = 0$ and $q^2 > 0$. The latter offers us the opportunity to work in the rest frame corresponding to q, leading to the identities

$$\vec{q} = \vec{0} \quad , \quad q_0 = \sqrt{q^2} \quad \text{and} \quad (l+q)^2 = l^2 + q^2 + 2l_0\sqrt{q^2}$$

to be used in (3.4). The n-dimensional l integration can be split into an l_0 integration and an Euclidean (n-1)-dimensional integration running over the spacial components of l. By introducing (n-1)-dimensional spherical coordinates and subsequently the new variable

$$\omega = \sqrt{\vec{l}^2 + m_1^2}$$

to replace the radiale coordinate $|\vec{l}|$, the n-dimensional l integral finally takes on the form :

$$\int d^n l = \int_{-\infty}^{\infty} dl_0 \int_{m_1}^{\infty} d\omega \int d\Omega_{n-1}\, \omega(\omega^2 - m_1^2)^{\frac{n-3}{2}}\,. \tag{3.5}$$

By performing first the l_0 integration and then the ω integral (3.4) reduces to the trivial result :

$8\pi^2$ 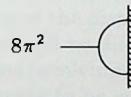 $\overset{q^2 \geq 0}{=} \theta(q^2 - [m_1+m_2]^2)\,(2\pi\mu)^{4-n}\, \frac{\Lambda^{\frac{n-3}{2}}}{(4q^2)^{\frac{n}{2}-1}}\, J\,,$ (3.6)

where Λ stands for the Kallén function $\lambda(q^2, m_1^2, m_2^2)$, defined by

$$\lambda(x,y,z) \equiv x^2 + y^2 + z^2 - 2xy - 2xz - 2yz\,, \tag{3.7}$$

and J for the integral over the angles :

$$J = \int d\Omega_{n-1} = 2\,\frac{\pi^{\frac{n-1}{2}}}{\Gamma(\frac{n-1}{2})}\,. \tag{3.8}$$

As the Cutkosky cutting rule will only lead to 2-propagator cuts in the case of 3- and 4-point integrals, this result also holds in those cases appart from just one extension to be found in J :

$$J = \int d\Omega_{n-1}\, \{ \text{ remaining propagators } \}^{-1}\,, \tag{3.9}$$

with the supplementary conditions

$$l_0 = -\frac{q^2 + m_1^2 - m_2^2}{2\sqrt{q^2}} \quad , \quad |\vec{l}| = \frac{\sqrt{\Lambda}}{2\sqrt{q^2}}$$

propagators in shaded region are to be conjugated . (3.10)

The remaining case $q^2 = 0$ will not render a non-zero result as a suitable choice of inertial frame will generate a conflict between the θ-functions and one of the δ-functions; because $m_1 > 0$ a choice leading to $q_0 < m_1$ will do the trick. We can summarize the above evaluation by the following result for the imaginary (absorptive) part of B_0 :

$$\mathrm{Im}_+ B_0(q^2) = \theta(q^2 - [m_1 + m_2]^2)\,(2\pi\mu)^{4-n}\,\frac{\Lambda^{\frac{n-3}{2}}}{(4q^2)^{\frac{n}{2}-1}}\,2\,\frac{\pi^{\frac{n-1}{2}}}{\Gamma\left(\frac{n-1}{2}\right)} \,. \tag{3.11}$$

The threshold indicated by the argument of the θ-function denotes in fact the physical threshold for the process describing the decay into the two intermediate state particles with masses m_1 and m_2. In fig. 7 the cut structure of the 2-point

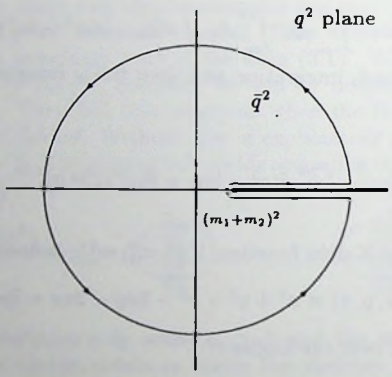

Fig. 7. Cauchy integral contour for $B_0(\bar{q}^2)$

integral $B_0(q^2)$ in the complex q^2 plane is displayed together with the definition of the contour to be used in the Cauchy integral for calculating its complete analytic expression at $q^2 = \bar{q}^2$. The circular part of the contour corresponds to a circle with infinite radius, so if we assume the function $B_0(q^2)/q^2$ to go to zero fast enough on

that part of the contour the following Cauchy integral can be derived :

$$B_0(q^2) = \frac{1}{2\pi i}\oint dq'^2 \frac{B_0(q'^2)}{q'^2 - q^2} = \frac{1}{2\pi i}\int_{(m_1+m_2)^2}^{\infty} dq'^2 \frac{\mathrm{disc}\, B_0(q'^2)}{q'^2 - q^2}$$

$$= \frac{1}{\pi}\int_{(m_1+m_2)^2}^{\infty} dq'^2 \frac{\mathrm{Im}_+ B_0(q'^2)}{q'^2 - q^2} \,. \qquad (3.12)$$

In case of absence of the proper amount of convergence of $B_0(q^2)/q^2$ on the infinite circular part of the contour, for instance when $B_0(q^2)$ tends to a constant there, the contribution coming from that circular part can be a non-zero one and hence should not be omitted. This is however not a genuine problem as we can decide on a different Cauchy integral in that case :

$$\frac{B_0(q^2)}{q^2 - q_0^2} = \frac{B_0(q_0^2)}{q^2 - q_0^2} + \frac{1}{\pi}\int_{(m_1+m_2)^2}^{\infty} dq'^2 \frac{\mathrm{Im}_+ B_0(q'^2)}{(q'^2 - q_0^2)(q'^2 - q^2)} \,. \qquad (3.13)$$

The Cauchy integrals (3.12) and (3.13) are called the dispersion integral respectively once subtracted dispersion integral of the function $B_0(q^2)$. This terminology reflects its close relation to similar integral representations in the analysis of forward light scattering in an absorptive medium [4]. Causality of the scattered wave, resulting in the possibility of applying the reflection principle of Schwartz, corresponds to the $i\epsilon$ - prescription for propagators (see last section). The optical theorem, connecting imaginary parts of scattering amplitudes for positive frequencies to the cross section of the absorption of light with those particular frequencies, can be related to the Cutkosky cutting rule, displaying unitarity at the diagram level.

The example given above is in fact not the most suitable one to show the strong points of the dispersion integral method for calculating scalar integrals. The strong points will be discussed in the next section when explicit dispersion integral calculations involving more complicated integral structures like 3- and 4-point integrals are going to be considered.

4 Dispersion integrals for IR-divergent scalar integrals

In this section we will consider a few general IR-divergent integrals which are of an electroweak origin. This last additional restriction means that the only possible divergences present in these integrals will be the UV and IR ones, the latter being caused by the coupling of a virtual photon to two external (on-shell) particles. As the IR-divergent scalar integrals will be of the 3- or more-point type we can forget about the UV divergences and hence will be allowed to perform these integrals in 4 dimensions. For our purposes (2- to 2-body processes) we will impose a further restriction by excluding 5- and more-point integrals.

The reason for selecting this particular type of integral to show dispersion integral techniques at work is twofold :

- these integrals are the main sources of the instabilities in numerical evaluations of EWRC effects. They contain IR-divergent terms as well as 'mass singular' double poles, which will both be cancelled by similar terms originating from real photonic corrections
- because of extra symmetries present in these integrals the combined use of the Cutkosky cutting rule and dispersion integral techniques will render transparent results displaying some of the particularly attractive aspects of this approach.

Consider the following most general form of an IR-divergent scalar 4-point integral of electroweak origin :

$$D_0(p_1, p_2, p_3, \lambda, m_1, m_0, m_4) \equiv \int \frac{d^4l}{i\pi^2} \{D_1 D_2 D_3 D_4\}^{-1} \quad (4.1)$$

with the denominators

$$\begin{aligned} D_1 &= l^2 - \lambda^2 + i\epsilon \\ D_2 &= (l + p_1)^2 - m_1^2 + i\epsilon \\ D_3 &= (l + p_1 + p_2)^2 - m_0^2 + i\epsilon \\ D_4 &= (l + p_1 + p_2 + p_3)^2 - m_4^2 + i\epsilon \, . \end{aligned} \quad (4.2)$$

The momenta in (4.2) corresponding to the diagram depicted in fig. 8 have the

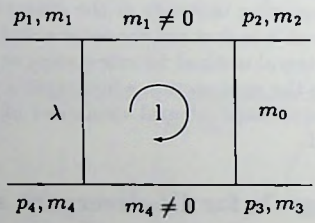

Fig. 8. IR-divergent scalar 4-point integral

following features :

$$\begin{aligned} & p_1 + p_2 + p_3 + p_4 = 0 \quad : \text{ momentum conservation} \\ & p_i^2 = m_i^2 \quad \text{for } i = 1, \ldots, 4 \\ & m_1, m_4 \, \epsilon \, I\!R^+ \quad : \text{ displaying the electroweak origin} \\ & (p_1 + p_4)^2 = (p_2 + p_3)^2 \equiv s \\ & (p_1 + p_2)^2 = (p_3 + p_4)^2 \equiv t \, . \end{aligned} \quad (4.3)$$

The parameters s and t are just the standard Mandelstam variables for the process $14 \to 23$. At this point we will restrict ourselves to real and positive masses m_0. Later on we will come back to that. For simplicity sake we will from now on leave out the long parameter list of D_0 except for the parameter in which the dispersion integral will be evaluated. In order to be able to give general results in a compact form we are led to define the following kinematical function :

$$K(z,m,m') \equiv \begin{cases} -\dfrac{\sqrt{1-\frac{4mm'}{[z-(m-m')^2]}}-1}{\sqrt{1-\frac{4mm'}{[z-(m-m')^2]}}+1} & \text{if } z \neq (m-m')^2 \\ -1 & \text{if } z = (m-m')^2 \end{cases} , \qquad (4.4)$$

where the parameters z, m, m' are in principle complex quantities. In the case $m' = m$ the function $K(s,m,m)$ takes on the form $-\frac{\sqrt{1-4m^2/s}-1}{\sqrt{1-4m^2/s}+1}$, which is a kinematical variable that finds frequent use in e^+e^- physics when the final state particles have the same mass.

The most important constituents in the forthcoming calculations will be the logarithm and dilogarithm. We define the logarithm of a complex quantity to have a cut along the negative real axis with a branching point situated at zero. The dilogarithm is defined by means of the integral representation

$$Li_2(z) = -\int_0^1 dt \, \frac{\log(1-zt)}{t} , \qquad (4.5)$$

where z may be a complex quantity. According to the cut structure of the logarithm the dilogarithm has a cut along the positive real axis with a branching point situated at $z = 1$. The discontinuity of both functions across the corresponding cuts are given by :

$$\begin{aligned} \lim_{\delta \downarrow 0} [\log(x+i\delta) - \log(x-i\delta)] &= 2i\pi \qquad (x<0) \\ \lim_{\delta \downarrow 0} [Li_2(x+i\delta) - Li_2(x-i\delta)] &= 2i\pi \log(x) \qquad (x>1) . \end{aligned} \qquad (4.6)$$

Because the integral (4.1) has kinematical singularities at $s = (m_1+m_4)^2$ and $t = m_0^2$ we will exclude these two situations from our calculation. This calculation will involve the evaluation of the dispersion integral in the parameter s. The choice of the parameter s is a purely practical one as it reveals the symmetries present in the integral in the best way (see fig. 9) by decomposing it via cutting into the scalar processes $14 \to 14$ and $23 \to 14$. In order to avoid problems with the other remaining parameters, bearing in mind that any cut in one of those parameters (the so-called cut invariants) will be of the form (3.6), we will start off with the restrictions m_2^2 , m_3^2 , $t < 0$. Later on the obtained expressions will also be extended

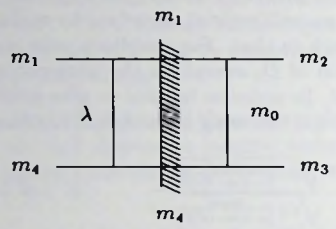

Fig. 9. s-channel cut

to non-negative values. Application of the Cutkosky cutting rule via the use of (3.6), (3.9) and (3.10) yields the following :

$$\mathrm{Im}_+ D_0(s) \overset{s\text{-channel}}{=\!=} \theta(s-[m_1+m_4]^2)\,\frac{\sqrt{\Lambda}}{4s}\,J\ , \tag{4.7}$$

with $\Lambda \equiv \lambda(s, m_1^2, m_4^2)$ as defined in (3.7) and the angular integral J given by

$$\begin{aligned} J &= \int d\Omega\,\left\{\,[(l-p_1)^2-\lambda^2+i\epsilon][(l+p_2)^2-m_0^2-i\epsilon]\,\right\}^{-1} \\ l_0 &= \frac{s+m_1^2-m_4^2}{2\sqrt{s}} \quad , \quad |\vec{l}\,| = \frac{\sqrt{\Lambda}}{2\sqrt{s}}\ . \end{aligned} \tag{4.8}$$

The sign difference between the l_0 conditions of (3.10) and (4.8) is caused by the direction of the integration momentum as compared to the direction of the energy flow, imposed by the shaded region of the cut. By a proper parametrization J can be brought in the form

$$J = \int d\Omega\ \{\,(a+b\cos\theta)(A+B\cos\theta+C\sin\theta\cos\phi)\,\}^{-1}\ . \tag{4.9}$$

Now we can make use of a general result displayed in appendix B and after neglecting λ whenever that is possible, bearing in mind that we have left out both kinematical singularities, we are left with

$$\begin{aligned} \mathrm{Im}_+ D_0(s) \overset{s\text{-channel}}{=\!=} \theta(s-[m_1+m_4]^2)\,&\frac{\pi}{\sqrt{\Lambda}\,(t-m_0^2)}\left\{2\log\left(\frac{m_0\lambda}{m_0^2-t}\right)\right. \\ &\left. +\sum_{\rho,\sigma=\pm1}\log(z-z_{\rho,\sigma})-2\log(z-1)-2\log(z+1)\right\}\ , \end{aligned} \tag{4.10}$$

with

$$z = \frac{s - m_1^2 - m_4^2 + \sqrt{\Lambda}}{2m_1 m_4} = \frac{1}{K(s, m_1, m_4)}$$

$$z_{\rho,\sigma} = -K^{\rho}(m_2^2, m_1, m_0)\, K^{\sigma}(m_3^2, m_4, m_0)\ . \qquad (4.11)$$

From the definition of the function K in (4.4) it can be seen that $z \in (1, \infty)$ because of the θ-function condition $s > (m_1 + m_4)^2$ and $z_{\rho,\sigma} < 0$ in view of the conditions imposed on the other cut invariants restricting them to negative values. So none of the arguments of the above logarithms will lie on a cut. Now we can apply the dispersion integral formalism and calculate D_0. Just as in the case of the other cut invariants the selected s-range will first be restricted to $s < 0$ in order to avoid the s-channel discontinuity of D_0 from entering the dispersion integral. Of course an extension of this s-range needs to be implemented later on.
The (unsubtracted) dispersion integral for D_0 looks as follows :

$$D_0(s) = \frac{1}{\pi} \int_{(m_1+m_4)^2}^{\infty} \frac{ds'}{s' - s}\, \mathrm{Im}_+ D_0(s')\ . \qquad (4.12)$$

Using formula (4.10) as input and introducing the new integration variable

$$z = K^{-1}(s', m_1, m_4)\ ,$$

leading to the replacements

$$\frac{ds'}{\sqrt{\Lambda'}} = \frac{dz}{z} \quad \text{and} \quad \frac{s' - s}{m_1 m_4} = \frac{(z - z_0)(z - z_0^{-1})}{z}\ ,$$

where z_0 and Λ' are shorthand notations for $K(s, m_1, m_4)$ and $\lambda(s', m_1^2, m_4^2)$, this reduces to the much simpler integral

$$D_0(s) = \frac{z_0}{m_1 m_4 (t - m_0^2)(z_0^2 - 1)} \int_1^{\infty} dz \left[\frac{1}{z - z_0} - \frac{1}{z - z_0^{-1}}\right] \left\{2 \log\left(\frac{m_0 \lambda}{m_0^2 - t}\right) + \sum_{\rho,\sigma=\pm 1} \log(z - z_{\rho,\sigma}) - 2\log(z-1) - 2\log(z+1)\right\}\ . \qquad (4.13)$$

Now the $z_{\rho,\sigma} \to z_{\rho,\sigma}^{-1}$ symmetry present in the integral can be exploited by realizing the following :

$$\int_1^{\infty} dz \left[\frac{1}{z - z_0} - \frac{1}{z - z_0^{-1}}\right] \left\{\log(z - y) + \log(z - y^{-1})\right\} = \int_0^{\infty} dz \left[\frac{1}{z - z_0} - \frac{1}{z - z_0^{-1}}\right] \log(z - y) - \int_0^{1} dz \left[\frac{1}{z - z_0} - \frac{1}{z - z_0^{-1}}\right] \{\log(z) + \log(-y)\}\ . \qquad (4.14)$$

To come to this expression the second logarithm on the left hand side has to be submitted to the transformation $z \to z^{-1}$. In this way we arrive at

$$D_0(s) = \frac{z_0}{m_1 m_4 (t-m_0^2)(z_0^2-1)} \left\{ \int_0^\infty dz \left[\frac{1}{z-z_0} - \frac{1}{z-z_0^{-1}} \right] \left[-\log(z+1) + \frac{1}{2} \sum_{\rho,\sigma=\pm 1} \log(z - z_{\rho,\sigma}) \right] + \int_0^1 dz \left[\frac{1}{z-z_0} - \frac{1}{z-z_0^{-1}} \right] \left[\log(z) - 2\log(1-z) + 2\log\left(\frac{m_0 \lambda}{m_0^2 - t} \right) \right] \right\} . \tag{4.15}$$

Now we can make use of a few integral identities : ($t \epsilon \mathbb{R}$)

$$\int_0^1 dz \left[\frac{1}{z-z_0} - \frac{1}{z-z_0^{-1}} \right] = -\log(-z_0)$$

$$\int_0^1 dz \left[\frac{1}{z-z_0} - \frac{1}{z-z_0^{-1}} \right] \log(1-z) = -Li_2\left(\frac{1}{1-z_0} \right) + Li_2\left(\frac{z_0}{z_0-1} \right)$$

$$\int_0^t dz \frac{\log(z-a)}{z-b} = \left[-Li_2\left(\frac{z-a}{z-b} \right) + \frac{1}{2}\log^2(z-b) + \{ \log(z-b) - \log(z-a) \} \log\left(\frac{a-b}{z-b} \right) \right]_{z=0}^{z=t} . \tag{4.16}$$

which even holds for complex a and b as can be seen from appendix C. In our calculation we are at the moment mainly dealing with the above integrals in the cases $t > 0$ and $a, b < 0$. This enables us to use a more pleasant form for the last integral identity, reading

$$\int_0^t dz \frac{\log(z-a)}{z-b} = \left[Li_2\left(\frac{a-b}{z-b} \right) + \frac{1}{2}\log^2(z-b) \right]_{z=0}^{z=t} . \tag{4.17}$$

This can easily be derived by applying the dilogarithm relation (D.3) given in appendix D. As a consequence of the above identities and the dilogarithm relations (D.2-D.6) of appendix D we arrive at the following integral results :

$$\frac{1}{2} \int_0^\infty dz \left[\frac{1}{z-z_0} - \frac{1}{z-z_0^{-1}} \right] \sum_{\rho,\sigma=\pm 1} \log(z - z_{\rho,\sigma}) = \frac{1}{2} \sum_{\rho,\sigma,\tau=\pm 1} \tau\, Li_2(1 - z_0^\tau z_{\rho,\sigma}) = \sum_{\rho,\sigma=\pm 1} \left\{ Li_2(1 - z_0 z_{\rho,\sigma}) + \frac{1}{4}\log^2(z_0 z_{\rho,\sigma}) \right\} \tag{4.18}$$

and

$$2 \int_0^1 dz \left[\frac{1}{z-z_0} - \frac{1}{z-z_0^{-1}} \right] \left\{ \frac{1}{2}\log(z) - \log(1-z) \right\} -$$

$$\int_0^\infty dz \left[\frac{1}{z-z_0} - \frac{1}{z-z_0^{-1}}\right] \log(z+1) = -Li_2(1-z_0^2) - \log^2(-z_0) \ . \tag{4.19}$$

Putting together all ingredients yields :

$$D_0(s) = \frac{z_0}{m_1 m_4 (t-m_0^2)(z_0^2-1)} \left\{ -2\log(-z_0)\log\left(\frac{m_0\lambda}{m_0^2-t}\right) + \frac{1}{4}\sum_{\rho,\sigma=\pm 1}\log^2(-z_{\rho,\sigma}) \right.$$
$$\left. - Li_2(1-z_0^2) + \sum_{\rho,\sigma=\pm 1} Li_2(1-z_0 z_{\rho,\sigma}) \right\} \ . \tag{4.20}$$

This is the final result for the scalar 4-point integral (4.1) restricted by the condition that all cut invariants are smaller than zero (well below any of the possible thresholds). The reason that the s-channel dispersion integral is sufficient to cover the dependence of D_0 on all other cut invariants is that any term present in D_0 which is not obtained from the s-channel dispersion integral survives on the infinite circular part of the contour as depicted in fig. 7 in the last section. But it is obvious that the s dependence of the original integral (4.1), via its multiplicative propagator character, ensures that no such term exists.

Maybe this is the right time to make a few remarks about the above approach of calculating scalar integrals as compared to already existing general integral formalisms. Because of the fact that the dispersion integral is just 1-dimensional, as compared to the basicly 3-dimensional integral obtained by Feynman parametrization of (4.1), any symmetry or systematics which might be present can more easily be exploited. Of course general integral formalisms like the one by 't Hooft and Veltman [5], which applies Feynman parametrization to end up with general formulae covering all physical parameter regions, are very much appreciated because of that very general character. However, they tend to obscure any systematic behaviour as protruding in the above described dispersion technique. At the moment the use of dispersion techniques is restricted to integrals which are likely to lead to numerical instabilities caused by the presence of IR divergences and 'mass singularities'. See for instance the integrals given in [6], used in [7], which were calculated by means of both above mentioned integration techniques. Extension of its range of applications to integrals which do not have these particularities might be considered in the future in order to come to an alternative general integral formalism which could be complementary to the already existing ones as far as insight and transparency are concerned. Any attempt to do so has up to now been restricted to physically imposed parameter choices (including several small masses like m_e).

After this intermezzo we return to the scalar 4-point integral under consideration, which is at this moment in a form valid well below all possible thresholds as set by 2-propagator cuts of the form (3.6). The continuation of expression (4.20)

to cover all possible real values for the cut invariants, whether they are physical or not, proceeds via an analytical continuation procedure involving the logarithms and dilogarithms. To this end we introduce a shorthand notation for the kinematical variables :

$$\begin{aligned} x_s &= -K(s+i\epsilon, m_1, m_4) \\ x_2 &= -K(m_2^2+i\epsilon, m_1, m_0) \\ x_3 &= -K(m_3^2+i\epsilon, m_4, m_0)\ . \end{aligned} \tag{4.21}$$

The positive infinitesimal imaginary parts ϵ constitute the $i\epsilon$ - propagator prescription as present in (4.1), which leads to the realization of analyticity on the upper half of the complex plane corresponding to any of the above mentioned cut invariants. All this results in the replacements $z_0 \to -x_s$ and $z_{\rho,\sigma} \to -x_2^\rho x_3^\sigma$ in (4.20). In the same way we could in fact have introduced $x_t = -K(t+i\epsilon, \lambda, m_0)$, but this automatically takes on the form $\frac{m_0\lambda}{m_0^2-t-i\epsilon}$ for $t \neq m_0^2$ as a consequence of the infinitesimal character of the photon mass λ. Notice that the introduction of the positive imaginary parts ϵ is necessary to extend the cut invariants above the corresponding thresholds in such a way that the correct imaginary parts, as predicted by the Cutkosky cutting rule, are reproduced. When the cut invariants cover all possible real values, the corresponding kinematical variables x_s, x_t, x_2, x_3 vary only on the first Riemann sheet, i.e. $-\pi < \arg(x_s, x_t, x_2, x_3) < \pi$, whereas their absolute values are smaller than 1 as a consequence of the infinitesimal imaginary parts ϵ. The fact that the kinematical variables vary only on the first Riemann sheet is of crucial importance to the analytical continuation procedure, allowing the arguments of some of the logarithms and dilogarithms to move on the corresponding Riemann surfaces beyond the first sheet as a result of the combined effect of a product of more than one kinematical variable. The continuation of terms of the form $\log(x_1 x_2 \cdots x_n)$ and $Li_2(1-x_1x_2\cdots x_n)$ is displayed in appendix E. Application of this procedure leads to the following result, valid for all real cut invariants and including all possible cuts :

$s \neq (m_1-m_4)^2$:

$$\begin{aligned} D_0(s) = \frac{x_s}{m_1 m_4 (t-m_0^2)(1-x_s^2)} \Bigg\{ & 2\log(x_s)\left[\log(1-x_s^2) - \log\left(\frac{m_0\lambda}{m_0^2-t-i\epsilon}\right)\right] \\ & + \frac{\pi^2}{2} + Li_2(x_s^2) + \log^2(x_2) + \log^2(x_3) - \sum_{\rho,\sigma=\pm 1} \Big[Li_2(x_s x_2^\rho x_3^\sigma) \\ & + \left\{\log(x_s) + \log(x_2^\rho) + \log(x_3^\sigma)\right\} \log(1-x_s x_2^\rho x_3^\sigma) \Big] \Bigg\} \end{aligned} \tag{4.22}$$

$s = (m_1-m_4)^2$:

$$D_0(s) = \frac{1}{2m_1 m_4 (t-m_0^2)} \Bigg\{ - \sum_{\rho=\pm 1} \frac{1+x_2 x_3^\rho}{1-x_2 x_3^\rho} \left[\log(x_2) + \log(x_3^\rho)\right]$$

$$+\ 2\log\left(\frac{m_0\lambda}{m_0^2-t-i\epsilon}\right)-2\Big\}\ . \tag{4.23}$$

The explicit division into the situations $s \neq (m_1-m_4)^2$ and $s=(m_1-m_4)^2$ is necessary as in the latter case $x_s = 1$ and consequently both numerator and denominator become zero in (4.22), demanding a limiting procedure for the determination of the possibly finite answer.

To finish the above example we will give a special form of (4.22) and (4.23) containing two sources of IR divergences, indicated by the parameter conditions $m_2 = m_1$, $m_3 = m_4$ and $m_0 = \lambda$. This leads to an expression containing just two cut invariants s and t given by :

$s \neq (m_1-m_4)^2$:

$$D_0(s) = \frac{-x_s}{m_1 m_4 t\,(1-x_s^2)}\left\{2\log(x_s)\log\left(\frac{\lambda^2}{-t-i\epsilon}\right)\right\} \tag{4.24}$$

$s=(m_1-m_4)^2$:

$$D_0(s) = \frac{1}{2m_1m_4t}\left\{2\log\left(\frac{\lambda^2}{-t-i\epsilon}\right)\right\}\ . \tag{4.25}$$

For more special forms involving the case $m_0 = 0$ and 'mass singularities' we can refer to [8]. Any of the above types of integrals appearing in the specific calculations of EWRC effects to the fermion pair production processes $e^+e^- \to f\bar{f}$ can be found in appendix F. At this point we should stress that the expressions (4.22) and (4.23) will remain of the same form when the mass m_0 is allowed to have a non-zero imaginary part, provided this imaginary part is a non-positive one. This in order to avoid crossing any cut while continuating the propagator D_3 in (4.2), containing the positive infinitesimal imaginary parts $+\epsilon$, to a resonant type of propagator involving a non-real mass m_0. This feature is particularly handy for the process $e^+e^- \to f\bar{f}$ when final state particles are considered with mass $< M_Z/2$.

Our survey of IR-divergent scalar integrals can now be completed by determining the expression for the scalar 3-point integral

$$C_0(p_1,p_2+p_3,\lambda,m_1,m_4) \equiv \int \frac{d^4l}{i\pi^2}\,\{D_1D_2D_4\}^{-1}\ , \tag{4.26}$$

with D_1, D_2 and D_4 as defined in (4.2), described diagrammatically by the scalar diagram of fig. 10. This integral can be linked directly to the 4-point integral (4.1) via

$$C_0(p_1,p_2+p_3,\lambda,m_1,m_4) = \lim_{m_0^2\to\infty}\left[-m_0^2\,D_0(p_1,p_2,p_3,\lambda,m_1,m_0,m_4)\right]\ . \tag{4.27}$$

The immediate consequence of this relation is a general expression for C_0 of the form (using once again a shorthand parameter list) :

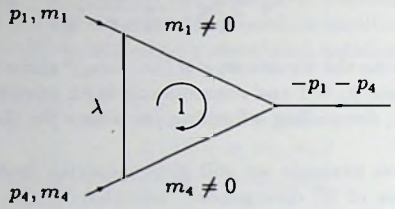

Fig. 10. IR-divergent scalar 3-point integral

$s \neq (m_1 - m_4)^2$:

$$C_0(s) = \frac{x_s}{m_1 m_4 (1-x_s^2)} \left\{ \log(x_s) \left[-\frac{1}{2} \log(x_s) + 2 \log(1-x_s^2) - \log\left(\frac{\lambda^2}{m_1 m_4}\right) \right] \right.$$
$$\left. - \frac{\pi^2}{6} + Li_2(x_s^2) + \frac{1}{2} \log^2\left(\frac{m_1}{m_4}\right) + Li_2\left(1 - x_s \frac{m_1}{m_4}\right) + Li_2\left(1 - x_s \frac{m_4}{m_1}\right) \right\} \tag{4.28}$$

$s = (m_1 - m_4)^2$:

$$C_0(s) = \frac{1}{2 m_1 m_4} \left\{ \log\left(\frac{\lambda^2}{m_1 m_4}\right) - 2 - \frac{1 + \frac{m_1}{m_4}}{1 - \frac{m_1}{m_4}} \log\left(\frac{m_1}{m_4}\right) \right\} . \tag{4.29}$$

Specific forms of this 3-point integral to be used in the calculations of EWRC effects to the fermion pair production processes $e^+e^- \to f\bar{f}$ can be found in appendix F. Note that the most general expressions for D_0 and C_0 have, for transparency reasons, not been written in a form containing as few dilogarithms as possible. The number of dilogarithms can be reduced from 5 to 4 in the D_0 expression and from 3 to 2 in the C_0 expression by application of the special two parameter dilogarithm relation displayed in appendix D. This, however, leads to all kinds of additional logarithms, accounting for the crossing of some cuts, which in general obscure any systematics that might be present.

5 Reduction of tensor integrals

Up to now our efforts have been focussed on the scalar integrals, the basic building blocks in any calculation of EWRC effects. The next step will be a discussion of ways to arrive at those scalar integrals starting off with some diagram contributing to the S-matrix of a particular process. To this end we will concentrate in this

section on the 2-, 3- and 4-point tensor integrals. First define the following :

$$
\begin{aligned}
A_0(M_1) &\equiv (2\pi\mu)^{4-n} \int \frac{d^n l}{i\pi^2} \frac{1}{D_1} \\
B_{\{0,\mu,\mu\nu\}}(p_1, M_1, M_2) &\equiv (2\pi\mu)^{4-n} \int \frac{d^n l}{i\pi^2} \frac{\{1,\, l_\mu,\, l_\mu l_\nu\}}{D_1 D_2} \\
C_{\{0,\mu,\mu\nu,\mu\nu\rho\}}(p_1, p_2, M_1, M_2, M_3) &\equiv (2\pi\mu)^{4-n} \int \frac{d^n l}{i\pi^2} \frac{\{1,\, l_\mu,\, l_\mu l_\nu,\, l_\mu l_\nu l_\rho\}}{D_1 D_2 D_3} \\
D_{\{0,\mu,\mu\nu,\mu\nu\rho\}}(p_1, p_2, p_3, M_1, M_2, M_3, M_4) &\equiv (2\pi\mu)^{4-n} \int \frac{d^n l}{i\pi^2} \frac{\{1,\, l_\mu,\, l_\mu l_\nu,\, l_\mu l_\nu l_\rho\}}{D_1 D_2 D_3 D_4} ,
\end{aligned}
\tag{5.1}
$$

with the denominators given by

$$
\begin{aligned}
D_1 &= l^2 - M_1^2 + i\epsilon \\
D_2 &= (l + p_1)^2 - M_2^2 + i\epsilon \\
D_3 &= (l + p_1 + p_2)^2 - M_3^2 + i\epsilon \\
D_4 &= (l + p_1 + p_2 + p_3)^2 - M_4^2 + i\epsilon \, .
\end{aligned}
\tag{5.2}
$$

The fact that the loop momentum integration is an n-dimensional one displays our wish for a little bit more generality, enabling us to extend any forthcoming method beyond the electroweak theory to, for instance, the massless theory of strong interactions (QCD), with its much richer structure of n-dimensionally regulated divergences (UV, IR and mass singular ones). In the case of integrals of pure electroweak origin the 4-point scalar and tensor integrals present in (5.1) will not need an n-dimensional treatment, because of the absence of real mass singularities (not labeled by a small mass) and UV divergences (for that given number of integration momenta in the numerator).

Because of the symmetry properties of the tensor integrals (5.1), they can be decomposed by applying Lorentz covariance into :

$$
\begin{aligned}
B_\mu &= p_{1\mu}\, B_1 \\
B_{\mu\nu} &= p_{1\mu} p_{1\nu}\, B_{21} + g_{\mu\nu}\, B_{22}
\end{aligned}
$$

$$
\begin{aligned}
C_\mu &= p_{1\mu}\, C_{11} + p_{2\mu}\, C_{12} \\
C_{\mu\nu} &= p_{1\mu} p_{1\nu}\, C_{21} + p_{2\mu} p_{2\nu}\, C_{22} + \{p_1\, p_2\}_{\mu\nu}\, C_{23} + g_{\mu\nu}\, C_{24} \\
C_{\mu\nu\rho} &= p_{1\mu} p_{1\nu} p_{1\rho}\, C_{31} + p_{2\mu} p_{2\nu} p_{2\rho}\, C_{32} + \{p_1\, p_1\, p_2\}_{\mu\nu\rho}\, C_{33} \\
&\quad + \{p_1\, p_2\, p_2\}_{\mu\nu\rho}\, C_{34} + \{p_1\, g\}_{\mu\nu\rho}\, C_{35} + \{p_2\, g\}_{\mu\nu\rho}\, C_{36}
\end{aligned}
$$

$$
D_\mu = p_{1\mu}\, D_{11} + p_{2\mu}\, D_{12} + p_{3\mu}\, D_{13}
$$

$$
\begin{aligned}
D_{\mu\nu} &= p_{1\mu}p_{1\nu}\,D_{21} + p_{2\mu}p_{2\nu}\,D_{22} + p_{3\mu}p_{3\nu}\,D_{23} \\
&\quad + \{p_1\,p_2\}_{\mu\nu}\,D_{24} + \{p_1\,p_3\}_{\mu\nu}\,D_{25} + \{p_2\,p_3\}_{\mu\nu}\,D_{26} + g_{\mu\nu}\,D_{27} \\
D_{\mu\nu\rho} &= p_{1\mu}p_{1\nu}p_{1\rho}\,D_{31} + p_{2\mu}p_{2\nu}p_{2\rho}\,D_{32} + p_{3\mu}p_{3\nu}p_{3\rho}\,D_{33} \\
&\quad + \{p_1\,p_1\,p_2\}_{\mu\nu\rho}\,D_{34} + \{p_1\,p_1\,p_3\}_{\mu\nu\rho}\,D_{35} + \{p_1\,p_2\,p_2\}_{\mu\nu\rho}\,D_{36} \\
&\quad + \{p_1\,p_3\,p_3\}_{\mu\nu\rho}\,D_{37} + \{p_2\,p_2\,p_3\}_{\mu\nu\rho}\,D_{38} + \{p_2\,p_3\,p_3\}_{\mu\nu\rho}\,D_{39} \\
&\quad + \{p_1\,p_2\,p_3\}_{\mu\nu\rho}\,D_{310} + \{p_1\,g\}_{\mu\nu\rho}\,D_{311} + \{p_2\,g\}_{\mu\nu\rho}\,D_{312} + \{p_3\,g\}_{\mu\nu\rho}\,D_{313}\ ,
\end{aligned}
\tag{5.3}
$$

where we have introduced shorthand notations like

$$
\{p_i\,p_j\,p_k\}_{\mu\nu\rho} \equiv \sum_{\sigma(i,j,k)} p_{\sigma(i)\mu}\,p_{\sigma(j)\nu}\,p_{\sigma(k)\rho}\ , \tag{5.4}
$$

with $\sigma(i,j,k)$ denoting all different permutations of (i,j,k), and

$$
\{p_i\,g\}_{\mu\nu\rho} \equiv p_{i\mu}\,g_{\nu\rho} + p_{i\nu}\,g_{\mu\rho} + p_{i\rho}\,g_{\mu\nu}\ . \tag{5.5}
$$

The coefficients $B_{j(k)}, C_{jk}$ and $D_{jk(l)}$, a notation taken over from [9], denote scalar functions depending on all possible invariants and the masses M_i. To avoid obscuring any transparency all the arguments of the tensor integrals and the coefficients related to them have been dropped in the above decomposition.

Examining for instance the last expression of (5.3), the determination of the coefficients $D_{jk(l)}$ will in principle lead to a 13×13 matrix problem. This can however be reduced to a 3×3 matrix problem as will be explained and elaborated below.

Because it is often a question of taste whether the tensor integral decomposition will be of the form (5.3) or in terms of linear combinations of the momenta p_1, p_2 and p_3 (e.g. an orthogonal set), we will at this moment try to be as general as possible.

The first step in the process of pinpointing the relations linking the coefficients $D_{jk(l)}$ to the scalar integrals will be the introduction of some shorthand notations. To this end we will indicate the combination of external momenta occuring in the propagators D_i given in (5.2) by Q_i, so

$$
Q_1 = 0 \qquad \text{and} \qquad Q_i = \sum_{j=1}^{i-1} p_j \quad \text{for } i > 1\ .
$$

Now we can introduce

$$
B_{\{0,\mu,\mu\nu\}}(k,l) \equiv (2\pi\mu)^{4-n} \int \frac{d^n l}{i\pi^2} \frac{\{1,\, l_\mu,\, l_\mu l_\nu\}}{D_k D_l}\bigg|_{Q_k=0} \tag{5.6}
$$

$$
C_{\{0,\mu,\mu\nu,\mu\nu\rho\}}(k,l,m) \equiv (2\pi\mu)^{4-n} \int \frac{d^n l}{i\pi^2} \frac{\{1,\, l_\mu,\, l_\mu l_\nu,\, l_\mu l_\nu l_\rho\}}{D_k D_l D_m}\bigg|_{Q_k=0}\ , \tag{5.7}
$$

where $(k,l,m) \subset (1,2,3,4)$ is an ordered set, hence $k < l < m$. The denominators in the above definitions are the ones to be found in (5.2). Looking for instance at the 3-point tensor integrals (5.7) the definition in the case $(k,l,m) = (2,3,4)$ deviates from the other ones as a consequence of the non-trivial condition $Q_2 = 0$ in order to have it in a form corresponding to the tensor integral definitions (5.1). The coefficients originating from the above tensor integrals will consequently be written in the form $B_{ij}(k,l)$ or $C_{ij}(k,l,m)$ defined according to (5.3). The reason for introducing these specific 3- and 2-point tensor integrals is to be found in the fact that they constitute the integrals which remain after one respectively two of the denominators have been divided out in the 4-point tensor integrals. Now we need some tools to project on the various momenta and combinations of momenta and the metric tensor. As the main tool necessary to achieve this we introduce the projective momenta P_l^μ defined by :

$$P_l^\mu \, p_{i\mu} = \delta_{il} \qquad \text{for} \quad l = 1,2,3 \; . \tag{5.8}$$

The existence of these projective momenta is directly related to the existence of the inverse matrix to the matrix

$$X = \begin{pmatrix} p_1^2 & p_1.p_2 & p_1.p_3 \\ p_1.p_2 & p_2^2 & p_2.p_3 \\ p_1.p_3 & p_2.p_3 & p_3^2 \end{pmatrix} \; . \tag{5.9}$$

So, the P_l can be constructed if $\det X \neq 0$, which is equivalent to the statement that the P_l can be constructed if the 4-momenta p_1, p_2, p_3 form an independent set. The matrix X corresponds to the reduction of the D_μ tensor integral :

$$\begin{pmatrix} p_1^\mu \\ p_2^\mu \\ p_3^\mu \end{pmatrix} D_\mu = X \begin{pmatrix} D_{11} \\ D_{12} \\ D_{13} \end{pmatrix} = \begin{pmatrix} R_{20} \\ R_{21} \\ R_{22} \end{pmatrix} \; , \tag{5.10}$$

with

$$\begin{aligned} R_{20} &= \frac{1}{2}\left[C_0(1,3,4) - C_0(2,3,4) + f_1 D_0 \right] \\ R_{21} &= \frac{1}{2}\left[C_0(1,2,4) - C_0(1,3,4) + f_2 D_0 \right] \\ R_{22} &= \frac{1}{2}\left[C_0(1,2,3) - C_0(1,2,4) + f_3 D_0 \right] \end{aligned}$$

$$f_1 = M_2^2 - M_1^2 - Q_2^2 \;\; , \;\; f_2 = M_3^2 - M_2^2 - Q_3^2 + Q_2^2 \;\; , \;\; f_3 = M_4^2 - M_3^2 - Q_4^2 + Q_3^2 \; . \tag{5.11}$$

This can be seen easily by realizing for example

$$p_1^\mu \, D_\mu \;\; = \;\; (2\pi\mu)^{4-n} \int \frac{d^n l}{i\pi^2} \, \frac{p_1.l}{D_1 D_2 D_3 D_4} = (2\pi\mu)^{4-n} \int \frac{d^n l}{i\pi^2} \, \frac{\frac{1}{2}\left[D_2 - D_1 + f_1 \right]}{D_1 D_2 D_3 D_4} \; . \tag{5.12}$$

In the case of the reduction of $D_{\mu\nu}$ this 3×3 matrix structure is maintained by including the projective momenta P_l as follows :

$$
\begin{aligned}
P_1^\mu D_{\mu\nu} \begin{pmatrix} p_1^\nu \\ p_2^\nu \\ p_3^\nu \end{pmatrix} &= X \begin{pmatrix} D_{21} \\ D_{24} \\ D_{25} \end{pmatrix} + \begin{pmatrix} D_{27} \\ 0 \\ 0 \end{pmatrix} = \begin{pmatrix} R_{30} \\ R_{31} \\ R_{32} \end{pmatrix} \\
P_2^\mu D_{\mu\nu} \begin{pmatrix} p_1^\nu \\ p_2^\nu \\ p_3^\nu \end{pmatrix} &= X \begin{pmatrix} D_{24} \\ D_{22} \\ D_{26} \end{pmatrix} + \begin{pmatrix} 0 \\ D_{27} \\ 0 \end{pmatrix} = \begin{pmatrix} R_{33} \\ R_{34} \\ R_{35} \end{pmatrix} \\
P_3^\mu D_{\mu\nu} \begin{pmatrix} p_1^\nu \\ p_2^\nu \\ p_3^\nu \end{pmatrix} &= X \begin{pmatrix} D_{25} \\ D_{26} \\ D_{23} \end{pmatrix} + \begin{pmatrix} 0 \\ 0 \\ D_{27} \end{pmatrix} = \begin{pmatrix} R_{36} \\ R_{37} \\ R_{38} \end{pmatrix}
\end{aligned}
\tag{5.13}
$$

where the expressions R_{3i}, consisting of coefficients originating from the already known reduction of D_μ and 3-point coefficients, can be found in appendix G. The remaining coefficient D_{27}, appearing in the above matrix expressions, which corresponds to the $g_{\mu\nu}$ term in the reduction (5.3), can be obtained directly by introducing the projective tensor

$$
P^{\mu\nu} \equiv \frac{1}{n-3} \left\{ g^{\mu\nu} - \sum_{j=1}^{3} P_j^\mu \, p_j^\nu \right\} , \tag{5.14}
$$

which has the nice features

$$
p_{i\mu} \, P^{\mu\nu} = 0 \quad \text{and} \quad g_{\mu\nu} \, P^{\mu\nu} = 1 . \tag{5.15}
$$

In this way one arrives at $P^{\mu\nu} D_{\mu\nu} = D_{27}$ leading to an expression for D_{27}, consisting of terms also present in R_{2i} and R_{3i}, which can be found in appendix G.

The above described use of the first two projective operators shows the essence of the projective operator method :

1. the contractions between the tensor integrals and the momenta p_1, p_2, p_3 or the metric tensor $g^{\mu\nu}$ are needed in order to get rid of one of the propagators, leading to tensor integrals of a lower-point type, or in order to reduce the rank of the tensor integral by one.

2. the projective operators, which need not be known explicitly in terms of the external momenta, are needed for the handling of the algebra, maintaining the most compact problem casting as possible.

We can now extend this recipe to the determination of the coefficients originating from the decomposition of $D_{\mu\nu\rho}$ as given in (5.3). Once again new projective tensors are indispensible to maintain the mere 3×3 matrix structure as compared to the

expected 13 × 13 matrix problem. First a projective tensor is needed which is in fact complementary to $P^{\mu\nu}$:

$$P^{\mu\nu}_{k,l} = P^{\mu}_{k}\, P^{\nu}_{l} - (P_k.P_l)\, P^{\mu\nu} \;, \tag{5.16}$$

which has the properties

$$P^{\mu\nu}_{k,l}\, g_{\mu\nu} = 0 \quad \text{and} \quad p_{i\mu}\, P^{\mu\nu}_{k,l}\, p_{j\nu} = \delta_{ik}\, \delta_{jl} \;. \tag{5.17}$$

This leads to the following set of matrix identities :

$$\begin{aligned}
P^{\mu\nu}_{1,1} D_{\mu\nu\rho} \begin{pmatrix} p^{\rho}_1 \\ p^{\rho}_2 \\ p^{\rho}_3 \end{pmatrix} &= X \begin{pmatrix} D_{31} \\ D_{34} \\ D_{35} \end{pmatrix} + \begin{pmatrix} 2D_{311} \\ 0 \\ 0 \end{pmatrix} = \begin{pmatrix} R_{43} \\ R_{44} \\ R_{45} \end{pmatrix} \\
P^{\mu\nu}_{2,2} D_{\mu\nu\rho} \begin{pmatrix} p^{\rho}_1 \\ p^{\rho}_2 \\ p^{\rho}_3 \end{pmatrix} &= X \begin{pmatrix} D_{36} \\ D_{32} \\ D_{38} \end{pmatrix} + \begin{pmatrix} 0 \\ 2D_{312} \\ 0 \end{pmatrix} = \begin{pmatrix} R_{46} \\ R_{47} \\ R_{48} \end{pmatrix} \\
P^{\mu\nu}_{3,3} D_{\mu\nu\rho} \begin{pmatrix} p^{\rho}_1 \\ p^{\rho}_2 \\ p^{\rho}_3 \end{pmatrix} &= X \begin{pmatrix} D_{37} \\ D_{39} \\ D_{33} \end{pmatrix} + \begin{pmatrix} 0 \\ 0 \\ 2D_{313} \end{pmatrix} = \begin{pmatrix} R_{49} \\ R_{50} \\ R_{51} \end{pmatrix} \\
P^{\mu\nu}_{2,1} D_{\mu\nu\rho} \begin{pmatrix} p^{\rho}_1 \\ p^{\rho}_2 \\ p^{\rho}_3 \end{pmatrix} &= X \begin{pmatrix} D_{34} \\ D_{36} \\ D_{310} \end{pmatrix} + \begin{pmatrix} D_{312} \\ D_{311} \\ 0 \end{pmatrix} = \begin{pmatrix} R_{52} \\ R_{53} \\ R_{54} \end{pmatrix} \;.
\end{aligned} \tag{5.18}$$

For explicit expressions for R_{4i} and R_{5i} we refer once again to appendix G. The second projective tensor will be needed for coefficients corresponding to the terms in the decomposition (5.3) containing the metric tensor $g_{\mu\nu}$:

$$P^{\mu\nu\rho}_{l} = p^{\mu}_{l}\, P^{\nu\rho} \;, \tag{5.19}$$

with the features

$$P^{\mu\nu\rho}_{i}\, g_{\mu\nu}\, p_{i\rho} = P^{\mu\nu\rho}_{l}\, g_{\mu\rho}\, p_{i\nu} = 0 \quad \text{and} \quad P^{\mu\nu\rho}_{l}\, g_{\nu\rho}\, p_{i\mu} = p_l.p_i \;. \tag{5.20}$$

This automatically yields

$$\begin{pmatrix} P^{\mu\nu\rho}_{1} \\ P^{\mu\nu\rho}_{2} \\ P^{\mu\nu\rho}_{3} \end{pmatrix} D_{\mu\nu\rho} = X \begin{pmatrix} D_{311} \\ D_{312} \\ D_{313} \end{pmatrix} \;. \tag{5.21}$$

The same kind of procedure can be adopted for the 2- and 3-point tensor integrals. As (5.6) and (5.7) cast them in a similar form compared to the 4-point tensor integrals, leading to a reduction in terms of just one respectively two of the three

momenta p_1, p_2, p_3, the corresponding projective operators can be deduced from the ones mentioned above. For simplicity sake we will take the one respectively two reduction momenta to be p_1 and p_1, p_2. The specific set of projective operators will be identical to the ones given above with just one replacement to be implemented in all projective tensor definitions :

$$P^{\mu\nu} \equiv \frac{1}{n-d+1} \left\{ g_{\mu\nu} - \sum_{j=1}^{d-1} P_j^\mu \, p_j^\nu \right\} , \tag{5.22}$$

where d denotes the number of propagators occurring in the denominator of the tensor integral. In the 3-point case for example this allows for a 2×2 matrix formulation of the C-coefficients appearing in (5.3). The results obtained by applying these projective operators can be found in appendix G. Because of the presence of UV divergences in case the number of integration momenta in the numerator exceeds $2d-5$, the n-dimensional treatment of the 2- and 3-point tensor integrals is unavoidable, even when we would restrict ourselves to integrals appearing in pure electroweak calculations.

It should be noted that the projective operators as given above take on particularly transparent forms in case one decides to work with an orthogonal basic momentum set k_1, k_2, k_3, being linear combinations of the momenta p_1, p_2 and p_3, and with the metric tensor $g_{\mu\nu}$ replaced by the projective operator $K^{\mu\nu}$ derived from (5.22). If we use these 4 objects to construct the Lorentz structures appearing in (5.3) the following self projective scheme can be derived :

- for the reduction of the d-point tensor integrals ($d = 2, 3$ or 4), as given by (5.1) with p_i replaced by k_i, we can instantly use the projective operators derived from (5.8) :

$$K_l^\mu = \frac{k_l^\mu}{k_l^2} \quad \text{for} \quad l = 1, \cdots, d-1 \quad , \tag{5.23}$$

which project on the momenta k_i according to $K_l^\mu \, k_{i\mu} = \delta_{li}$. They can be used to project on any string of external momenta appearing in (5.3) by just combining the corresponding projective momenta to form an analogous string. This is a consequence of the fact that $g^{\mu\nu}$ has been replaced by $K^{\mu\nu}$. The condition $\det X \neq 0$ as appearing in the general case ensures that none of the momenta k_i are lightlike ($k_i^2 = 0$) and hence that the above projective operators exist. In general it involves application of a diagonalization procedure to the matrix X in order to arrive at an orthogonal momentum set. In the case of massless theories however, like for instance QCD, an orthogonal set is a natural approach. Consider for example a 2- to 2-body process with lightlike external momenta $p_1, \cdots, p_4$, then the linear combinations $p_1 + p_2$, $p_1 + p_3$ and $p_2 + p_3$ will form an orthogonal set as a consequence of momentum conservation.

- for the determination of coefficients corresponding to Lorentz structures containing the metric tensor replacement $K^{\mu\nu}$ we can apply this very operator $K^{\mu\nu}$ as derived from (5.22) :

$$K^{\mu\nu} \equiv \frac{1}{n-d+1} \left\{ g^{\mu\nu} - \sum_{j=1}^{d-1} \frac{k_j^\mu k_j^\nu}{k_j^2} \right\} . \tag{5.24}$$

Because of the symmetric form of $K^{\mu\nu}$ its projective nature is extended to

$$k_{i\mu} K^{\mu\nu} = K^{\mu\nu} k_{i\nu} = 0 \quad \text{and} \quad (n-d+1) K^{\mu\nu} K_{\mu\nu} = 1 . \tag{5.25}$$

This reveals the self projective nature of the 4 objects we have decided upon above. One is now able to project on strings containing one $K_{\mu\nu}$ tensor and any set of external momenta, as appearing in the reduction of tensor integrals of rank>2, by combining the corresponding projective tensor and projective momenta in the same way. For example, $(n-d+1) K^{\mu\nu} K_i^\rho$ projects on the corresponding string $K_{\mu\nu} k_{i\rho}$ and hence on the symmetric reduction Lorentz structure $\{k_i K\}_{\mu\nu\rho}$.

As an example of the use of such an orthogonal approach in the framework of the EWRC calculations we will investigate how the IR-divergent scalar integrals of the last section appear when tensor structures corresponding to the 4-point integral (4.1) are under consideration. So, we will restrict ourselves to a 4-dimensional treatment of the 4-point tensor integrals of (5.1), with the supplementary conditions $M_1 = \lambda$, $M_2 = m_1$, $M_3 = m_0$, $M_4 = m_4$ and $p_i^2 = m_i^2$. First we will discuss some general features of how the IR-divergent scalar 3- and 4-point integrals enter the tensor integral reduction. In case of just one source of IR divergences these divergences will have their origin in that part of the integration region where the 4-momentum of the photon becomes zero. In our example this corresponds to $l \to 0$ which automatically leads to the conclusion that the coefficients given in (5.3) will be IR-finite. So, we can conclude that the IR-divergent scalar integrals enter the reduction in the form of the IR-finite combination $(t-m_0^2)\, D_0 - C_0(1,2,4)$, where the first integral can be taken from (4.22) or (4.23) and the second one from (4.28) or (4.29). In order to find the Lorentz structure accompanying this IR-finite combination we will have to construct a momentum set that projects on the scalar 4-point integral. This is achieved by introducing

$$\begin{aligned} k_+ &\equiv p_1 + \frac{m_1}{m_4} p_4 \quad , \quad k_- \equiv p_1 - \frac{m_1}{m_4} p_4 \\ k_0 &\equiv p_2 - \left(\frac{p_2.k_+}{k_+^2} \right) k_+ - \left(\frac{p_2.k_-}{k_-^2} \right) k_- , \end{aligned} \tag{5.26}$$

which constitutes an orthogonal momentum set (k_+, k_-, k_0) with corresponding projective operators. The momentum k_0 is the one that enables us to project on the

scalar 4-point integral because of the following properties :

$$
\begin{aligned}
k_+.l &= \frac{1}{2}\left\{D_2 - D_1 - \frac{m_1}{m_4}\left[D_4 - D_1\right]\right\} \\
k_-.l &= \frac{1}{2}\left\{D_2 - D_1 + \frac{m_1}{m_4}\left[D_4 - D_1\right]\right\} \\
k_0.l &= \frac{1}{2}\left\{D_3 - D_2 - \left[t - m_0^2\right]\right\} - \left(\frac{p_2.k_+}{k_+^2}\right) k_+.l - \left(\frac{p_2.k_-}{k_-^2}\right) k_-.l \\
g^{\mu\nu}\, l_\mu l_\nu &= l^2 = D_1 \ , \qquad (5.27)
\end{aligned}
$$

where λ has been neglected whenever possible. The only term in (5.27) not leading to a reduction of the number of propagators D_i $(i = 1, \cdots, 4)$ by one is the $-\frac{1}{2}\left[t - m_0^2\right]$ term originating from $p_2.l$. So, the only possibility of arriving at an expression containing D_0 is offered by those projective operators that contain terms only consisting of k_0. They are given by :

- $K_0^\mu = \frac{k_0^\mu}{k_0^2}$ to be used in the reduction of D_μ
- $K^{\mu\nu} \to -\frac{k_0^\mu k_0^\nu}{k_0^2}$ to be used in the reduction of $D_{\mu\nu}$
- $K_0^\mu\, K_0^\nu = \frac{k_0^\mu k_0^\nu}{k_0^4}$ to be used in the reduction of $D_{\mu\nu}$
- $K_0^\mu\, K^{\nu\rho} \to -\frac{k_0^\mu k_0^\nu k_0^\rho}{k_0^4}$ to be used in the reduction of $D_{\mu\nu\rho}$
- $K_0^\mu\, K_0^\nu\, K_0^\rho = \frac{k_0^\mu k_0^\nu k_0^\rho}{k_0^6}$ to be used in the reduction of $D_{\mu\nu\rho}$.

Introducing the shorthand notation for the IR-finite combination of the scalar 3- and 4-point integrals with one source of IR divergences

$$
D_{(1)}^{IR-finite} = (t - m_0^2)\, D_0 - C_0(1,2,4) \qquad (5.28)
$$

the above projective operators result in the following reductions :

$$
\begin{aligned}
D^\mu &\to -\left(\frac{k_0^\mu}{2\, k_0^2}\right) D_{(1)}^{IR-finite} \\
D^{\mu\nu} &\to -\left(\frac{k_0^2 K^{\mu\nu} - k_0^\mu k_0^\nu}{4\, k_0^4}\right) (t - m_0^2)\, D_{(1)}^{IR-finite} \\
D^{\mu\nu\rho} &\to +\left(\frac{k_0^2\, \{k_0\, K\}^{\mu\nu\rho} - k_0^\mu k_0^\nu k_0^\rho}{8\, k_0^6}\right) (t - m_0^2)^2\, D_{(1)}^{IR-finite} \ . \qquad (5.29)
\end{aligned}
$$

We can easily extend this procedure to the case of two sources of IR divergences : $m_0 = \lambda$, $m_1 = m_2$ and $m_4 = m_3$. The second part of the integration region

leading to the supplementary IR-divergent behaviour corresponds to the limit $l \to -p_1 - p_2 = -Q_3$, whereas the IR-finite combination

$$D_{(2)}^{IR-finite} = t\, D_0 - 2\, C_0(1,2,4) \tag{5.30}$$

will represent the finite contribution of the integrals (4.24) or (4.25) and (4.28) or (4.29). Using the above approach, while at the same time bearing in mind that the limit $l \to -Q_3$ will render the IR-divergent content of the tensor integrals, we arrive at :

$$\begin{aligned}
D^{\mu} &\to -Q_3^{\mu}\,\frac{C_0(1,2,4)}{t} - \left(\frac{k_0^{\mu}}{2\,k_0^2}\right) D_{(2)}^{IR-finite} \\
D^{\mu\nu} &\to Q_3^{\mu}\,Q_3^{\nu}\,\frac{C_0(1,2,4)}{t} - \left(\frac{k_0^2 K^{\mu\nu} - k_0^{\mu}k_0^{\nu}}{4\,k_0^4}\right) t\, D_{(2)}^{IR-finite} \\
D^{\mu\nu\rho} &\to -Q_3^{\mu}\,Q_3^{\nu}\,Q_3^{\rho}\,\frac{C_0(1,2,4)}{t} + \left(\frac{k_0^2\,\{k_0\,K\}^{\mu\nu\rho} - k_0^{\mu}k_0^{\nu}k_0^{\rho}}{8\,k_0^6}\right) t^2\, D_{(2)}^{IR-finite}\,.
\end{aligned} \tag{5.31}$$

This shows how in an elegant way, without any brute force, information about the occurrence of IR-divergent scalar 3- and 4-point integrals in the reduction of tensor integrals can be obtained by application of some simple projective methods.

References

[1] G. 't Hooft and M. Veltman, "Diagrammar" in "Particle Interactions at Very High Energies", Summer Institute on Elementary Particle Physics, Leuven 1973, eds. D. Speiser, F. Halzen, J. Weyers, Plenum Press, London 1974.

[2] G. Kallén, Helv. Phys. Acta **25** (1952) 417;
H. Lehmann, Nuovo Cimento **11** (1954) 342.

[3] R.J. Eden, P.V. Landshoff, D.I. Olive and J.C. Polkinghorne, "The Analytic S-Matrix", Cambridge Univ. Press 1966.

[4] J.D. Bjorken and S.D. Drell, "Relativistic Quantum Fields", McGraw-Hill, New York 1965.

[5] G. 't Hooft and M. Veltman, Nucl. Phys. **B153** (1979) 365.

[6] T. Sack, Ph.D. Thesis, Würzburg 1987.

[7] M. Böhm, A. Denner, T. Sack, W. Beenakker, F. Berends and H. Kuijf, Nucl. Phys. **B304** (1988) 463.

[8] W. Beenakker and A. Denner, Leiden Preprint 1988,
to be published in Nucl. Phys. **B**.

[9] G. Passarino and M. Veltman, Nucl. Phys. **B160** (1979) 151.

Chapter IV

Fermion pair production from e^+e^- annihilation

1 Introduction

In this chapter we will discuss the various aspects of the production of light as well as heavy fermions from e^+e^- collisions being the most important set of processes to give information about Z gauge boson related quantities. Via the examination of the Z resonance valuable information is gained concerning the Z mass and width [1,2], whereas various on-resonance asymmetries will provide us with strong tests of the electroweak standard model at the quantum level as well as high precision quantities necessary for probing the unknown model parameters M_H, m_i and the possibility of theoretical concepts lying beyond the restricted area of the electroweak standard model [3,4]. To this end much care has to be taken with the implementation of the EWRC effects and polarization of the $e^\pm$ beams. The specific division into light and heavy fermion production as mentioned above has its origin in the fact that the presence of light final state fermions allows for a much more transparent treatment of the EWRC effects [5], as we will neglect the corresponding small masses (compared to for instance the CM energy or $M_{W,Z}$) in the EWRC effects whenever possible. So, in order to keep things as compact as possible we will show explicit light fermion expressions whenever it makes sense to do so. The heavy final state fermions will be indicated by

$$f_H \quad : \quad \text{consisting of the top quark and maybe further generations of quarks and charged leptons} \tag{1.1}$$

and the light final state fermions by

$$f_L \quad : \quad \text{consisting of the remaining quarks and leptons, except the electron and its neutrino .} \tag{1.2}$$

The reason for leaving out the electron and its neutrino from the list of possible final state fermions is to be found in the fact that they lead to process characteristics deviating from the ones corresponding to the other final state fermions. This is caused by the fact that in addition t-channel exchange contributions corresponding to the scattering process have to be included when final state fermions are involved originating from the same fermion doublet as the initial state fermions ($e^{\pm}$). Furthermore the EWRC effects on e^+e^- and $\nu_e\bar{\nu}_e$ production processes have already been discussed extensively in the literature [6,7]. It should be noted that the pure annihilation process in those cases will be covered like the other fermionic final state processes by the following discussions.

2 Conventions and Born cross sections

In this section we want to set up our notation and give some general structures necessary to present the matrix elements. Further we will give some lowest order (Born) results for the differential as well as total cross sections and for some on-resonance asymmetries. This will involve the incorporation of the possibility of longitudinal $e^{\pm}$ beam polarization. As far as possible we will neglect and hence omit the electron mass m_e. In general we will refer to the fermion pair production process from e^+e^- annihilation as $e^+e^- \to f\bar{f}$, whereas in special cases we will explicitly indicate whether we are dealing with light (f_L) or heavy (f_H) final state particles. The 4-momenta and helicities (by definition ± 1) of the initial state (incoming) electron and positron are denoted by p_-, κ_- and p_+, κ_+ respectively, while we will use q, η and $\bar{q}, \bar{\eta}$ for the final state (outgoing) fermions f and $\bar{f}$. The masses of the corresponding particles will be indicated by m_e and m_f. As we will only be concerned with 2-particle final state cross sections in the forthcoming evaluations the following standard set of Mandelstam variables will be used :

$$\begin{aligned} s &= (p_+ + p_-)^2 = (q + \bar{q})^2 \\ t &= (p_+ - \bar{q})^2 = (p_- - q)^2 \\ u &= (p_+ - q)^2 = (p_- - \bar{q})^2 \,. \end{aligned} \tag{2.1}$$

In the CM system of the electron-positron pair we will adopt the following conventions valid for the 2-particle final state processes :

$$p_{\pm} = (E, 0, 0, \mp E)$$

$$q = (E, E\beta \sin\theta, 0, E\beta\cos\theta) \quad , \quad \bar{q} = (E, -E\beta\sin\theta, 0, -E\beta\cos\theta)$$

$\beta = \sqrt{1 - m_f^2/E^2}$: the final state fermion velocity

$$\theta = \angle(e^-, f) \ : \text{the scattering angle} \tag{2.2}$$

and hence we can rewrite the standard set of Mandelstam variables (2.1) in the CM system as follows :

$$\begin{aligned} s &= 4E^2 \\ \beta &= \sqrt{1 - 4m_f^2/s} \\ t &= m_f^2 - \frac{s}{2}(1 - \beta\cos\theta) \\ u &= m_f^2 - \frac{s}{2}(1 + \beta\cos\theta) \ . \end{aligned} \tag{2.3}$$

Because of the fact that the electron and positron are essentially massless as compared to the beam energy E, except when the before mentioned 'mass singularities' come into play, the matrix element for the process $e^+e^- \to f\bar{f}$ will vanish in case e^- and e^+ have equal helicities, as enforced by the presence of initial state chiral symmetry. This allows for the following notation for the 2-particle final state helicity amplitudes :

$$M(\kappa_+, \kappa_-; \eta, \bar{\eta}; s, t) = M(\kappa; \eta, \bar{\eta}; s, t) \ , \tag{2.4}$$

with

$$\kappa = \kappa_- = -\kappa_+ \ . \tag{2.5}$$

We have chosen our normalization such that M is related in the CM system to the differential cross section per initial state helicity via

$$\frac{d\sigma}{d\Omega}(\kappa; s, \cos\theta) = \frac{\alpha^2}{4s} N_c^f \beta \sum_{\eta,\bar{\eta}} |M(\kappa; \eta, \bar{\eta}; s, t)|^2 \ . \tag{2.6}$$

The colour factor

$$N_c^f = \begin{cases} 1 & \text{if f=lepton} \\ 3 & \text{if f=quark} \end{cases} \tag{2.7}$$

distinguishes quark and lepton final states with respect to their colour content. The general helicity amplitude (2.4) covering Born as well as higher order contributions can be decomposed, when we restrict ourselves to Born and first order contributions, into a set of 4 basic helicity amplitudes $M_i^{\rho\kappa}$ and corresponding form factors $L_i^{\rho\kappa}$, containing all gauge group details, according to :

$$M(\kappa; \eta, \bar{\eta}; s, t) = \sum_{i=1}^{4} \sum_{\rho=\pm 1} M_i^{\rho\kappa} L_i^{\rho\kappa} \ , \tag{2.8}$$

with the basic helicity amplitudes

$$
\begin{aligned}
M_1^{\rho\kappa} &= [\bar{u}_f(q)\,\gamma^\mu \omega_\rho\, v_f(\bar{q})]\,[\bar{v}_e(p_+)\,\gamma_\mu \omega_\kappa\, u_e(p_-)] \\
M_2^{\rho\kappa} &= [\bar{u}_f(q)\,\not{p}_+ \omega_\rho\, v_f(\bar{q})]\,[\bar{v}_e(p_+)\,\frac{1}{2}(\not{q}-\not{\bar{q}})\omega_\kappa\, u_e(p_-)] \\
M_3^{\rho\kappa} &= [\bar{u}_f(q)\,\omega_\rho\, v_f(\bar{q})]\,[\bar{v}_e(p_+)\,\frac{1}{2}(\not{q}-\not{\bar{q}})\omega_\kappa\, u_e(p_-)] \\
M_4^{\rho\kappa} &= [\bar{u}_f(q)\,\gamma^\mu \not{p}_+ \omega_\rho\, v_f(\bar{q})]\,[\bar{v}_e(p_+)\,\gamma_\mu \omega_\kappa\, u_e(p_-)]\,,
\end{aligned}
\tag{2.9}
$$

where we have suppressed the final state helicities $\eta, \bar{\eta}$ as they will be summed anyhow. It should be noted that no summation is and from now on will be intended when helicity related indices (like κ, ρ) are repeated. In the above basic helicity amplitude set we have used the chiral projectors

$$
\omega_\lambda = \frac{1+\lambda\gamma_5}{2} \quad , \quad \lambda = \pm 1\,. \tag{2.10}
$$

For the initial state $e^\pm$ these chiral projectors also are projectors on helicity states because $s \gg m_e^2$, whereas due to the possibility of finite masses for the final state fermions the quantity λ in (2.10) does not necessarily coincide with the f or $\bar{f}$ helicity. In case we are dealing with for example final state muons, with negligible mass compared to the beam energy E, the parameter ρ corresponds to the helicity η of the muon.

In lowest order the γ- and Z-exchange diagrams of fig. 1 contribute. Higgs bo-

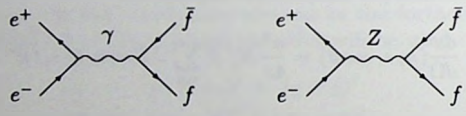

Fig. 1. γ and Z exchange Born diagrams

son exchange is neglected since it is suppressed by a factor $\frac{m_e}{M_W}$ originating from the Yukawa coupling between electrons and the Higgs bosons. Applying the decomposition (2.8) only the first basic helicity amplitude is present in the Born approximation :

$$
M^{(0)}(\kappa;\eta,\bar{\eta};s,t) = \sum_\rho M_1^{\rho\kappa} L_1^{(0)\,\rho\kappa}\,, \tag{2.11}
$$

with

$$
L_1^{(0)\,\rho\kappa} = \frac{Q_e Q_f}{s} + g_e^\kappa g_f^\rho\, \frac{\chi_Z^{(0)}(s)}{s}\,. \tag{2.12}
$$

This involves besides the charge fractions $Q_{e,f}$ the left and right handed coupling constants of the fermions to the Z gauge boson

$$g^{-}_{e,f} = \frac{I^{e,f}_3 - s^2_w Q_{e,f}}{s_w c_w} \quad , \quad g^{+}_{e,f} = -Q_{e,f}\frac{s_w}{c_w} \tag{2.13}$$

and the lowest order Z propagator function

$$\chi^{(0)}_Z(s) = \frac{s}{s - M^2_Z + iM_Z\Gamma^0_Z} \, , \tag{2.14}$$

containing the tree level width Γ^0_Z (see section 4) which can be written as a sum over all partial fermionic decay widths $\Gamma^0_Z(f\bar{f})$ for $m_f < M_Z/2$:

$$\Gamma^0_Z = \sum_f \Gamma^0_Z(f\bar{f}) \, . \tag{2.15}$$

As soon as we are going to include 1-loop corrections to the Born matrix element, constituting part of the EWRC effects, we have to take into account the interference of (2.11) with the first order contribution $M^{(1)}(\kappa;\eta,\bar{\eta};s,t)$. As long as we are not interested in final state polarizations we have to sum them, leading to a first order contribution of the form

$$2\,\mathrm{Re}\left[\sum_{\eta,\bar{\eta}} M^{(1)}(\kappa;\eta,\bar{\eta};s,t)\, M^{(0)\,*}(\kappa;\eta,\bar{\eta};s,t)\right] \tag{2.16}$$

appearing in the calculation of the differential cross section (2.6) with definite initial state helicities. For unpolarized beams we have to average over the initial state electron and positron helicities :

$$\frac{d\sigma}{d\Omega}(s,\cos\theta) = \frac{1}{4}\left[\frac{d\sigma}{d\Omega}(+;s,\cos\theta) + \frac{d\sigma}{d\Omega}(-;s,\cos\theta)\right] \, . \tag{2.17}$$

The interference (2.16) of the Born helicity amplitude with the first order one can be evaluated in terms of the interferences of the basic helicity amplitudes (2.9) with the one appearing in the Born approximation (2.11) :

$$\sum_{\eta,\bar{\eta}} M^{\rho\kappa}_i \left(M^{\rho'\kappa}_1\right)^* \tag{2.18}$$

to be found in appendix H.

Introducing the vector and axial vector couplings

$$v_{e,f} = \frac{1}{2}\left(g^{+}_{e,f} + g^{-}_{e,f}\right) \quad , \quad a_{e,f} = \frac{1}{2}\left(g^{-}_{e,f} - g^{+}_{e,f}\right) \tag{2.19}$$

the result for the longitudinally polarized initial state Born cross section in the CM system can be written in the following way (without neglecting m_f) :

$$\begin{aligned}\frac{d\sigma}{d\Omega}^{(0)}(\kappa;s,\cos\theta) &= \frac{\alpha^2}{4s}N_c^f\beta\left\{\left([1+\kappa^2]\,G_1(s)-2\kappa\,H_1(s)\right)(1+\cos^2\theta)\right.\\ &+\left([1+\kappa^2]\,G_2(s)-2\kappa\,H_2(s)\right)\frac{4m_f^2}{s}\sin^2\theta\\ &+\left.\left([1+\kappa^2]\,G_3(s)-2\kappa\,H_3(s)\right)2\beta\cos\theta\right\}. \quad (2.20)\end{aligned}$$

The functions $G_i(s)$ and $H_i(s)$ are given by :

$$\begin{aligned}G_1(s) &= Q_e^2Q_f^2+2v_ev_fQ_eQ_f\,\mathrm{Re}\,\chi_Z^{(0)}(s)+(v_e^2+a_e^2)(v_f^2+\beta^2a_f^2)\,|\chi_Z^{(0)}(s)|^2\\ G_2(s) &= Q_e^2Q_f^2+2v_ev_fQ_eQ_f\,\mathrm{Re}\,\chi_Z^{(0)}(s)+(v_e^2+a_e^2)v_f^2\,|\chi_Z^{(0)}(s)|^2\\ G_3(s) &= 2a_ea_fQ_eQ_f\,\mathrm{Re}\,\chi_Z^{(0)}(s)+4v_ea_ev_fa_f\,|\chi_Z^{(0)}(s)|^2\\ H_1(s) &= 2a_ev_fQ_eQ_f\,\mathrm{Re}\,\chi_Z^{(0)}(s)+2v_ea_e(v_f^2+\beta^2a_f^2)\,|\chi_Z^{(0)}(s)|^2\\ H_2(s) &= 2a_ev_fQ_eQ_f\,\mathrm{Re}\,\chi_Z^{(0)}(s)+2v_ea_ev_f^2\,|\chi_Z^{(0)}(s)|^2\\ H_3(s) &= 2v_ea_fQ_eQ_f\,\mathrm{Re}\,\chi_Z^{(0)}(s)+2(v_e^2+a_e^2)v_fa_f\,|\chi_Z^{(0)}(s)|^2\,. \quad (2.21)\end{aligned}$$

Consequently the differential Born cross section for unpolarized initial state electrons and positrons will only contain the $G_i(s)$:

$$\begin{aligned}\frac{d\sigma}{d\Omega}^{(0)}(s,\cos\theta) &= \frac{1}{4}\left[\frac{d\sigma}{d\Omega}^{(0)}(+;s,\cos\theta)+\frac{d\sigma}{d\Omega}^{(0)}(-;s,\cos\theta)\right]\\ &= \frac{\alpha^2}{4s}N_c^f\beta\left\{G_1(s)(1+\cos^2\theta)+\frac{4m_f^2}{s}G_2(s)\sin^2\theta+2\,G_3(s)\,\beta\cos\theta\right\}. \quad (2.22)\end{aligned}$$

As a preparation to the forthcoming calculations of total cross sections and on-resonance asymmetries we are led to define a couple of shorthand notations :

- σ^F will denote the forward cross section :

$$\sigma^F \equiv \int_{\theta<\pi/2} d\Omega\,\frac{d\sigma}{d\Omega}(s,\cos\theta)$$

- σ^B will denote the backward cross section :

$$\sigma^B \equiv \int_{\theta>\pi/2} d\Omega\,\frac{d\sigma}{d\Omega}(s,\cos\theta)$$

- σ_L, σ_L^F and σ_L^B will denote the longitudinally polarized total, forward and backward cross sections for left handed ($\kappa=-$) electrons

- σ_R, σ_R^F and σ_R^B will denote the longitudinally polarized total, forward and backward cross sections for right handed ($\kappa = +$) electrons
- σ_0 will denote the pointlike muon cross section :

$$\sigma_0 = \sigma_0(e^+e^- \to \gamma^* \to \mu^+\mu^-) = \frac{4\pi\alpha^2}{3s} .$$

Using these notations and (2.20) or (2.22) we can write :

$$\sigma^{(0)}(e^+e^- \to f\bar{f}) = \sigma_0 N_c^f \beta \left(G_1(s) + \frac{2m_f^2}{s} G_2(s) \right) \tag{2.23}$$

$$\sigma_{L/R}^{(0)}(e^+e^- \to f\bar{f}) = 2\sigma_0 N_c^f \beta \left(G_1(s) +/- H_1(s) + \frac{2m_f^2}{s} [G_2(s) +/- H_2(s)] \right) . \tag{2.24}$$

There are three on-resonance asymmetries to be considered (neglecting higher order terms proportional to $[\Gamma_Z^0/M_Z]^2$) :

1. the unpolarized forward-backward (FB) asymmetries, sometimes referred to as the charge asymmetries,

$$A_{FB}^{(0)}(e^+e^- \to f\bar{f}) = \frac{\sigma^F - \sigma^B}{\sigma^F + \sigma^B} \overset{s=M_Z^2}{=\!=} \frac{3}{4}\beta_Z \frac{G_3(M_Z^2)}{G_1(M_Z^2) + \frac{2m_f^2}{M_Z^2} G_2(M_Z^2)}$$

$$\approx \frac{3}{4}\beta_Z \left(\frac{2v_e a_e}{v_e^2 + a_e^2} \right) \left(\frac{2v_f a_f}{v_f^2 (1 + \frac{2m_f^2}{M_Z^2}) + \beta_Z^2 a_f^2} \right) , \tag{2.25}$$

where β_Z denotes the on-resonance final state fermion velocity.

2. the left-right (LR) asymmetries

$$A_{LR}^{(0)}(e^+e^- \to f\bar{f}) = \frac{\sigma_L - \sigma_R}{\sigma_L + \sigma_R} \overset{s=M_Z^2}{=\!=} \frac{H_1(M_Z^2) + \frac{2m_f^2}{M_Z^2} H_2(M_Z^2)}{G_1(M_Z^2) + \frac{2m_f^2}{M_Z^2} G_2(M_Z^2)}$$

$$\approx \frac{2v_e a_e}{v_e^2 + a_e^2} \tag{2.26}$$

3. the polarized forward-backward (FBpol) asymmetries

$$A_{FB}^{pol\ (0)}(e^+e^- \to f\bar{f}) = \frac{\sigma_L^F - \sigma_L^B - [\sigma_R^F - \sigma_R^B]}{\sigma_L^F + \sigma_L^B + \sigma_R^F + \sigma_R^B}$$

$$\overset{s=M_Z^2}{=\!=} \frac{3}{4}\beta_Z \frac{H_3(M_Z^2)}{G_1(M_Z^2) + \frac{2m_f^2}{M_Z^2} G_2(M_Z^2)} \approx \frac{3}{4}\beta_Z \frac{2v_f a_f}{v_f^2 (1 + \frac{2m_f^2}{M_Z^2}) + \beta_Z^2 a_f^2} . \tag{2.27}$$

In this way one gets information about two things: first of all the above asymmetries will shed some light on the question of universality of the fermion couplings to the Z gauge boson, whether fermions with the same isospin and charge couple in the same way, and secondly assuming that very universality as a result of the standard model concepts information is gained on $\sin^2\theta_w$. This last aspect is a consequence of the fact that the above asymmetries can be rewritten in terms of the quantities

$$\begin{aligned} A_f &\equiv \beta_Z \frac{2v_f a_f}{v_f^2(1+\frac{2m_f^2}{M_Z^2})+\beta_Z^2 a_f^2} \\ &= \beta_Z \frac{2(1-4s_w^2|Q_f|)}{\beta_Z^2+(1+\frac{2m_f^2}{M_Z^2})(1-4s_w^2|Q_f|)^2} , \end{aligned} \tag{2.28}$$

which leads in case of light final state fermions f_L to the following compact solely $\sin^2\theta_w$ depending form :

$$A_{f_L} = \frac{2v_{f_L}a_{f_L}}{v_{f_L}^2+a_{f_L}^2} = \frac{2(1-4s_w^2|Q_{f_L}|)}{1+(1-4s_w^2|Q_{f_L}|)^2} . \tag{2.29}$$

Even at this point we are getting some insight in the reason why the on-resonance A_{LR} is so very well suited for probing the standard model and what is lying beyond. The fact that the on-resonance A_{LR} is almost independent of the final state fermion specifications (at least at Born level) allows for an inclusive measurement, which means that we will not lose any statistics by having to identify the specific fermions in the final state. A property which starts to vanish when off-resonance s values are considered.

3 Electroweak radiative corrections

3.1 General framework

Since we can neglect the Higgs boson exchange contribution, being suppressed by a factor $\frac{m_e}{M_W}$, our sample of electroweak radiative corrections to $e^+e^- \to f\bar{f}$ consists of the γ and Z propagator corrections, the γ- and Z-fermion vertex corrections, the box contributions involving 2 gauge boson exchange and the real photon bremsstrahlung contributions. We can divide those EWRC effects, contributing terms of $\mathcal{O}(\alpha^3)$ to the various cross sections and of $\mathcal{O}(\alpha)$ to the asymmetries, into :

1. virtual corrections consisting of selfenergies, vertex corrections and box contributions. They can be accounted for by adding the corresponding 1-loop expression to the matrix element for the 4-fermion processes :

$$\delta M = \delta M_S + \delta M_V + \delta M_B . \tag{3.1}$$

2. real photon bremsstrahlung $e^+e^- \to f\bar{f}\gamma$: the integration over the soft photon phase space yields a 2-particle final state cross section which cancels the IR singularities present in (3.1).

As a consequence of the application of the multiplicative 'on-shell' renormalization scheme as briefly mentioned in section 7 of chapter II it has become customary to subdivide the radiative corrections to $e^+e^- \to f\bar{f}$ into the following gauge invariant classes :

a. the 'QED corrections', consisting of those diagrams which contain an extra photon attached to the original Born diagrams. They therefore cover all the real and virtual photonic corrections to the γ as well as Z exchange Born diagrams.

b. the 'weak corrections', consisting of the remaining 1-loop diagrams : γ vacuum polarization, Z self energy and γZ mixing, non-photonic vertex corrections, box contributions with two massive gauge boson exchange and non-photonic external fermion self energies entering in the form of wave function renormalization factors.

Separating off the QED corrections makes sense since they depend on the details of the experiments via the applied cuts to the final state photons. Although they are considered not very interesting with respect to the underlying theory they are in general large at LEP/SLC energies and hence need some care. Moreover, the unbroken $U(1)_{em}$ symmetry allows us to treat the renormalization as well as the evaluations in this QED sector completely independent of the details of the full electroweak structure. The weak corrections will be treated in the subsections 3.2 - 3.4, whereas the QED corrections can be found in subsection 3.5.

3.2 Self energy corrections and neutral gauge boson propagation

The analogy to QED advocates to fix the electron field renormalization constants for the left and right handed components by imposing the condition that the residue of the pole should be equal to 1 on the renormalized electron propagator (and analogously on the other charged lepton propagators) . Consequently there is no wave function renormalization factor for external $e^\pm$ lines as well as for all other sequential charged lepton lines. On the other hand, due to only one doublet renormalization constant Z_L , displaying the multiplicative character of the applied renormalization scheme [5], the corresponding neutrino partners get a finite wave function renormalization factor when they occur as external particles. The extension of this prescription to the quark doublets involves an ambiguity since there both $I_3 = +1/2$ and $I_3 = -1/2$ members have electromagnetic couplings to the photon. In order to maintain the analogy to the lepton sector we take over the condition for the

$I_3 = -1/2$ quarks to propagate with residue 1, i.e. no wave function renormalization factors for external lines. Then external $I_3 = +1/2$ quarks automatically get finite wave function renormalization factors which we will treat together with the vertex corrections in the next subsection.

The next order contributions to the vector boson propagators can be summarized in terms of the 1PI renormalized transverse self energies $\hat{\Sigma}^{\gamma}(s)$, $\hat{\Sigma}^{Z}(s)$ and $\hat{\Sigma}^{\gamma Z}(s)$. We only need the transverse parts as the longitudinal parts will be suppressed by a factor $\frac{m_f^2}{s}$. Because of the γZ mixing self energies the at the classical level diagonal mass matrix (*II*.5.2) will acquire off diagonal components leading to an intertwining of the propagation of photons and Z gauge bosons. The radiatively corrected complex of neutral gauge boson propagators consequently has a matrix structure which can be determined by inversion of

$$D^{-1}_{\mu\nu} = ig_{\mu\nu} \begin{pmatrix} s + \hat{\Sigma}^{\gamma}(s) & \hat{\Sigma}^{\gamma Z}(s) \\ \hat{\Sigma}^{\gamma Z}(s) & s - M_Z^2 + \hat{\Sigma}^{Z}(s) \end{pmatrix} . \tag{3.2}$$

The 1-loop 1PI renormalized transverse self energies $\hat{\Sigma}^{\gamma,Z,\gamma Z}(s)$ can be found in appendix I. After inversion we arrive at

$$D_{\mu\nu} = -ig_{\mu\nu} \begin{pmatrix} D_{\gamma}(s) & D_{\gamma Z}(s) \\ D_{\gamma Z}(s) & D_{Z}(s) \end{pmatrix} , \tag{3.3}$$

with

$$\begin{aligned} D_{\gamma}(s) &= \left\{ s + \hat{\Sigma}^{\gamma}(s) - \frac{[\hat{\Sigma}^{\gamma Z}(s)]^2}{s - M_Z^2 + \hat{\Sigma}^{Z}(s)} \right\}^{-1} \\ D_{Z}(s) &= \left\{ s - M_Z^2 + \hat{\Sigma}^{Z}(s) - \frac{[\hat{\Sigma}^{\gamma Z}(s)]^2}{s + \hat{\Sigma}^{\gamma}(s)} \right\}^{-1} \\ D_{\gamma Z}(s) &= -\frac{\hat{\Sigma}^{\gamma Z}(s)}{s - M_Z^2 + \hat{\Sigma}^{Z}(s)} D_{\gamma}(s) = -\frac{\hat{\Sigma}^{\gamma Z}(s)}{s + \hat{\Sigma}^{\gamma}(s)} D_{Z}(s) . \end{aligned} \tag{3.4}$$

In perturbation language this should be interpreted as follows :

1. the gauge invariant part of the 1PI renormalized transverse gauge boson self energies $\hat{\Sigma}(s)$ can be resummed to all orders according to the solution of Dyson's equation, which involves extending the series beyond its radius of convergence. The expansion in terms of powers of $\frac{\alpha}{\pi}$ enters the resummed expression in the form of a corresponding expansion of $\hat{\Sigma}(s)$. Restricting ourselves to $\mathcal{O}(\alpha)$ corrections to the Born propagators this corresponds for instance to the inclusion of the 1-loop 1PI corrections originating from fermion

loops (being gauge invariant by themselves) and in case of $D_Z(s)$ also some 2-loop 1PI corrections at $s = M_Z^2$ leading to an imaginary part constituting $\mathcal{O}(\alpha)$ corrections to the lowest order (fermionic) width of the Z gauge boson (see section 4). In this way we will have incorporated the to all orders resummed leading logarithmic contributions

$$\left[\frac{\alpha}{\pi}\log\left(\frac{m_f^2}{s}\right)\right]^n ,$$

constituting the dominant contributions to the real parts of the diagonal self energies, and in case of $D_Z(s)$ the $\mathcal{O}(\alpha)$ corrected fermionic width. These $\mathcal{O}(\alpha)$ corrections to the Z gauge boson width are provided with an approximated linear near resonance s-dependence motivated by the lowest order near resonance behaviour.

2. the remaining gauge depending 1PI contributions to $\hat{\Sigma}(s)$ enter the expansion of the neutral gauge boson propagators in terms of powers of $\frac{\alpha}{\pi}$ in a perturbative way and should not be resummed because of their close relation, as far as gauge dependence is concerned, to the perturbatively treated vertex corrections and box contributions.

When one also considers the real part of the terms in (3.4) containing $[\,\hat{\Sigma}^{\gamma Z}(s)\,]^2$ one effectively takes into account second order corrections to the real part of the Born propagators. For large mass splitting in the top-bottom doublet ($m_t \geq 150$ GeV) these terms will lead to corrections exceeding the aimed experimental uncertainties for some of the measurable quantities. This is however not the complete story as we should in fact include all second order contributions present in (3.4) to come to a conclusive statement regarding the inclusion or exclusion of higher order corrections. Recent calculations involving leading top mass evaluations [8] give indications that the lowest order large mass splitting effects are reduced by the inclusion of second order contributions, especially those originating from the Yukawa sector which is a breeding place for large mass splitting effects because of the fermion mass depending couplings between the fermions and the Higgs bosons. This stresses the importance of a complete second order leading top mass evaluation in the near future. To avoid an inadequate and incomplete treatment of higher order effects we will exclude them from our evaluations and stick to the $\mathcal{O}(\alpha)$ corrections to the Born propagators seen in the light of the above given interpretation of what we mean by an expansion in terms of powers of $\frac{\alpha}{\pi}$.

Combining the above considerations with the Born matrix element (2.11) we arrive at

$$M^{(0)}(\kappa;\eta,\bar{\eta};s,t) + \delta M_S(\kappa;\eta,\bar{\eta};s,t) \;\rightarrow\; \frac{1}{s}\sum_\rho M_1^{\rho\kappa}\{\,Q_e Q_f\,\chi_\gamma(s) + g_e^\kappa g_f^\rho\,\chi_Z(s) + [\,Q_e g_f^\rho + Q_f g_e^\kappa\,]\,\chi_{\gamma Z}(s)\,\}\,, \qquad (3.5)$$

with

$$\begin{aligned}
\chi_\gamma(s) &= s\, D_\gamma(s) \\
\chi_Z(s) &= s\, D_Z(s) \\
\chi_{\gamma Z}(s) &= -s\, D_{\gamma Z}(s) = \frac{\hat{\Sigma}^{\gamma Z}(s)}{s}\, \chi_Z(s)
\end{aligned} \tag{3.6}$$

and $D_{\gamma,Z,\gamma Z}(s)$ as given in (3.4). The 'dressed' Born part, from now on to be used instead of the Born matrix element (2.11), consists of the first two terms of (3.5) :

$$M^{(0)}_{dr.}(\kappa;\eta,\bar{\eta};s,t) = \frac{1}{s}\sum_\rho M_1^{\rho\kappa}\left\{ Q_e Q_f\, \chi_\gamma(s) + g_e^\kappa g_f^\rho\, \chi_Z(s) \right\}, \tag{3.7}$$

whereas the remaining γZ mixing self energy term appearing in (3.5) will enter any calculation including $\mathcal{O}(\alpha)$ corrections from now on as a self energy correction to this dressed Born matrix element. This once again in order to avoid a possibly misplaced inclusion of higher order terms. For later use we will make a separation between the dressed matrix elements related to γ and Z exchange according to :

$$\begin{aligned}
M^{(0)}_\gamma(\kappa;\eta,\bar{\eta};s,t) &= Q_e Q_f\, \frac{\chi_\gamma(s)}{s} \sum_\rho M_1^{\rho\kappa} \\
M^{(0)}_Z(\kappa;\eta,\bar{\eta};s,t) &= g_e^\kappa \frac{\chi_Z(s)}{s} \sum_\rho g_f^\rho\, M_1^{\rho\kappa}
\end{aligned} \tag{3.8}$$

3.3 Weak vertex corrections

As the influence of the mass of the light final state fermions is very small, even at Born level, we will neglect that mass when considering further $\mathcal{O}(\alpha)$ corrections, except in the case of 'mass singularities' present in some of the QED corrections. The weak vertex corrections can be divided into 4 separate contributions :

$$\delta M_V^{weak} = \delta M_{ee\gamma}^{weak} + \delta M_{eeZ}^{weak} + \delta M_{ff\gamma}^{weak} + \delta M_{ffZ}^{weak}, \tag{3.9}$$

according to the corrections to the 4 types of vertices present in the Born diagrams of fig. 1. Because of the resonant behaviour of the Z propagator and in order to maintain a gauge invariant treatment of the radiative corrections, as the gauge depending part of the self energy corrections is related to part of the weak vertex corrections, the above given weak vertex corrections will involve a resummation of the propagators connecting the two fermion currents. This resummation will be of the same diagonal type as the one appearing in the dressed Born matrix element (3.7). It should be noted that the final state vertex corrections are not irreducible in case of $I_3 = +1/2$ final state fermions as they will also include the external wave function renormalization factors mentioned in the last subsection. The weak

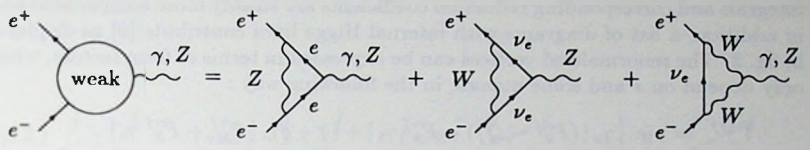

Fig. 2. Weak $ee\gamma$ and eeZ vertex corrections

contributions from the renormalized initial state $ee\gamma$ and eeZ vertices (see fig. 2) can be brought in the general form (2.8) as follows :

$$\begin{aligned}
\delta M^{weak}_{ee\gamma}(\kappa;\eta,\bar{\eta};s,t) &= -\frac{\alpha}{4\pi}\left\{-Q_e(g_e^\kappa)^2\,\Lambda_2(s,M_Z)+2\delta_{\kappa-}\,F_L^{\gamma l}\right\} Q_f\,\frac{\chi_\gamma(s)}{s}\sum_\rho M_1^{\rho\kappa}\\
\delta M^{weak}_{eeZ}(\kappa;\eta,\bar{\eta};s,t) &= \frac{\alpha}{4\pi}\left\{(g_e^\kappa)^3\,\Lambda_2(s,M_Z)+2\delta_{\kappa-}\,F_L^{Zl}\right\}\frac{\chi_Z(s)}{s}\sum_\rho g_f^\rho\,M_1^{\rho\kappa}\ ,
\end{aligned} \tag{3.10}$$

where $\delta_{\kappa-}$ projects on amplitudes with left handed $\kappa=-$ electrons :

$$\delta_{\kappa-}=\begin{cases}1 & \text{for } \kappa=-\\ 0 & \text{for } \kappa=+\end{cases} \tag{3.11}$$

and

$$\begin{aligned}
F_L^{\gamma l} &= \frac{3}{4s_w^2}\,\Lambda_3(s,M_W)\\
F_L^{Zl} &= \frac{1}{8s_w^3c_w}\,\Lambda_2(s,M_W)-\frac{3c_w}{4s_w^3}\,\Lambda_3(s,M_W)\ .
\end{aligned} \tag{3.12}$$

The invariant functions $\Lambda_{2,3}$ are given by :

$$\begin{aligned}
\Lambda_2(s,M) &= -\frac{7}{2}-2w-(2w+3)\log(-w)+2(1+w)^2\left\{Li_2\left(1+\frac{1}{w}\right)-\frac{\pi^2}{6}\right\}\\
\Lambda_3(s,M) &= \frac{5}{6}-\frac{2w}{3}-\frac{2w+1}{3}\sqrt{1-4w}\,\log(x)+\frac{2}{3}w(w+2)\log^2(x)\ ,
\end{aligned} \tag{3.13}$$

where

$$w\equiv\frac{M^2}{s+i\epsilon}\quad,\quad x\equiv\frac{\sqrt{1-4w}-1}{\sqrt{1-4w}+1}=-K(s+i\epsilon,M,M)\ .$$

The weak vertex corrections corresponding to the final state fermions are more involved. Without neglecting fermion mass terms the analytical expressions for the

integrals and corresponding reduction coefficients are sizably more complicated and, in addition, a list of diagrams with internal Higgs lines contribute [9] as displayed in fig. 3. The renormalized vertices can be expressed in terms of form factors, which only depend on s and some masses, in the following way :

$$\begin{aligned}
\hat{\Gamma}^{\gamma ff}_{\mu} &= ie\left\{\gamma_\mu[(F_V^{\gamma f}-Q_f)-F_A^{\gamma f}\gamma_5]+(q-\bar{q})_\mu[F_M^{\gamma f}+F_E^{\gamma f}\gamma_5]\right. \\
&\quad \left.-(q+\bar{q})_\mu[F_S^{\gamma f}+F_P^{\gamma f}\gamma_5]\right\} \\
\hat{\Gamma}^{Zff}_{\mu} &= ie\left\{\gamma_\mu[(F_V^{Zf}+v_f)-(F_A^{Zf}+a_f)\gamma_5]+(q-\bar{q})_\mu[F_M^{Zf}+F_E^{Zf}\gamma_5]\right. \\
&\quad \left.-(q+\bar{q})_\mu[F_S^{Zf}+F_P^{Zf}\gamma_5]\right\}\ , \qquad (3.14)
\end{aligned}$$

resulting in a general contribution to the matrix element which reduces because of current and axial current conservation at the initial state $ee\gamma$ and $ee\!\!\not{Z}$ vertices and CP invariance, resulting in the absence of electric dipole moments at 1-loop level ($F_E = 0$), to

$$\begin{aligned}
\delta M^{weak}_{ff\gamma}(\kappa;\eta,\bar{\eta};s,t) &= -Q_e\frac{\chi_\gamma(s)}{s}\sum_\rho\left\{M_1^{\rho\kappa}[F_V^{\gamma f}-\rho F_A^{\gamma f}]+2M_3^{\rho\kappa}F_M^{\gamma f}\right\} \\
\delta M^{weak}_{ffZ}(\kappa;\eta,\bar{\eta};s,t) &= g_e^\kappa\frac{\chi_Z(s)}{s}\sum_\rho\left\{M_1^{\rho\kappa}[F_V^{Zf}-\rho F_A^{Zf}]+2M_2^{\rho\kappa}F_M^{Zf}\right\}\ . \qquad (3.15)
\end{aligned}$$

In case of light final state fermions, except for the bottom quark, compact expressions like the ones in (3.10) are recovered. In that case we find for the surviving form factors :

$$\begin{aligned}
F_V^{\gamma f_L}(s) &= \frac{\alpha}{4\pi}\{-Q_{f_L}(v_{f_L}^2+a_{f_L}^2)\Lambda_2(s,M_Z)+F_L^{\gamma f_L}\} \\
F_A^{\gamma f_L}(s) &= \frac{\alpha}{4\pi}\{-2Q_{f_L}v_{f_L}a_{f_L}\Lambda_2(s,M_Z)+F_L^{\gamma f_L}\} \\
F_V^{Z f_L}(s) &= \frac{\alpha}{4\pi}\{v_{f_L}(v_{f_L}^2+3a_{f_L}^2)\Lambda_2(s,M_Z)+F_L^{Z f_L}\} \\
F_A^{Z f_L}(s) &= \frac{\alpha}{4\pi}\{a_{f_L}(3v_{f_L}^2+a_{f_L}^2)\Lambda_2(s,M_Z)+F_L^{Z f_L}\}\ , \qquad (3.16)
\end{aligned}$$

with

$$\begin{aligned}
F_L^{\gamma f_L} &= \frac{3I_3^{f'_L}}{2s_w^2}\Lambda_3(s,M_W)-\frac{Q_{f'_L}}{4s_w^2}\Lambda_2(s,M_W) \\
F_L^{Z f_L} &= -\frac{3c_w I_3^{f'_L}}{2s_w^3}\Lambda_3(s,M_W)+\frac{g^-_{f'_L}}{4s_w^2}\Lambda_2(s,M_W)\ , \qquad (3.17)
\end{aligned}$$

where f' denotes the isospin partner (=doublet partner) of f.

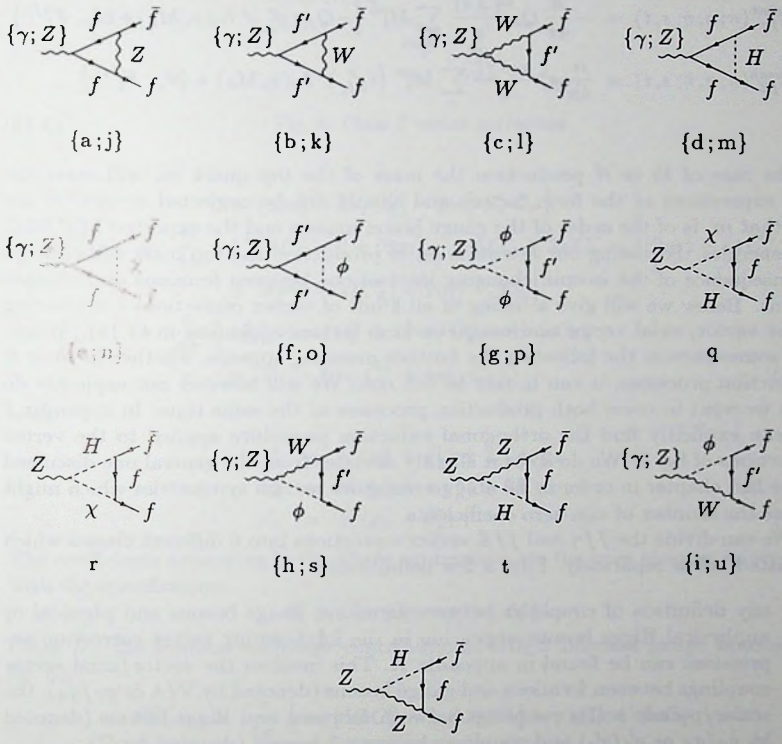

Fig. 3. Weak $ff\gamma$ and ffZ vertex corrections

The magnetic (F_M) form factors can be neglected as their contribution will be suppressed by a factor $\{m^2_{f_L}; m_{f_L} m_{f'_L}\}/s$ compared to the contributions originating from the vector (F_V) and axial vector (F_A) form factors. From this we can derive

$$\delta M^{weak}_{ff\gamma}(\kappa;\eta,\bar{\eta};s,t) = -\frac{\alpha}{4\pi} Q_e \frac{\chi_\gamma(s)}{s} \sum_\rho M_1^{\rho\kappa} \left\{ -Q_{f_L} (g^\rho_{f_L})^2 \Lambda_2(s,M_Z) + 2\delta_{\rho-} F_L^{\gamma f_L} \right\}$$

$$\delta M^{weak}_{ffZ}(\kappa;\eta,\bar{\eta};s,t) = \frac{\alpha}{4\pi} g_e^\kappa \frac{\chi_Z(s)}{s} \sum_\rho M_1^{\rho\kappa} \left\{ (g^\rho_{f_L})^3 \Lambda_2(s,M_Z) + 2\delta_{\rho-} F_L^{Z f_L} \right\} . \tag{3.18}$$

In the case of $b\bar{b}$ or $t\bar{t}$ production the mass of the top quark m_t will enter the final expressions of the form factors and should not be neglected in view of the fact that m_t is of the order of the gauge boson masses and the expected LEP/SLC CM energies. Focussing our attention on $b\bar{b}$ production the top mass will enter as a consequence of the isospin changing interactions between fermions and charged bosons. Below we will give a listing of all kinds of vertex corrections contributing to the vector, axial vector and magnetic form factors appearing in (3.15). Whenever somewhere in the following the bottom mass m_b appears, whether in $b\bar{b}$ or $t\bar{t}$ production processes, it can in fact be left out. We will however not explicitly do so as we want to cover both production processes at the same time. In appendix J one can explicitly find the orthogonal reduction procedure applied to the vertex corrections of fig. 3. We do so as it slightly deviates from the general one discussed in the last chapter in order to be able to recognize certain symmetries which might reduce the number of non-zero coefficients.

We can divide the $ff\gamma$ and ffZ vertex corrections into 6 different classes which are listed below separately. First a few definitions :

- any definition of couplings between fermions, gauge bosons and physical or unphysical Higgs bosons appearing in the forthcoming vertex correction expressions can be found in appendix K. This involves the vector/axial vector couplings between fermions and gauge bosons (denoted by V/A or g_V/g_A), the scalar/pseudo scalar couplings between fermions and Higgs bosons (denoted by g_S/g_P or g'_S/g'_P) and couplings between 3 bosons (denoted by G).

- in case we are dealing with a fermionic internal line we will indicate the corresponding mass by m_f which is equal to $m_{f'}$ in case of isospin changing charged current interactions or m_f in case of isospin preserving neutral current interactions.

Class I: the gauge boson exchange contributions (see fig. 4).

$$F_V^I(s) = \frac{\alpha}{4\pi} \Big\{ \lambda_V^+ [4C_2^0 - 2 + (8m_f^2 - 2s) C_2^+ + 2s\, C_2^- - 4(4m_f^2 - s) C_1^+$$

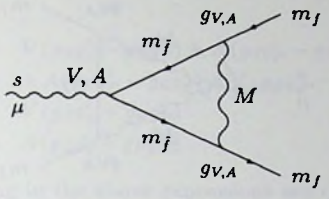

Fig. 4. Class I vertex correction

$$
\begin{aligned}
& + (6m_f^2 - 2s)\, C_0\,] - 2m_{\tilde{f}}^2\, \lambda_V^-\, C_0 \Big\} \\
F_A^I(s) &= \frac{\alpha}{4\pi} \Big\{ \lambda_A^+\, [\, 4C_2^0 - 2 + (8m_f^2 - 2s)\, C_2^+ + 2s\, C_2^- - 4(2m_f^2 - s)\, C_1^+ \\
& + 2(m_f^2 - s)\, C_0\,] - 2m_{\tilde{f}}^2\, \lambda_A^-\, C_0 \Big\} \\
F_M^I(s) &= \frac{\alpha}{4\pi} \Big\{ \lambda_V^+\, [\, -8m_f\, C_2^+ + 12 m_f\, C_1^+ - 4 m_f\, C_0\,] \\
& + \lambda_V'\, [\, -8 m_{\tilde{f}}\, C_1^+ + 4 m_{\tilde{f}}\, C_0\,] \Big\}\ , \qquad (3.19)
\end{aligned}
$$

with

$$
\begin{aligned}
\lambda_V^{\pm} &= V\,(g_V^2 + g_A^2) \pm 2A\, g_V g_A \\
\lambda_A^{\pm} &= \pm A\,(g_V^2 + g_A^2) + 2V\, g_V g_A \\
\lambda_V' &= V\,(g_V^2 - g_A^2)\ . \qquad (3.20)
\end{aligned}
$$

The coefficients appearing in the above expressions are the ones given in appendix J with the specification

$$\bar{C} \equiv \bar{C}(-\bar{q}, q, m_{\tilde{f}}, m_{\tilde{f}}, M)\ .$$

Class II: the fermion exchange contributions with 2 internal gauge bosons (see fig. 5).

$$
\begin{aligned}
F_V^{II}(s) &= \frac{\alpha}{4\pi} \Big\{ \lambda_V\, [\, 12\, C_2^0 - 2 + 2(4m_f^2 - s)\, C_2^+ + 2s\, C_2^- \\
& - 4(4m_f^2 - s)\, C_1^+\,] + 6 m_f m_{\tilde{f}}\, \lambda_V'\, C_0 \Big\} \\
F_A^{II}(s) &= \frac{\alpha}{4\pi} \Big\{ \lambda_A\, [\, 12\, C_2^0 - 2 + 2(4m_f^2 - s)\, C_2^+ + 2s\, C_2^- \\
& - 4(m_f^2 - s)\, C_1^+\,] \Big\} \\
F_M^{II}(s) &= \frac{\alpha}{4\pi} \Big\{ \lambda_V\, [\, 8 m_f\, C_2^+ + 2 m_f\, C_1^+\,] - 6 m_{\tilde{f}}\, \lambda_V'\, C_1^+ \Big\}\ , \qquad (3.21)
\end{aligned}
$$

with

$$\lambda_V = G\,(g_V^2 + g_A^2)$$

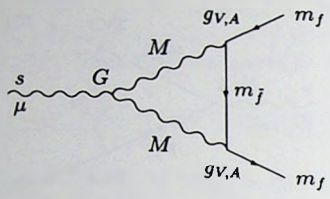

Fig. 5. Class *II* vertex correction

$$\begin{aligned} \lambda_A &= 2G\, g_V g_A \\ \lambda'_V &= G\,(g_V^2 - g_A^2)\,. \end{aligned} \tag{3.22}$$

The coefficients appearing in the above expressions are the ones given in appendix J with the specification

$$C \equiv C(-\bar{q}, q, M, M, m_{\tilde{f}})\,.$$

The following classes of contributions are in the light fermion case (except for $b\bar{b}$ production) suppressed by at least a factor $\{m_{f_L}^2; m_{f'_L}^2; m_{f_L} m_{f'_L}\}/\{M_W^2; s\}$.

Class *III*: Higgs boson exchange contributions (see fig. 6).

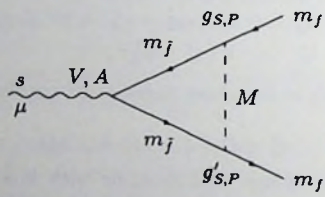

Fig. 6. Class *III* vertex correction

$$\begin{aligned} F_V^{III}(s) &= \frac{\alpha}{4\pi}\Big\{\lambda_V^+\,[\,2\,C_2^0 - \frac{1}{2} + (4m_f^2 - s)\,C_2^+ + s\,C_2^- - m_f^2\,C_0\,] \\ &\quad - m_{\tilde{f}}^2\,\lambda_V^-\,C_0 - 2m_f m_{\tilde{f}}\,\lambda'_V\,C_0\Big\} \\ F_A^{III}(s) &= \frac{\alpha}{4\pi}\Big\{\lambda_A^+\,[\,2\,C_2^0 - \frac{1}{2} + (4m_f^2 - s)\,C_2^+ + s\,C_2^- + m_f^2\,C_0 \\ &\quad - 4m_f^2\,C_1^+\,] - m_{\tilde{f}}^2\,\lambda_A^-\,C_0 + 2m_f m_{\tilde{f}}\,\lambda'_A\,[\,2\,C_1^+ - C_0\,]\Big\} \\ F_M^{III}(s) &= \frac{\alpha}{4\pi}\Big\{\lambda_V^+\,[\,-4m_f\,C_2^+ + 2m_f\,C_1^+\,] + 2m_{\tilde{f}}\,\lambda'_V\,C_1^+\Big\}\,, \end{aligned} \tag{3.23}$$

with

$$\begin{aligned}
\lambda_V^{\pm} &= V(g_S g'_S - g_P g'_P) \pm A(g_S g'_P - g_P g'_S) \\
\lambda_A^{\pm} &= \pm A(g_P g'_P - g_S g'_S) + V(g_P g'_S - g_S g'_P) \\
\lambda'_V &= V(g_S g'_S + g_P g'_P) \\
\lambda'_A &= A(g_S g'_S + g_P g'_P) \,. \qquad (3.24)
\end{aligned}$$

The coefficients appearing in the above expressions are the same as the ones appearing in the expressions of Class *I*.

Class *IV*: fermion exchange contributions with 2 internal Higgs bosons (see fig. 7).

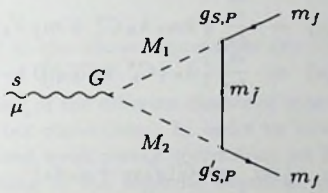

Fig. 7. Class *IV* vertex correction

$$\begin{aligned}
F_V^{IV}(s) &= \frac{\alpha}{4\pi}\left\{2\,\lambda_V\,C_2^0\right\} \\
F_A^{IV}(s) &= \frac{\alpha}{4\pi}\left\{2\,\lambda_A\,C_2^0\right\} \\
F_M^{IV}(s) &= \frac{\alpha}{4\pi}\left\{\lambda_V\,[4m_f\,C_2^+ - 2m_f\,C_1^+] + m_f\,\lambda'_V\,[2\,C_1^+ - C_0]\right\}\,, \qquad (3.25)
\end{aligned}$$

with

$$\begin{aligned}
\lambda_V &= G(g_S g'_S - g_P g'_P) \\
\lambda_A &= G(g_P g'_S - g_S g'_P) \\
\lambda'_V &= G(g_S g'_S + g_P g'_P) \,. \qquad (3.26)
\end{aligned}$$

The coefficients appearing in the above expressions are the ones given in appendix J with the specification

$$\bar{C} \equiv \bar{C}(-\bar{q}, q, M_1, M_2, m_f) \,.$$

Class *V*: fermion exchange contributions with 1 internal gauge boson at the top and 1 internal Higgs boson at the bottom (see fig. 8).

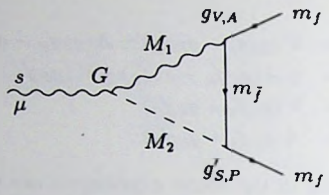

Fig. 8. Class V vertex correction

$$
\begin{aligned}
F_V^V(s) &= \frac{\alpha}{4\pi}\left\{-2m_f\,\lambda_V\,C_1^- + m_{\tilde{f}}\,\lambda'_V\,C_0\right\} \\
F_A^V(s) &= \frac{\alpha}{4\pi}\left\{2m_f\,\lambda_A\,C_1^+ + m_{\tilde{f}}\,\lambda'_A\,C_0\right\} \\
F_M^V(s) &= \frac{\alpha}{4\pi}\left\{\lambda_V\,[\,C_1^+ + C_1^-\,]\right\}\,, \qquad (3.27)
\end{aligned}
$$

with

$$
\begin{aligned}
\lambda_V &= G\,(g'_S g_V + g'_P g_A) \\
\lambda_A &= G\,(g'_S g_A + g'_P g_V) \\
\lambda'_V &= G\,(g'_S g_V - g'_P g_A) \\
\lambda'_A &= G\,(g'_S g_A - g'_P g_V)\,. \qquad (3.28)
\end{aligned}
$$

The coefficients appearing in the above expressions are the same as the ones appearing in the expressions of Class *IV*.

Class *VI*: fermion exchange contributions with 1 internal Higgs boson at the top and 1 internal gauge boson at the bottom (see fig. 9).

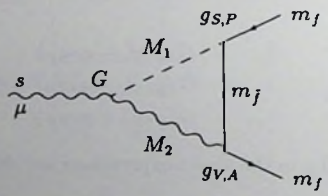

Fig. 9. Class *VI* vertex correction

$$
\begin{aligned}
F_V^{VI}(s) &= \frac{\alpha}{4\pi}\left\{2m_f\,\lambda_V\,C_1^- + m_f\,\lambda'_V\,C_0\right\} \\
F_A^{VI}(s) &= \frac{\alpha}{4\pi}\left\{-2m_f\,\lambda_A\,C_1^+ + m_f\,\lambda'_A\,C_0\right\} \\
F_M^{VI}(s) &= \frac{\alpha}{4\pi}\left\{\lambda_V\,[C_1^+ - C_1^-]\right\}\,, \qquad (3.29)
\end{aligned}
$$

with

$$
\begin{aligned}
\lambda_V &= G(g_S g_V - g_P g_A) \\
\lambda_A &= G(g_P g_V - g_S g_A) \\
\lambda'_V &= G(g_S g_V + g_P g_A) \\
\lambda'_A &= G(g_S g_A + g_P g_V)\,. \qquad (3.30)
\end{aligned}
$$

The coefficients appearing in the above expressions are the same as the ones appearing in the expressions of Class *IV*.

This completes the listing of the different classes of contributions to the fermion - neutral gauge boson vertex corrections. In order to have all the ingredients to construct the unrenormalized weak vertex corrections we list the detailed content of the form factors according to the separate Feynman diagrams of fig. 3. The separate contribution of each diagram to the various form factors is denoted by F_V^a, F_A^a, F_M^a ; F_V^b, F_A^b, F_M^b ; $\cdots$. For each of the diagrams $a, \cdots, v$ the corresponding couplings from the following tables have to be inserted into the expressions for the form factors as prescribed by the class that particular diagram belongs to. Diagrams $a, \cdots, i$ are the weak vertex corrections to the $ff\gamma$ vertex, diagrams $j, \cdots, v$ are the weak vertex corrections to the ffZ vertex. It should be noted that the mass content of these diagrams can immediately be read off from fig. 3, consequently no mass parameters will be included in the tables below.

$ff\gamma$ vertex correction diagrams $a, \cdots, j$					
	class	$\lambda_V^{\pm}$ or λ_V	λ'_V	$\lambda_A^{\pm}$ or λ_A	λ'_A
a	*I*	$-Q_f(v_f^2+a_f^2)$	$-Q_f(v_f^2-a_f^2)$	$-2Q_f v_f a_f$	
b	*I*	$-Q_{f'}/4s_w^2$	0	$-Q_{f'}/4s_w^2$	
c	*II*	$-I_3^f/2s_w^2$	0	$-I_3^f/2s_w^2$	
d	*III*	$-Q_f\mu_f^2$	$-Q_f\mu_f^2$	0	0
e	*III*	$-Q_f\mu_f^2$	$Q_f\mu_f^2$	0	0
f	*III*	$-Q_{f'}(\mu_f^2+\mu_{f'}^2)$	$2Q_{f'}\mu_f\mu_{f'}$	$Q_{f'}(\mu_f^2-\mu_{f'}^2)$	0
g	*IV*	$-2I_3^f(\mu_f^2+\mu_{f'}^2)$	$4I_3^f\mu_f\mu_{f'}$	$2I_3^f(\mu_f^2-\mu_{f'}^2)$	
h	*V*	$-I_3^f m_f/2s_w^2$	$I_3^f m_{f'}/2s_w^2$	$-I_3^f m_f/2s_w^2$	$I_3^f m_{f'}/2s_w^2$
i	*VI*	$-I_3^f m_f/2s_w^2$	$I_3^f m_{f'}/2s_w^2$	$I_3^f m_f/2s_w^2$	$I_3^f m_{f'}/2s_w^2$

ffZ vertex correction diagrams $k, \cdots, x$					
	class	$\lambda_V^{\pm}$ or λ_V	λ'_V	$\lambda_A^{\pm}$ or λ_A	λ'_A
j	*I*	$v_f(v_f^2+a_f^2 \pm 2a_f^2)$	$v_f(v_f^2-a_f^2)$	$\pm a_f(v_f^2+a_f^2 \pm 2v_f^2)$	
k	*I*	$g_{f'}^{\mp}/4s_w^2$	0	$g_{f'}^{\mp}/4s_w^2$	
l	*II*	$c_w I_3^f/2s_w^3$	0	$c_w I_3^f/2s_w^3$	
m	*III*	$v_f\mu_f^2$	$v_f\mu_f^2$	$\mp a_f\mu_f^2$	$a_f\mu_f^2$
n	*III*	$v_f\mu_f^2$	$-v_f\mu_f^2$	$\mp a_f\mu_f^2$	$-a_f\mu_f^2$
o	*III*	$\mu_f^2 g_{f'}^{\mp} + \mu_{f'}^2 g_{f'}^{\pm}$	$-2v_{f'}\mu_f\mu_{f'}$	$-\mu_f^2 g_{f'}^{\mp} + \mu_{f'}^2 g_{f'}^{\pm}$	$-2a_{f'}\mu_f\mu_{f'}$
p	*IV*	$-2\alpha_f(\mu_f^2+\mu_{f'}^2)$	$4\alpha_f\mu_f\mu_{f'}$	$2\alpha_f(\mu_f^2-\mu_{f'}^2)$	
q	*IV*	0	0	$2a_f\mu_f^2$	
r	*IV*	0	0	$2a_f\mu_f^2$	
s	*V*	$-a_f m_f$	$-a_{f'}m_{f'}$	$-a_f m_f$	$-a_{f'}m_{f'}$
t	*V*	$-v_f m_f/2s_w^2c_w^2$	$-v_{f'}m_{f'}/2s_w^2c_w^2$	$-a_f m_f/2s_w^2c_w^2$	$-a_{f'}m_{f'}/2s_w^2c_w^2$
u	*VI*	$-a_f m_f$	$-a_{f'}m_{f'}$	$a_f m_f$	$-a_{f'}m_{f'}$
v	*VI*	$-v_f m_f/2s_w^2c_w^2$	$-v_{f'}m_{f'}/2s_w^2c_w^2$	$a_f m_f/2s_w^2c_w^2$	$-a_{f'}m_{f'}/2s_w^2c_w^2$

Thereby we have used the following abbreviations :

$$\begin{aligned} \mu_f &\equiv \frac{m_f}{2s_w M_W} = \frac{m_f}{2s_w c_w M_Z} \\ \alpha_f &\equiv a_f(s_w^2 - c_w^2)\,. \end{aligned} \tag{3.31}$$

The sum of the diagrams listed above yields the unrenormalized weak vertex corrections. The renormalized vertices are obtained by adding the corresponding counter terms as specified in [5]. Since we want to include the on-shell self energy contributions from the external fermions, entering in the form of wave function renormalization factors, we obtain our renormalized vertex corrections as displayed graphically by :

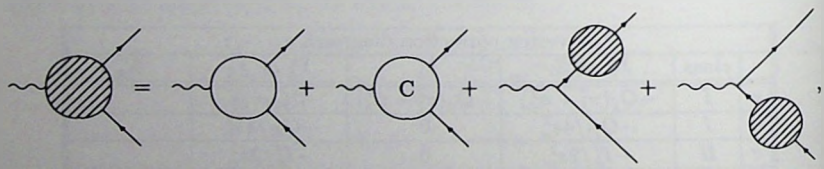

where the empty blob denotes the sum of the Feynman graphs and the one containing the C the counter terms. The vertex counter terms combined with the fermion wave function renormalization factors can be expressed in terms of contributions to the vector (C_V) and axial vector (C_A) form factors according to :

$$C_V^{f,weak} = -Q_f C_1^f - Q_f(\delta Z_1^\gamma - \delta Z_2^\gamma) - v_f(\delta Z_1^{\gamma Z} - \delta Z_2^{\gamma Z})$$

$$
\begin{aligned}
C_A^{\gamma f,weak} &= -Q_f C_2^f - a_f (\delta Z_1^{\gamma Z} - \delta Z_2^{\gamma Z}) \\
C_V^{Z f,weak} &= v_f C_1^f + a_f C_2^f + v_f (\delta Z_1^Z - \delta Z_2^Z) + Q_f (\delta Z_1^{\gamma Z} - \delta Z_2^{\gamma Z}) \\
C_A^{Z f,weak} &= a_f C_1^f + v_f C_2^f + a_f (\delta Z_1^Z - \delta Z_2^Z) \,, \qquad (3.32)
\end{aligned}
$$

with

$$
(\delta Z_1 - \delta Z_2)^{\gamma,\gamma Z,Z} = -\frac{\alpha}{2\pi} \Delta_{M_W} \left(1, \frac{c_w}{s_w}, \frac{c_w^2}{s_w^2}\right) , \qquad (3.33)
$$

where the UV-divergent quantity Δ_M is defined in appendix G. The weak renormalization constants C_1^f, C_2^f, related to the left and right handed fermionic renormalization constants, are given by the on-shell ($q^2 = m_f^2$) expressions :

$$
\begin{aligned}
C_1^f &= \frac{\alpha}{4\pi} \mathrm{Re} \Big\{ (v_f^2 + a_f^2) [2 B_1(q^2, m_f, M_Z) + 1] + \frac{1}{4 s_w^2} [2 B_1(q^2, m_{f'}, M_W) + 1] \\
&+ \mu_f^2 [B_1(q^2, m_f, M_H) + B_1(q^2, m_f, M_Z) + B_1(q^2, m_{f'}, M_W)] \\
&+ \mu_{f'}^2 B_1(q^2, m_{f'}, M_W) + 2 m_f^2 \Big(v_f^2 [2 B_1'(q^2, m_f, M_Z) \\
&+ 4 B_0'(q^2, m_f, M_Z)] + a_f^2 [2 B_1'(q^2, m_f, M_Z) - 4 B_0'(q^2, m_f, M_Z)] \\
&+ \frac{1}{2 s_w^2} B_1'(q^2, m_{f'}, M_W) + \mu_f^2 [B_1'(q^2, m_f, M_H) + B_1'(q^2, m_f, M_Z) \\
&+ B_1'(q^2, m_{f'}, M_W) + B_0'(q^2, m_f, M_Z) - B_0'(q^2, m_f, M_H)] \\
&+ \mu_{f'}^2 [B_1'(q^2, m_{f'}, M_W) + 2 B_0'(q^2, m_{f'}, M_W)] \Big) \Big\} \qquad (3.34)
\end{aligned}
$$

and

$$
\begin{aligned}
C_2^f &= -\frac{\alpha}{4\pi} \mathrm{Re} \Big\{ -2 v_f a_f [2 B_1(q^2, m_f, M_Z) + 1] - \frac{1}{4 s_w^2} [2 B_1(q^2, m_{f'}, M_W) + 1] \\
&+ (\mu_f^2 - \mu_{f'}^2) B_1(q^2, m_{f'}, M_W) \Big\} \,, \qquad (3.35)
\end{aligned}
$$

where B_0' and B_1' denote the derivatives of B_0 and B_1 with respect to q^2. For the functions B_0 and B_1 we refer to appendix G. Now we have all the ingredients for constructing the form factors appearing in (3.15). The weak $ff\gamma$ form factors are given by

$$
\begin{aligned}
F_V^{\gamma f,weak}(s) &= \sum_a^i F_V(s) + C_V^{\gamma f,weak} \\
F_A^{\gamma f,weak}(s) &= \sum_a^i F_A(s) + C_A^{\gamma f,weak} \\
F_M^{\gamma f,weak}(s) &= \sum_a^i F_M(s) \,, \qquad (3.36)
\end{aligned}
$$

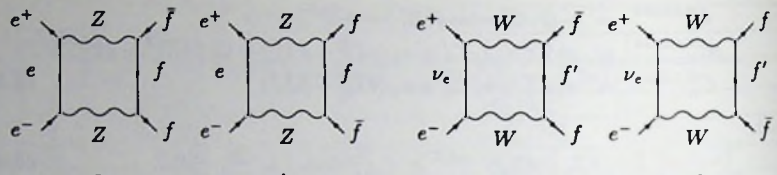

Neutral current weak boxes

Charged current weak boxes
diagram c contributes for $I_3^f = -1/2$
diagram d contributes for $I_3^f = +1/2$

Fig. 10. Neutral and charged current weak boxes

whereas the weak ffZ form factors are given by

$$F_V^{Zf,weak}(s) = \sum_j^v F_V(s) + C_V^{Zf,weak}$$
$$F_A^{Zf,weak}(s) = \sum_j^v F_A(s) + C_A^{Zf,weak}$$
$$F_M^{Zf,weak}(s) = \sum_j^v F_M(s) \; . \tag{3.37}$$

3.4 Weak box contributions

The UV-finite weak box contributions to the 1-loop matrix element (3.1) can be divided into a neutral current and a charged current part :

$$\delta M_B^{weak} = \delta M_B^{NC} + \delta M_B^{CC} \; , \tag{3.38}$$

each of which is characterized by the exchange of two massive gauge bosons. As these weak box contributions are not resonant no resummation is needed. Because of the suppression by a factor $\frac{m_e}{M_W}$, originating from the Yukawa couplings between the initial state e^+e^- and the Higgs bosons, any Higgs boson exchange box contribution can be neglected. In terms of the diagrams of fig. 10 the neutral current weak box contributions correspond to diagrams a and b, whereas in the case of the charged current box contribution only the direct (diagram c) or crossed (diagram d) box is present depending on the isospin I_3^f of the final state fermion. Each of these

box contributions allows for a decomposition according to (2.8), yielding :

$$\delta M = \sum_{i=1}^{4} \sum_{\rho} M_i^{\rho\kappa} \left\{ \delta^{\rho}_{-\kappa} B_i^{(1)\kappa} + \delta^{\rho}_{\kappa} B_i^{(2)\kappa} \right\} , \tag{3.39}$$

with

$$\begin{aligned}
B_1^{(1)\kappa} &= \lambda_\kappa^-(2B_1 - 2B_2^c) + \bar{\lambda}_\kappa^+(B_7 + B_7^c) - \bar{\lambda}_\kappa^-(B_8 + B_8^c) \\
B_1^{(2)\kappa} &= \lambda_\kappa^+(2B_2 - 2B_1^c) + \bar{\lambda}_\kappa^+(B_8 + B_8^c) - \bar{\lambda}_\kappa^-(B_7 + B_7^c) \\
B_2^{(1)\kappa} &= 2\lambda_\kappa^- B_3^c \\
B_2^{(2)\kappa} &= 2\lambda_\kappa^+ B_3 \\
B_3^{(1)\kappa} &= 2\lambda_\kappa^+ B_4 - 2\lambda_\kappa^- B_4^c + \bar{\lambda}_\kappa^+(B_{10}^c - B_9^c) - \bar{\lambda}_\kappa^-(B_{10} - B_9) \\
B_3^{(2)\kappa} &= 2\lambda_\kappa^+ B_5 - 2\lambda_\kappa^- B_5^c + \bar{\lambda}_\kappa^+(B_9 + B_{10}) - \bar{\lambda}_\kappa^-(B_9^c + B_{10}^c) \\
B_4^{(1)\kappa} &= \bar{\lambda}_\kappa^+ B_6^c - \bar{\lambda}_\kappa^- B_6 \\
B_4^{(2)\kappa} &= \bar{\lambda}_\kappa^+ B_6 - \bar{\lambda}_\kappa^- B_6^c .
\end{aligned} \tag{3.40}$$

The functions $B_1, \ldots, B_{10}$ corresponding to the direct box contributions a and c only depend on the external momenta and internal masses :

$$B_i \equiv P_f^- \, F_i(p_+, -\bar{q}, -q, M_1, M_2, M_3, M_4) \tag{3.41}$$

and the functions $B_1^c, \ldots, B_{10}^c$ corresponding to the crossed box contributions b and d are obtained as :

$$B_i^c \equiv P_f^+ \, F_i(p_+, -q, -\bar{q}, M_1, M_2, M_3, M_4) , \tag{3.42}$$

where the parameter list of the F_i coincides with the parameter list appearing in the 4-point tensor integrals they are related to. The symbols $P_f^{\pm}$ (=0,1) have been introduced to select the direct or crossed box contributions in the charged current case. The functions $F_1, \ldots, F_{10}$ can be expressed in terms of the 4-point tensor integral coefficients of (*III*.5.3) and the scalar 3- and 4-point integrals defined according to (*III*.5.7) respectively (*III*.5.1), using the above mentioned parameter list, in the following way :

$$\begin{aligned}
F_1 &= \frac{\alpha}{4\pi} \left[(M_3^2 - t) \, D_0 + C_0(1,2,4) + C_0(2,3,4) \right] \\
F_2 &= 2 \frac{\alpha}{4\pi} D_{27} \\
F_3 &= 2 \frac{\alpha}{4\pi} \left[D_{11} + D_{24} - D_{25} \right] \\
F_4 &= 2 m_f \frac{\alpha}{4\pi} \left[D_{12} + D_{22} - D_{26} \right]
\end{aligned}$$

$$
\begin{aligned}
F_5 &= -2m_f \frac{\alpha}{4\pi} [\, D_{13} + D_{26} - D_{23} \,] \\
F_6 &= -2M_3 \frac{\alpha}{4\pi} D_{11} \\
F_7 &= -2M_3 m_f \frac{\alpha}{4\pi} D_{12} \\
F_8 &= -2M_3 m_f \frac{\alpha}{4\pi} D_{13} \\
F_9 &= -2M_3 \frac{\alpha}{4\pi} [\, D_{12} - D_{13} \,] \\
F_{10} &= 2M_3 \frac{\alpha}{4\pi} [\, D_{12} + D_{13} \,] \,. \qquad (3.43)
\end{aligned}
$$

For the separate neutral or charged current weak box contributions we have to insert the following in (3.40-3.42) :

$$
\begin{aligned}
\text{neutral current boxes} \;:\; & \lambda_\kappa^\pm = (g_e^\kappa)^2 (g_f^{\pm\kappa})^2 \;,\; \bar{\lambda}_\kappa^\pm = (g_e^\kappa)^2 g_f^\kappa g_{f'}^{-\kappa} \;,\; P_f^\pm = 1 \\
& \text{and} \quad M_1, M_2, M_3, M_4 = m_e, M_Z, m_f, M_Z \\
\text{charged current boxes} \;:\; & \lambda_\kappa^+ = \delta_{\kappa -}/4 s_w^4 \;,\; \lambda_\kappa^- = \bar{\lambda}_\kappa^\pm = 0 \;,\; P_f^\pm = (\frac{1}{2} \pm I_3^f) \\
& \text{and} \quad M_1, M_2, M_3, M_4 = 0, M_W, m_{f'}, M_W \;. \qquad (3.44)
\end{aligned}
$$

As an example we give the charged current box contribution in terms of the functions F_i :

$$
\begin{aligned}
\delta M_B^{CC} = \frac{\delta_{\kappa -}}{2 s_w^4} \Big\{ (\frac{1}{2} - I_3^f) \Big[& M_1^{--} F_2(p_+, -\bar{q}, -q, 0, M_W, m_{f'}, M_W) \\
& + M_2^{--} F_3(p_+, -\bar{q}, -q, 0, M_W, m_{f'}, M_W) \\
& + M_3^{--} F_5(p_+, -\bar{q}, -q, 0, M_W, m_{f'}, M_W) \\
& + M_3^{+-} F_4(p_+, -\bar{q}, -q, 0, M_W, m_{f'}, M_W) \Big] \\
- (\frac{1}{2} + I_3^f) & \Big[M_1^{--} F_1(p_+, -q, -\bar{q}, 0, M_W, m_{f'}, M_W) \Big] \Big\} \;. \qquad (3.45)
\end{aligned}
$$

3.5 QED corrections

The $\mathcal{O}(\alpha)$ QED corrections complete our survey of EWRC effects to fermion pair production from e^+e^- annihilation. They constitute in fact the major part of those EWRC effects as a consequence of large contributions originating from interactions between particles with small masses. The QED sector can be treated as being decoupled from the weak part of the theory as a result of its direct relation to the unbroken gauge group $U(1)_{em}$ which survives the symmetry breaking mechanism and hence will be treated as such. As far as we are interested in probing typical aspects of the electroweak standard model like the quantum effects from weak interactions or its dependence on the unknown model parameters m_t and M_H, the QED

corrections could be regarded as being not very interesting. The fact, however, that they cover a major part of the complete electroweak quantum effects makes it mandatory to have a precise knowledge of the QED sector to be able to recognize the interesting weak sector. Apart from the fact that the QED corrections are in general large as compared to the weak corrections there is yet another distinguishing feature to be found in the dependence of the QED corrections on the details of the experiments via the applied cuts to the final state photons of the inclusively treated 3-particle final state.

The calculations in the QED sector need special care as that very QED sector is a breeding place for, finally vanishing, IR divergences and 'mass singular' double poles. For this reason the special techniques of the last chapter have been developed. In order to arrive at results which are free of those IR divergences and 'mass singular' double poles it will be sufficient to restrict ourselves to the 2-particle final states and to the soft part of the inclusively treated 3-particle final states, introducing a fixed energy cutoff $\omega \ll \sqrt{s}$ for the emitted photon in the CM frame of the initial state electron-positron pair. This leads to expressions which are closely related to the expressions corresponding to the weak corrections as the energy loss in the photon and Z gauge boson propagators are very small. In the case of the resonant Z propagator we have, however, to be careful as a result of the fact that the energy loss due to soft photon radiation of the initial state e^+e^- is not necessarily small compared to the size of the Z resonance shape. The remaining part of the allowed photon phase space restricted by all kinds of detector bound cuts will be referred to as the phase space corresponding to hard photon radiation. This hard part, being free of any divergences, can be treated separately by means of Monte Carlo techniques [10].

The QED corrections to the $ee\gamma$, $ff\gamma$ and eeZ, ffZ vertices as displayed in fig. 11 lead after renormalization to the following contributions to δM_V appearing in (3.1) :

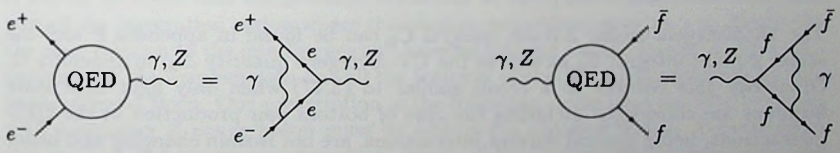

Fig. 11. QED vertex corrections to the $ee\gamma$, eeZ and $ff\gamma$, ffZ vertices

$$\delta M_V^{QED} = \delta M_{ee\gamma}^{QED} + \delta M_{eeZ}^{QED} + \delta M_{ff\gamma}^{QED} + \delta M_{ffZ}^{QED} \,. \tag{3.46}$$

It should be noted that because of the presence of 'mass singular' terms some care has to be taken when neglecting small fermion masses in explicit expressions for

those QED vertex corrections. Bearing that in mind and performing the in this case unavoidable resummation we arrive at

$$\delta M^{QED}_{ee\gamma}(\kappa;\eta,\bar{\eta};s,t) + \delta M^{QED}_{eeZ}(\kappa;\eta,\bar{\eta};s,t) = \frac{\alpha}{4\pi}\, Q_e^2\, \Lambda_1(s,m_e)\, M^{(0)}_{dr.}(\kappa;\eta,\bar{\eta};s,t)\;, \tag{3.47}$$

with

$$\begin{aligned}\Lambda_1(s,m) &= \left[2\log\left(\frac{\lambda^2}{-s-i\epsilon}\right) + \log\left(\frac{-s-i\epsilon}{m^2}\right)\right]\left[\log\left(\frac{-s-i\epsilon}{m^2}\right) - 1\right] \\ &\quad + 2\log\left(\frac{-s-i\epsilon}{m^2}\right) + 4\left(\frac{\pi^2}{12} - 1\right), \end{aligned} \tag{3.48}$$

for the combined $ee\gamma$ and eeZ QED vertex corrections which are proportional to the dressed Born matrix element. Because of finite mass effects the same does not hold in the case of heavy final state fermions :

$$\begin{aligned}\delta M^{QED}_{ff\gamma}(\kappa;\eta,\bar{\eta};s,t) &= Q_e Q_f \frac{\chi_\gamma(s)}{s} \sum_\rho \{\Lambda(s,m_f)\, M_1^{\rho\kappa} + 2\Lambda_M(s,m_f)\, M_3^{\rho\kappa}\} \\ \delta M^{QED}_{ffZ}(\kappa;\eta,\bar{\eta};s,t) &= g_e^\kappa \frac{\chi_Z(s)}{s} \sum_\rho \Big\{[\Lambda(s,m_f)\, g_f^\rho - 4m_f \rho \Lambda_M(s,m_f)\, a_f]\, M_1^{\rho\kappa} \\ &\qquad + 2\Lambda_M(s,m_f)\, v_f\, M_3^{\rho\kappa}\Big\}\;, \end{aligned} \tag{3.49}$$

with

$$\begin{aligned}\Lambda(s,m_f) &\equiv \frac{\alpha}{4\pi} Q_f^2 \Big\{-2(s-2m_f^2)\, C_0(-\bar{q},q+\bar{q},\lambda,m_f,m_f) - 4 - 2\log\left(\frac{\lambda^2}{m_f^2}\right) \\ &\qquad - 3[\, B_0(s,m_f,m_f) - \Delta_{m_f} - 2\,]\Big\} \\ \Lambda_M(s,m_f) &\equiv \frac{\alpha}{4\pi} Q_f^2 \frac{2m_f}{4m_f^2 - s}\,[\, B_0(s,m_f,m_f) - \Delta_{m_f} - 2\,]\;. \end{aligned} \tag{3.50}$$

The IR-divergent scalar 3-point integral C_0 can be found in appendix F and the scalar 2-point integral B_0 as well as the UV-divergent quantity Δ_M in appendix G. Obviously this reduces to a result similar to (3.47) when only light final state fermions are considered including the case of bottom pair production as the QED interactions, being neutral current interactions, are not isospin changing and hence keep any top quark from entering the $bb\gamma$ or bbZ vertex corrections.

The QED box contributions (see fig. 12) consist of photonic corrections to both the γ and Z exchange Born diagrams :

$$\delta M_B^{QED} = \delta M_B^{\gamma\gamma} + \delta M_B^{\gamma Z} + \delta M_B^{Z\gamma}\;. \tag{3.51}$$

The structure of the corresponding contributions to the $\mathcal{O}(\alpha)$ corrected matrix element is almost the same as in the case of boxes with two heavy gauge boson

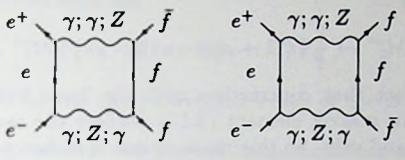

Fig. 12. QED boxes

exchange given by (3.39-3.43). The first step is to specify the mass parameters and the various couplings which have to be inserted :

$$\begin{aligned}
\gamma\gamma \text{ boxes} \quad &: \quad \lambda_\kappa^\pm = \bar{\lambda}_\kappa^\pm = Q_e^2 Q_f^2 \ , \ P_f^\pm = 1 \\
&\quad \text{and} \quad M_1, M_2, M_3, M_4 = m_e, \lambda, m_f, \lambda \\
\gamma Z \text{ boxes} \quad &: \quad \lambda_\kappa^\pm = \bar{\lambda}_\kappa^\mp = Q_e Q_f g_e^\kappa g_f^{\pm\kappa} \ , \ P_f^\pm = 1 \\
&\quad \text{and} \quad M_1, M_2, M_3, M_4 = m_e, \lambda, m_f, M_Z \\
Z\gamma \text{ boxes} \quad &: \quad \lambda_\kappa^\pm = \bar{\lambda}_\kappa^\pm = Q_e Q_f g_e^\kappa g_f^{\pm\kappa} \ , \ P_f^\pm = 1 \\
&\quad \text{and} \quad M_1, M_2, M_3, M_4 = m_e, M_Z, m_f, \lambda \ . \qquad (3.52)
\end{aligned}$$

The second step involves the inclusion of the resummations as a consequence of the resonant nature of the γZ and $Z\gamma$ boxes. Now we have to be careful! There are two things which have to be kept in mind :

- the resummed propagators are situated inside the box integral
- we have to maintain the gauge invariant prescription.

It should be noted that the resonant behaviour of these boxes originates from that part of the integration region where the photon momentum goes to zero displaying the close relation to the interference soft bremsstrahlung contributions. In that particular limit the resummation has all the features of the Born resummation leading to the dressed Born. Our prescription is the following : calculate the box integrals with a complex Z gauge boson mass by adding the physical width. This removes the unpleasant loop momentum dependence of the resummed propagators from the integrals and at the same time incorporates the resonance effects originating from the remaining part of the integration region. Afterwards the result will be given the full s dependence of the dressed Born propagators by multiplying with an appropriate factor. This of course involves an approximation as we will give the non-resonant parts the same s dependence as the resonant parts.

In the case of light final state fermions these box contributions take on a particularly compact form (compared to the general expressions) provided we apply the

following replacement :

$$M_2^{\rho\kappa} \to \frac{1}{4}\left\{t\,(1+\rho\kappa) - u\,(1-\rho\kappa)\right\} M_1^{\rho\kappa} \ ,$$

which displays the fact that contraction with the basic helicity amplitude $M_1^{\rho\kappa}$ appearing in the Born matrix element (2.11) renders the same result for the left hand and the right hand side. So this replacement is in fact an effective one rather than an absolute one. Applying integral and reduction techniques described in the last chapter we arrive at the following QED box contributions :

1. the $\gamma\gamma$ boxes yield a contribution given by

$$\delta M_B^{\gamma\gamma} = Q_e^2 Q_f^2 \frac{\chi_\gamma(s)}{s} \sum_\rho M_1^{\rho\kappa} \left\{V^{\gamma\gamma} + \rho\kappa\, A^{\gamma\gamma}\right\} \ , \tag{3.53}$$

with

$$\begin{aligned} A^{\gamma\gamma} &= \frac{\alpha}{2\pi}\left[G(s,t) + G(s,u)\right] \\ V^{\gamma\gamma} &= \frac{\alpha}{2\pi}\left[G(s,t) - G(s,u) + 2\log\left(\frac{\lambda^2}{-s-i\epsilon}\right)\log\left(\frac{t}{u}\right)\right] \end{aligned} \tag{3.54}$$

and

$$G(s,t) = \frac{s}{2\,(s+t)}\log\left(\frac{t}{s+i\epsilon}\right) - \frac{s\,(s+2t)}{4\,(s+t)^2}\left[\log^2\left(\frac{t}{s+i\epsilon}\right) + \pi^2\right] \ . \tag{3.55}$$

2. the γZ and $Z\gamma$ boxes yield a contribution given by

$$\delta M_B^{\gamma Z} + \delta M_B^{Z\gamma} = Q_e Q_f g_e^\kappa \frac{\chi_Z(s)}{s} \sum_\rho M_1^{\rho\kappa} g_f^\rho \left\{V^{\gamma Z} + \rho\kappa\, A^{\gamma Z}\right\} \ , \tag{3.56}$$

with

$$\begin{aligned} A^{\gamma Z} &= \frac{\alpha}{2\pi}\left[A(s,t) + A(s,u)\right] \\ V^{\gamma Z} &= \frac{\alpha}{2\pi}\left[A(s,t) - A(s,u) + 2\,Li_2\left(1+\frac{M^2}{t}\right) - 2\,Li_2\left(1+\frac{M^2}{u}\right)\right. \\ &\qquad \left. +\ 4\log\left(\frac{M\lambda}{M^2-s}\right)\log\left(\frac{t}{u}\right)\right] \end{aligned} \tag{3.57}$$

and

$$\begin{aligned} A(s,t) &= \frac{s-M^2}{s+t}\left\{\log\left(\frac{t}{s-M^2}\right) + \frac{M^2}{s}\log\left(1-\frac{s}{M^2}\right)\right. \\ &\quad + \frac{s+2t+M^2}{s+t}\left[\log\left(-\frac{t}{M^2}\right)\log\left(\frac{M^2-s}{M^2+t}\right) + Li_2\left(\frac{s}{M^2}\right)\right. \\ &\qquad \left.\left. -\ Li_2\left(-\frac{t}{M^2}\right)\right]\right\} \ , \end{aligned} \tag{3.58}$$

using the shorthand notation

$$M^2 \equiv M_Z^2 - iM_Z\Gamma_Z \ ,$$

where Γ_Z stands for the $\mathcal{O}(\alpha)$ corrected width of the Z gauge boson.

The Feynman diagrams for real photon bremsstrahlung as displayed in fig. 13 are obtained from the Born ones by attaching a photon to each charged fermion line. We will indicate the separate bremsstrahlung matrix elements corresponding

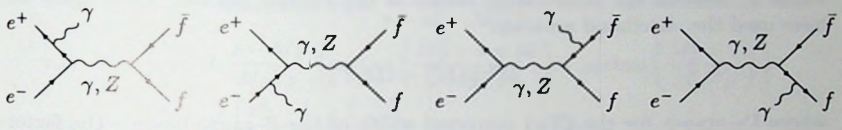

Fig. 13. Real photon bremsstrahlung diagrams

to the γ and Z exchange Born diagrams by

$$M_{brems} = M^{\gamma}_{brems} + M^{Z}_{brems} \ . \tag{3.59}$$

For our aim to come to an IR-finite cross section the soft photon approximation will be sufficient. In many situations of practical experimental interest also hard photons have to be included. They can be incorporated in a second step by means of Monte Carlo techniques independently of the electroweak virtual corrections [10]. With k denoting the 4-momentum of the emitted photon the soft approximation is characterized in the CM system of the initial state electron-positron pair by

$$\begin{aligned} &\lambda \leq k_0 \leq \omega \ll \sqrt{s} \\ &s = (p_+ + p_-)^2 \\ &s' = (p_+ + p_- - k)^2 = (q + \bar{q})^2 \\ &s - s' = 4Ek_0 \ , \end{aligned} \tag{3.60}$$

for a fixed maximum photon energy ω and an IR mass regulator λ in analogy to the IR regulation method adopted in the case of the virtual QED corrections listed above. The energy loss in the photon and Z gauge boson propagators due to single soft photon emission is very small, but in the case of a near resonance Z propagator and soft photon radiation off the initial state e^+e^- not necessarily negligible compared to the size of the resonance related to the width of the Z gauge boson. Applying the soft approximation we arrive at the following resummed matrix

elements for single soft photon radiation according to a soft version of the notation of (3.59) :

$$M^{\gamma}_{soft} = -e\left\{Q_f\left[\frac{\bar{q}^\mu}{\bar{q}.k}-\frac{q^\mu}{q.k}\right]+Q_e\left[\frac{p_-^\mu}{p_-.k}-\frac{p_+^\mu}{p_+.k}\right]\right\}\epsilon_\mu M_\gamma^{(0)}(\kappa;\eta,\bar{\eta};s,t)$$
$$M^{Z}_{soft} = -e\left\{Q_f\left[\frac{\bar{q}^\mu}{\bar{q}.k}-\frac{q^\mu}{q.k}\right]+Q_e\frac{s-M^2}{s'-M^2}\left[\frac{p_-^\mu}{p_-.k}-\frac{p_+^\mu}{p_+.k}\right]\right\}\epsilon_\mu M_Z^{(0)}(\kappa;\eta,\bar{\eta};s,t)\,, \tag{3.61}$$

where ϵ_μ denotes the polarization vector of the emitted photon. Once again we have used the shorthand notation

$$M^2 \equiv M_Z^2 - iM_Z\Gamma_Z\,,$$

where Γ_Z stands for the $\mathcal{O}(\alpha)$ corrected width of the Z gauge boson. The factor $(s-M^2)/(s'-M^2)$ in the last term is, in analogy to the QED boxes, an approximate form of $\chi_Z(s')/\chi_Z(s)$ in order to be able to perform the soft photon phase space integral. The soft approximation as has been applied to the full bremsstrahlung matrix elements involves neglecting all terms proportional to some positive power in k in the numerator while at the same time keeping the k dependence in the Z gauge boson propagators as far as initial state bremsstrahlung is concerned (changing the energy in the Z propagator). Consequently the spinors are identical to the ones appearing when considering 2-particle final states with corresponding 4-momentum conservation $p_+ + p_- = q + \bar{q}$. After integrating isotropically over the photon phase space restricted by $k_0 \le \omega$ this results in a 2-particle cross section

$$\frac{d\sigma}{d\Omega}^{soft}(\kappa;s,\cos\theta) = \frac{\alpha^2}{4s}N_c^f\,\beta\sum_{\eta,\bar{\eta}}\Big\{\delta^{\gamma\gamma}_{soft}\,|M_\gamma^{(0)}(\kappa;\eta,\bar{\eta};s,t)|^2+\delta^{ZZ}_{soft}\,|M_Z^{(0)}(\kappa;\eta,\bar{\eta};s,t)|^2$$
$$+2\,\mathrm{Re}\left[\delta^{\gamma Z}_{soft}\,M_Z^{(0)}(\kappa;\eta,\bar{\eta};s,t)\,M_\gamma^{(0)\,*}(\kappa;\eta,\bar{\eta};s,t)\right]\Big\}\,, \tag{3.62}$$

where the soft factors δ_{soft} displaying the multiplicative character of the soft corrections with respect to the Born cross section constituents are given by :

$$\begin{aligned}\delta^{\gamma\gamma}_{soft} &= \gamma_{IR}+\gamma_\delta+\gamma_{fin}\\ \delta^{\gamma Z}_{soft} &= \gamma_{IR}+\gamma_\delta^{int}+\gamma_{fin}\\ \delta^{ZZ}_{soft} &= \gamma_{IR}+\gamma_\delta^{res}+\gamma_{tail}+\gamma_{fin}\,.\end{aligned} \tag{3.63}$$

The functions contained in the soft factors can be expressed as

$$\gamma_{IR} = -\frac{\alpha}{\pi}\log\left(\frac{\lambda^2}{s}\right)\left\{Q_e^2\,B_e+Q_f^2\,B_f+Q_eQ_f\,B_{int}\right\}$$

$$
\begin{aligned}
\gamma_\delta &= \frac{2\alpha}{\pi}\log(\delta)\left\{Q_e^2 B_e + Q_f^2 B_f + Q_e Q_f B_{int}\right\} \\
\gamma_\delta^{int} &= \frac{2\alpha}{\pi}\left\{Q_e^2 B_e \log\left(\delta\,\frac{s-M^2}{s-s\delta-M^2}\right) + Q_f^2 B_f \log(\delta)\right. \\
&\quad \left. + \frac{1}{2} Q_e Q_f B_{int} \log\left(\delta^2\,\frac{s-M^2}{s-s\delta-M^2}\right)\right\} \\
\gamma_\delta^{res} &= \frac{2\alpha}{\pi}\left\{Q_e^2 B_e \log\left|\delta\,\frac{s-M^2}{s-s\delta-M^2}\right| + Q_f^2 B_f \log(\delta)\right. \\
&\quad \left. + Q_e Q_f B_{int} \log\left|\delta\,\frac{s-M^2}{s-s\delta-M^2}\right|\right\} \\
\gamma_{tail} &= \frac{2\alpha}{\pi} Q_e^2 B_e \frac{s-M_Z^2}{M_Z\Gamma_Z}\left\{\arctan\left(\frac{M_Z^2-s+s\delta}{M_Z\Gamma_Z}\right) - \arctan\left(\frac{M_Z^2-s}{M_Z\Gamma_Z}\right)\right\} \\
\gamma_{fin} &= -\frac{\alpha}{\pi}\left\{Q_e^2\left[\frac{\pi^2}{3} - \frac{1}{2} + \frac{1}{2}B_e^2\right]\right. \\
&\quad + Q_f^2\left[\frac{1}{\beta}\log(-x_f) + \frac{s-2m_f^2}{s\beta}\left(2\,Li_2(1+x_f) + \frac{1}{2}\log^2(-x_f)\right)\right] \\
&\quad \left. + 2Q_eQ_f\left[Li_2\left(1-\frac{1-\beta}{1-\beta\cos\theta}\right) + Li_2\left(1-\frac{1+\beta}{1-\beta\cos\theta}\right)\right.\right. \\
&\quad \left.\left. - Li_2\left(1-\frac{1-\beta}{1+\beta\cos\theta}\right) - Li_2\left(1-\frac{1+\beta}{1+\beta\cos\theta}\right)\right]\right\}\,,
\end{aligned}
\tag{3.64}
$$

where we have introduced the following shorthand notations :

$$
\begin{aligned}
\delta &\equiv \frac{2\omega}{\sqrt{s}} = \frac{\omega}{E} \\
x_f &\equiv -K(s,m_f,m_f) = \frac{\beta-1}{\beta+1} \\
B_e &\equiv \log\left(\frac{s}{m_e^2}\right) - 1 \\
B_{int} &\equiv 2\,\log\left(\frac{1-\beta\cos\theta}{1+\beta\cos\theta}\right) \\
B_f &\equiv -\frac{s-2m_f^2}{s\beta}\log(-x_f) - 1\,.
\end{aligned}
\tag{3.65}
$$

4 The width of the Z gauge boson

4.1 Introduction

One of the basic measurements to take place at LEP and SLC will be the determination of the width of the Z gauge boson with an accuracy of about 50 MeV, probably 20 MeV [1,2]. This requires an adequate theoretical accuracy on the elctroweak corrected Γ_Z of about 10 MeV as the uncertainty from the experimental error in α_S can be estimated to be about 12 MeV. Furthermore the width of the Z gauge boson is an important constituent of the expressions related to fermion pair production from e^+e^- annihilation as has become clear from the last sections. The precise value of Γ_Z is also of great importance to the precision measurement of M_Z because of the fact that bremsstrahlung emission from the initial state influences the Z resonance line shape significantly with Γ_Z acting as a measure of that peak deformation [11]. For these purposes it is necessary (see section 3) to treat next order corrections to the Z width. We will give explicit expressions for the $\mathcal{O}(\alpha)$ corrections to the various partial fermionic widths describing the decay modes $Z \to f\bar{f}$ which means that we will in this way cover 2-loop corrections to the imaginary part of the inverse Z propagator $D_Z^{-1}(s)$ at $s = M_Z^2$. We pay attention to the partial widths as they will give information about the weak coupling constants for the various types of fermions at the level of quantum corrections. To this end we will also cover fermionic decay modes with specific helicities. The notation adopted here is the one used in [12].

4.2 Lowest order results

In lowest order the Z propagator has the Breit-Wigner form

$$D_Z^{(0)}(s) = \frac{1}{s - M_Z^2 + iM_Z\Gamma_Z^0} \,. \tag{4.1}$$

The lowest order total width Γ_Z^0 is related to the 1-loop 1PI renormalized transverse self energy $\hat{\Sigma}^Z(s)$ of the Z gauge boson by

$$M_Z\Gamma_Z^0 = \mathrm{Im}\,\hat{\Sigma}^Z(s = M_Z^2) = \mathrm{Im}\,\Sigma^Z(s = M_Z^2) \,. \tag{4.2}$$

It can be written as the sum of the partial fermionic decay widths $\Gamma_Z^0(f\bar{f})$ with $m_f < M_Z/2$ as follows :

$$\Gamma_Z^0 = \sum_f \Gamma_Z^0(f\bar{f}) \,. \tag{4.3}$$

It should be noted that the present experimental status is such that the decay mode $Z \to t\bar{t}$ has been ruled out as $m_t > M_Z/2$. The partial widths appearing in (4.3)

can be expressed in terms of the vector and axial vector coupling constants (2.19) of the fermion f to the Z gauge boson in the following way :

$$\Gamma_Z^0(f\bar{f}) = N_c^f \frac{\alpha}{3} M_Z \beta_Z \left\{ v_f^2 (1 + \frac{2m_f^2}{M_Z^2}) + a_f^2 \beta_Z^2 \right\} , \tag{4.4}$$

where the definitions of any of the occuring objects can be found in section 2. For actual calculations the dependece on s_w^2 respectively M_W will be eliminated as discussed in section 7 of chapter II.

Making use of the lowest order version of relation (*II*.7.3), which means taking Δr to be 0, and (*II*.7.4) we can write down another possible tree level representation of the partial decay width

$$\bar{\Gamma}_Z^0(f\bar{f}) = N_c^f \frac{G_\mu M_Z^3}{24\pi\sqrt{2}} \beta_Z \left\{ \beta_Z^2 + [1 - 4|Q_f| s_w^2]^2 (1 + \frac{2m_f^2}{M_Z^2}) \right\} \tag{4.5}$$

leading to the Born total width in the G_μ representation :

$$\bar{\Gamma}_Z^0 = \sum_f \bar{\Gamma}_Z^0(f\bar{f}) . \tag{4.6}$$

Because of their applicability to approximations for on-resonance cross sections and asymmetries in 4-fermion processes we will also consider the case of Z decay modes with definite helicities. To this end we introduce the spin projection operators

$$\Sigma(s_f) = \frac{1 + \gamma_5 \not{s}_f}{2} \quad \text{and} \quad \Sigma(\bar{s}_f) = \frac{1 + \gamma_5 \not{\bar{s}}_f}{2} , \tag{4.7}$$

where s_f and $\bar{s}_f$ denote the spin polarization vectors corresponding to f respectively $\bar{f}$, which have the features

$$s_f^2 = \bar{s}_f^2 = -1 \quad \text{and} \quad s_f.q = \bar{s}_f.\bar{q} = 0 . \tag{4.8}$$

As a consequence of the general spin projection operator identity

$$\Sigma(s) + \Sigma(-s) = 1 \tag{4.9}$$

the above spin projection operators allow for a decomposition into polarized states. In order to describe definite helicity states by means of the spin polarization vectors s_f^η and $\bar{s}_f^{\bar{\eta}}$ we have to add the extra conditions

$$\frac{\vec{s}_f^{\,\eta}}{|\vec{s}_f^{\,\eta}|} = \eta \frac{\vec{q}}{|\vec{q}|} \quad \text{and} \quad \frac{\vec{\bar{s}}_f^{\,\bar{\eta}}}{|\vec{\bar{s}}_f^{\,\bar{\eta}}|} = \bar{\eta} \frac{\vec{\bar{q}}}{|\vec{\bar{q}}|} , \tag{4.10}$$

where η and $\bar{\eta}$ denote the helicities of the final state fermions. In the CM system of the fermions hence in the rest system of the decaying Z these spin polarization vectors s_f^η and $\bar{s}_f^{\bar{\eta}}$ take on the form

$$\begin{aligned} s_f^\eta &= \frac{\eta}{\beta_Z}\left[\frac{q}{m_f} - \frac{2m_f}{M_Z}\frac{q+\bar{q}}{M_Z}\right] \\ \bar{s}_f^{\bar{\eta}} &= \frac{\bar{\eta}}{\beta_Z}\left[\frac{\bar{q}}{m_f} - \frac{2m_f}{M_Z}\frac{q+\bar{q}}{M_Z}\right] . \end{aligned} \tag{4.11}$$

Implementing the spin projection operators corresponding to the helicity related spin polarization vectors (4.11) in the fermion currents leads to the following effective behaviour :

$$\begin{aligned} \Sigma(s_f^\eta)\,u(q) &= \left[\frac{1+\frac{\eta}{\beta_Z}\gamma_5\left(1-\frac{2m_f}{M_Z}\gamma_0\right)}{2}\right] u(q) \equiv \bar{\Sigma}_\eta\, u(q) \\ \bar{u}(q)\,\Sigma(s_f^\eta) &= \bar{u}(q)\left[\frac{1-\frac{\eta}{\beta_Z}\gamma_5\left(1+\frac{2m_f}{M_Z}\gamma_0\right)}{2}\right] \equiv \bar{u}(q)\,\bar{\Sigma}_\eta \\ \Sigma(\bar{s}_f^{\bar{\eta}})\,v(\bar{q}) &= \left[\frac{1-\frac{\bar{\eta}}{\beta_Z}\gamma_5\left(1+\frac{2m_f}{M_Z}\gamma_0\right)}{2}\right] v(\bar{q}) = \bar{\Sigma}_{\bar{\eta}}\,v(\bar{q}) \\ \bar{v}(\bar{q})\,\Sigma(\bar{s}_f^{\bar{\eta}}) &= \bar{v}(\bar{q})\left[\frac{1+\frac{\bar{\eta}}{\beta_Z}\gamma_5\left(1-\frac{2m_f}{M_Z}\gamma_0\right)}{2}\right] = \bar{v}(\bar{q})\,\Sigma_{\bar{\eta}} . \end{aligned} \tag{4.12}$$

By applying the above given helicity projection operators we can decompose the lowest order partial Z width according to (4.9) into contributions originating from the various decay modes with definite helicity :

$$\Gamma_Z^0(f\bar{f}) = \sum_{\eta,\bar{\eta}} \Gamma_Z^0(f,\eta;\bar{f},\bar{\eta}) , \tag{4.13}$$

with

$$\begin{aligned} \Gamma_Z^0(f,\eta;\bar{f},\bar{\eta}) &= N_c^f \frac{\alpha}{24} M_Z \beta_Z \left\{\delta_{-\bar{\eta}}^{\eta}\left[(1+\beta_Z)\,g_f^\eta + (1-\beta_Z)\,g_f^{-\eta}\right]^2\right. \\ &\qquad \left. + 2\,\frac{m_f^2}{M_Z^2}\,\delta_{\bar{\eta}}^{\eta}\left[g_f^+ + g_f^-\right]^2\right\} . \end{aligned} \tag{4.14}$$

The small fermion mass limit renders the well known result

$$\Gamma_Z^0(f_L,\eta;\bar{f}_L,\bar{\eta}) = N_c^{f_L}\frac{\alpha}{6} M_Z\,\delta_{-\bar{\eta}}^{\eta}\,(g_{f_L}^\eta)^2 . \tag{4.15}$$

4.3 QCD corrections

QCD corrections to the hadronic partial widths for $Z \to q\bar{q}$ can easily be included by multiplying each electroweak corrected partial width $\Gamma_{ew}(q\bar{q})$ by the QCD correction factor $1 + \delta^q_{QCD}$ [13,14], which yields in the massless quark approximation :

$$\Gamma_{ew+QCD}(q\bar{q}) = \Gamma_{ew}(q\bar{q}) \left\{ 1 + \frac{\alpha_s(M_Z^2)}{\pi} + \left(\frac{\alpha_s(M_Z^2)}{\pi} \right)^2 (1.98 - 0.115\, n_f) \right\} , \quad (4.16)$$

with n_f = number of flavours.

This QCD part will be included using the following value for α_s :

$$\alpha_s(M_Z^2) = 0.12 \pm 0.02 , \quad (4.17)$$

according to [15]

$$\alpha_s([34\ \text{GeV}]^2) = 0.138 \pm 0.023 . \quad (4.18)$$

For QCD corrections involving massive quarks we can refer to [13,16]. When considering bottom quarks, the heaviest of the Z decay fermions, these mass effects prove to be not very important, just as in fact the second order term of (4.16).

4.4 Electroweak corrections

The partial widths (4.4) in lowest order are influenced by next order corrections in terms of the vector boson self energies, external wave function renormalization factors of the fermions, irreducible vertex corrections and real photonic corrections. The result is a physical electroweak corrected quantity that is hence free of gauge dependence and which is related to the gauge independent imaginary part of the on-shell renormalized transverse Z gauge boson self energy.

The first modification of the lowest order Z propagator (4.1) will be the replacement of the constant width term by the 1PI renormalized transverse Z gauge boson self energy $\hat{\Sigma}^Z(s)$ taken from appendix I :

$$D_Z(s) = \frac{1}{s - M_Z^2 + \mathrm{Re}\,\hat{\Sigma}^Z(s) + i\,\mathrm{Im}\,\hat{\Sigma}^Z(s)} , \quad (4.19)$$

where $\mathrm{Re}\,\hat{\Sigma}^Z(M_Z^2) = 0$ due to the 'on-shell' renormalization procedure. In subsection 3.2 one can find the interpretation of this modified Z propagator in perturbation language. Around the Z pole approximately a Breit-Wigner form

$$D_Z(s) = \frac{1}{1 + \hat{\Pi}^Z(M_Z^2)} \frac{1}{s - M_Z^2 + iM_Z\Gamma_Z^1} \quad (4.20)$$

is recovered by a redefinition of the total width

$$\Gamma_Z^1 = \frac{\Gamma_Z^0}{1 + \hat{\Pi}^Z(M_Z^2)} \quad (4.21)$$

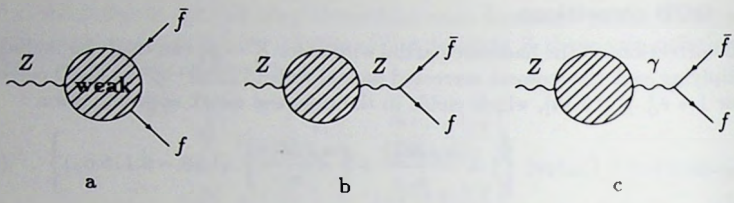

Fig. 14. Weak corrections to the $Z \to f\bar{f}$ partial widths

with Γ_Z^0 from (4.3) and

$$\hat{\Pi}^Z(M_Z^2) = \frac{\partial \operatorname{Re} \hat{\Sigma}^Z}{\partial s}(M_Z^2) \; . \tag{4.22}$$

This global normalization (4.21) corresponds to a resummed version of the wave function renormalization of the Z line as displayed in the decay diagram b of fig. 14. This resummation concerns only the gauge independent part as mentioned before. For each partial width this means that (4.4) has to be multiplied by a common factor :

$$\Gamma_Z^1(f\bar{f}) = \Gamma_Z^0(f\bar{f}) \left(1 + \hat{\Pi}^Z(M_Z^2)\right)^{-1} \; . \tag{4.23}$$

Furthermore, the relation (*II*.7.3) can be utilized in order to reexpress this in terms of the Fermi constant G_μ, yielding :

$$\Gamma_Z^1(f\bar{f}) = \bar{\Gamma}_Z^0(f\bar{f}) \frac{1 - \Delta r}{1 + \hat{\Pi}^Z(M_Z^2)} \tag{4.24}$$

with $\bar{\Gamma}_Z^0(f\bar{f})$ from (4.5). $\bar{\Gamma}_Z^0$ turns out to be a sufficiently good approximation (for $m_t < 100$ GeV and $M_H = 100, 1000$ GeV) including already the major part of the 1-loop corrections as a consequence of the fact that the large leading logarithmic contributions from the light fermions

$$\frac{\alpha}{3\pi} \sum_{f_L} Q_{f_L}^2 \log\left(\frac{M_Z^2}{m_{f_L}^2}\right)$$

present in both Δr and $\hat{\Pi}^Z(M_Z^2)$ (see appendix I) cancel in (4.24).

In addition to (4.24) we have to incorporate the γZ mixing contribution and the vertex corrections combined with the external fermion self energies as displayed in diagram c respectively diagram a of fig. 14. In case of the $Z \to b\bar{b}$ decay channel the full top mass dependence coming from virtual top quarks present in the vertex corrections to the bbZ vertex as discussed in the last section will be taken into account. All small fermion mass effects will be neglected in those vertex corrections.

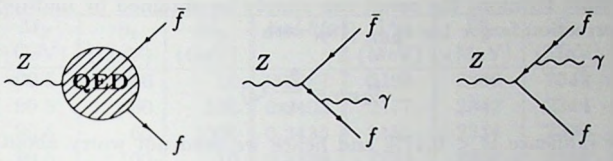

Fig. 15. QED corrections to the $Z \to f\bar{f}$ partial widths

Others than $Z \to f\bar{f}$ decay channels in higher order of the coupling constant (3-body decays) are very small [17]. The largest contribution of that sort comes from $Z \to Hf\bar{f}$ [18] contributing about 5 MeV for a light Higgs (10 GeV).

The final result for the partial width can be written in the following way :

$$\Gamma_Z(f\bar{f}) = \left(\Gamma_Z^0(f\bar{f}) + \Delta\Gamma_Z(f\bar{f})\right)\left(1+\hat{\Pi}^Z(M_Z^2)\right)^{-1} , \tag{4.25}$$

with

$$\Delta\Gamma_Z(f\bar{f}) = \frac{2}{3} N_c^f \, \alpha M_Z \, \mathrm{Re}\left\{ v_f \left[F_V^{Zf,weak}(M_Z^2) + Q_f \frac{\hat{\Sigma}^{\gamma Z}(M_Z^2)}{M_Z^2} \right] + a_f F_A^{Zf,weak}(M_Z^2) \right\} . \tag{4.26}$$

The 1-loop 1PI renormalized γZ mixing self energy $\hat{\Sigma}^{\gamma Z}(M_Z^2)$ can be found in appendix I. The finite vector and axial vector form factors $F_{V,A}^{Zf,weak}$ which include the fermion wave function renormalization factors can be taken from (3.37) in case of the $b\bar{b}$ decay mode and from (3.16) in case of the other light fermion decay modes. Using the following weak corrections to the left and right handed coupling constants :

$$\Delta g_f^\rho = F_V^{Zf,weak}(M_Z^2) + Q_f \frac{\hat{\Sigma}^{\gamma Z}(M_Z^2)}{M_Z^2} - \rho \, F_A^{ZF,weak}(M_Z^2) , \tag{4.27}$$

we can write

$$\Delta\Gamma_Z(f,\eta;\bar{f},\bar{\eta}) = \frac{\alpha}{3} N_c^f \, M_Z \, \delta_{-\eta}^{\eta} \, g_f^\eta \, \mathrm{Re}\left(\Delta g_f^\eta\right) . \tag{4.28}$$

This allows for an expression for the total weak corrected Z gauge boson width per helicity according to (4.25), consisting of (4.14) and (4.28) :

$$\Gamma_Z(f,\eta;\bar{f},\bar{\eta}) = \left(\Gamma_Z^0(f,\eta;\bar{f},\bar{\eta}) + \Delta\Gamma_Z(f,\eta;\bar{f},\bar{\eta})\right)\left(1+\hat{\Pi}^Z(M_Z^2)\right)^{-1} . \tag{4.29}$$

Finally we have to include the QED corrections (see fig. 15) due to virtual photon exchange and real photon bremsstrahlung integrated over the full phase space. For

light final state fermions the result can simply be obtained by multiplying (4.25) with the correction factor $1 + \delta^f_{QED}$ [19], with

$$\delta^f_{QED} = \frac{3\alpha}{4\pi} Q_f^2 \,. \tag{4.30}$$

Its relative influence is $< 0.17\%$ and hence we need not worry about any small corrections coming from the mass of the bottom quark the heaviest of the Z decay fermions.

4.5 Z width : results and discussion

All results going to be presented in this subsection are generated with the following fermion mass parameters as input :

$$m_e = 0.000511 \text{ GeV} \quad , \quad m_\mu = 0.10566 \text{ GeV} \quad , \quad m_\tau = 1.7842 \text{ GeV}$$

$$m_u = m_d = 0.04145 \text{ GeV}$$

$$m_c = 1.5 \text{ GeV} \quad , \quad m_s = 0.15 \text{ GeV} \quad , \quad m_b = 4.5 \text{ GeV} \,.$$

The masses of the light quarks are the effective quark masses representing a suitable parametrization of the dispersion integral results for the hadronic vacuum polarization to be used in the expressions for the renormalized transverse gauge boson self energies as discussed in appendix I. When considering fermion pair production processes involving these light quarks our lack of knowledge about the precise values of the corresponding masses is of no consequence to the practical applications as all remaining finite mass effects vanish for $m_q \to 0$ [20].

Besides the quantities α, G_μ, M_Z, which are sufficient to determine Γ_Z at the tree level, the unknown parameters M_H and m_t enter the higher order result. For our numerical discussion we proceed in the following way. After specifying the values for M_Z, M_H, m_t we derive from ($I\!I$.7.3) the corresponding value for M_W respectively $\sin^2\theta_w$ thus fixing the coupling constants v_f and a_f and the next order terms (4.25) and (4.26). Table 1 contains the total electroweak corrected Z gauge boson width Γ_Z, so QCD corrections are excluded. The tree level values Γ^0_Z correspond to the standard parametrization given in (4.3), $\bar{\Gamma}^0_Z$ is the tree level width (4.6) in the G_μ representation. For top masses not too large ($m_t < 100$ GeV) and $M_H = 100, 1000$ GeV $\bar{\Gamma}^0_Z$ gives already an approximation for the total electroweak corrected width which is good within 3 MeV. For large top masses, however, $\bar{\Gamma}^0_Z$ becomes insufficient as well; in some cases the parametrization Γ^0_Z is the better one. In the case $M_H = 10$ GeV the attempt to use $\bar{\Gamma}^0_Z$ as an approximation for the total electroweak corrected width is less successful : at $m_t = 100$ GeV the deviation is about 10 MeV equaling the aimed theoretical accuracy.

M_Z (GeV)	m_t (GeV)	M_H (GeV)	$\sin^2\theta_w$	Γ_Z^0 (MeV)	$\bar{\Gamma}_Z^0$ (MeV)	Γ_Z (MeV)
90.5	60	10	0.2387	2190	2346	2342
90.5	60	100	0.2403	2177	2342	2344
90.5	60	1000	0.2435	2151	2334	2336
90.5	100	10	0.2338	2233	2357	2348
90.5	100	100	0.2354	2219	2353	2351
90.5	100	1000	0.2386	2191	2346	2344
90.5	150	10	0.2278	2289	2372	2359
90.5	150	100	0.2295	2273	2368	2361
90.5	150	1000	0.2328	2242	2360	2354
90.5	230	10	0.2143	2427	2408	2383
90.5	230	100	0.2161	2407	2403	2386
90.5	230	1000	0.2196	2370	2394	2379
91.0	60	10	0.2350	2235	2394	2390
91.0	60	100	0.2366	2221	2390	2393
91.0	60	1000	0.2397	2194	2382	2385
91.0	100	10	0.2301	2279	2406	2396
91.0	100	100	0.2317	2265	2402	2399
91.0	100	1000	0.2349	2236	2394	2391
91.0	150	10	0.2241	2337	2422	2407
91.0	150	100	0.2257	2322	2417	2410
91.0	150	1000	0.2290	2290	2409	2402
91.0	230	10	0.2106	2483	2459	2432
91.0	230	100	0.2123	2463	2454	2435
91.0	230	1000	0.2158	2424	2444	2428
91.5	60	10	0.2315	2279	2442	2438
91.5	60	100	0.2330	2265	2438	2441
91.5	60	1000	0.2361	2237	2431	2433
91.5	100	10	0.2265	2327	2455	2445
91.5	100	100	0.2281	2311	2451	2448
91.5	100	1000	0.2313	2281	2443	2440
91.5	150	10	0.2205	2387	2472	2456
91.5	150	100	0.2221	2371	2467	2459
91.5	150	1000	0.2254	2337	2458	2451
91.5	230	10	0.2070	2539	2511	2481
91.5	230	100	0.2087	2519	2505	2485
91.5	230	1000	0.2122	2423	2495	2477

Table 1. Total electroweak corrected Z gauge boson width and tree level approximations

The Higgs and top mass dependences of the total width Γ_Z as well as various partial decay widths are put together in table 2 for a fixed value of the Z gauge boson mass ($M_Z = 91$ GeV) and for 5 quark flavours in (4.16). These numbers were generated by the program ZSHAPE [21] based on [5] and this thesis. As far as

m_t (GeV)	M_H (GeV)	$\sin^2\theta_w$	$\Gamma_{Z\to\nu\bar{\nu}}$ (MeV)	$\Gamma_{Z\to e^+e^-}$ (MeV)	$\Gamma_{Z\to u\bar{u}}$ (MeV)	$\Gamma_{Z\to d\bar{d}}$ (MeV)	$\Gamma_{Z\to b\bar{b}}$ (MeV)	Γ_Z (MeV)
60	10	0.2350	164.7	82.6	292.6	378.0	375.6	2458
60	100	0.2366	165.0	82.7	292.7	378.3	376.0	2461
60	1000	0.2397	164.7	82.5	291.4	376.9	374.6	2452
100	10	0.2301	165.0	82.8	293.8	379.3	375.8	2465
100	100	0.2317	165.4	82.9	293.9	379.7	376.1	2468
100	1000	0.2349	165.1	82.7	292.6	378.3	374.8	2459
150	10	0.2241	165.7	83.1	295.8	381.6	375.2	2476
150	100	0.2257	166.0	83.3	295.9	382.0	375.5	2479
150	1000	0.2290	165.7	83.1	294.7	380.6	374.2	2471
230	10	0.2106	167.2	83.8	300.4	387.2	373.3	2501
230	100	0.2123	167.6	84.0	300.6	387.6	373.7	2504
230	1000	0.2158	167.3	83.8	299.4	386.2	372.5	2497

Table 2. Total and partial widths of the Z gauge boson for M_Z=91 GeV ($n_f = 5$)

the total width is concerned the variation with m_t is strong enough that it has to be taken into account if one wants a theoretical precision of 10 MeV. For example the variation of m_t between 60 and 150 GeV leads to an increase in Γ_Z by 18 MeV for $M_H = 100$ GeV. On the other hand, the variation of Γ_Z with the Higgs mass remains smaller than 10 MeV. This is a consequence of the fact that the 1-loop EWRC effects only depend logarithmically on the Higgs mass in the large Higgs mass limit [22]. This is the so-called Higgs mass screening. The uncertainties in the hadronic sector as a consequence of the in appendix I mentioned dispersion integral and related mass fit for the light quarks leads to small uncertainties in Γ_Z ($\approx \pm 1$ MeV) which is of no practical importance.

Also the partial decay widths have a variation with the Higgs mass which is not very striking : 0.4 MeV for the leptonic channels and somewhat more in the hadronic decay modes, but still smaller than 1.5 MeV.

The dependence on m_t is strongest in the $Z \to u\bar{u}$ and $Z \to d\bar{d}$ decays. In the $Z \to b\bar{b}$ decay, however, the top mass dependence is much weaker as a consequence of the additional top mass dependence entering via the vertex corrections involving Yukawa couplings of the isospin changing type cancelling partly the top mass contributions from the reducible gauge boson self energy contributions. This

is exhibited in more detail in table 3 (for $M_Z = 91$ GeV, $M_H = 100$ GeV and without QCD corrections). There the tree level approximations $\bar{\Gamma}^0_Z(f\bar{f})$ as defined

m_t (GeV)	$\bar{\Gamma}^0_Z(d\bar{d})$ (MeV)	$\Delta\Gamma_Z^{weak}(d\bar{d})$ (MeV)	$\bar{\Gamma}^0_Z(b\bar{b})$ (MeV)	$\Delta\Gamma_Z^{weak}(b\bar{b})$ (MeV)
60	363.2	0.5	359.5	0.2
100	365.4	-0.5	361.8	-1.9
150	368.1	-1.0	364.5	-5.2
230	374.4	-1.8	370.8	-13.2

Table 3. Top mass dependence of the weak corrections to $Z \to d\bar{d}, b\bar{b}$

in (4.5) are slightly different for d and b quarks due to the finite mass m_b. The determination of $\sin^2\theta_w$ by means of (*II*.7.3) and the dependence of Δr on m_t are responsible for the variation of $\bar{\Gamma}^0_Z(f\bar{f})$ with the value of m_t. The weak corrections

$$\Delta\Gamma_Z^{weak}(f\bar{f}) = \Gamma_Z(f\bar{f}) - \bar{\Gamma}^0_Z(f\bar{f}) \,, \tag{4.31}$$

containing the weak corrected partial width $\Gamma_Z(f\bar{f})$ from (4.25), induce additional top quark contributions. Those entering via the $Z - Z$ and $Z - \gamma$ propagator corrections are identical for both d and b, whereas the vertex corrections and external quark self energies yield different corrections for d and b final states. For $b\bar{b}$ they tend to cancel the increase of the lowest order term for larger m_t.

Concluding this subsection, our discussion of the Z width has shown that the electroweak corrections play a role for precision experiments, in particular the top mass dependence. The variation with the Higgs mass does not exceed the aimed experimental accuracy.

5 Results and discussion

In this section we will present a range of results covering indirect effects of the unknown mass parameters M_H and m_t entering via the radiative corrections to physically accessible quantities as well as direct top quark production from e^+e^- annihilation. We will not present any Z line shape results as it has been discussed recently to its full extent [11]. In the last section we have discussed the explicit Higgs and top mass dependences of the total as well as partial decay widths of the Z gauge boson. Now we will do the same for the near resonance asymmetries defined in section 2.

$m_t = 60$ GeV			
$\sqrt{s}$	Higgs mass in GeV		
(GeV)	10	100	1000
88.5	-.2245	-.2255	-.2281
89.0	-.1772	-.1783	-.1807
89.5	-.1295	-.1307	-.1330
90.0	-.0818	-.0830	-.0852
90.5	-.0343	-.0356	-.0376
91.0	0.0126	0.0113	0.0094
91.5	0.0588	0.0574	0.0556
92.0	0.1039	0.1024	0.1008
92.5	0.1477	0.1462	0.1447
93.0	0.1901	0.1886	0.1872
93.5	0.2309	0.2293	0.2282

$m_t = 100$ GeV			
$\sqrt{s}$	Higgs mass in GeV		
(GeV)	10	100	1000
88.5	-.2226	-.2236	-.2260
89.0	-.1754	-.1765	-.1788
89.5	-.1278	-.1290	-.1311
90.0	-.0802	-.0814	-.0835
90.5	-.0329	-.0341	-.0360
91.0	0.0140	0.0126	0.0109
91.5	0.0600	0.0586	0.0570
92.0	0.1049	0.1035	0.1021
92.5	0.1487	0.1472	0.1459
93.0	0.1909	0.1894	0.1883
93.5	0.2317	0.2301	0.2291

$m_t = 150$ GeV			
$\sqrt{s}$	Higgs mass in GeV		
(GeV)	10	100	1000
88.5	-.2196	-.2207	-.2230
89.0	-.1726	-.1738	-.1760
89.5	-.1253	-.1265	-.1285
90.0	-.0779	-.0792	-.0811
90.5	-.0308	-.0321	-.0339
91.0	0.0157	0.0144	0.0128
91.5	0.0615	0.0601	0.0586
92.0	0.1062	0.1047	0.1034
92.5	0.1497	0.1482	0.1470
93.0	0.1917	0.1902	0.1892
93.5	0.2322	0.2306	0.2297

$m_t = 230$ GeV			
$\sqrt{s}$	Higgs mass in GeV		
(GeV)	10	100	1000
88.5	-.2137	-.2149	-.2170
89.0	-.1673	-.1686	-.1705
89.5	-.1206	-.1219	-.1237
90.0	-.0739	-.0752	-.0768
90.5	-.0275	-.0288	-.0303
91.0	0.0184	0.0170	0.0157
91.5	0.0635	0.0621	0.0610
92.0	0.1076	0.1061	0.1052
92.5	0.1504	0.1489	0.1481
93.0	0.1919	0.1904	0.1897
93.5	0.2319	0.2303	0.2298

Table 4. Weak corrected forward-backward asymmetry for $M_Z = 91$ GeV

$m_t = 60$ GeV			
$\sqrt{s}$	Higgs mass in GeV		
(GeV)	10	100	1000
88.5	0.0971	0.0911	0.0822
89.0	0.1020	0.0957	0.0864
89.5	0.1068	0.1002	0.0905
90.0	0.1113	0.1044	0.0943
90.5	0.1155	0.1083	0.0979
91.0	0.1194	0.1120	0.1013
91.5	0.1231	0.1154	0.1044
92.0	0.1264	0.1186	0.1072
92.5	0.1294	0.1214	0.1098
93.0	0.1321	0.1240	0.1121
93.5	0.1346	0.1262	0.1142

$m_t = 100$ GeV			
$\sqrt{s}$	Higgs mass in GeV		
(GeV)	10	100	1000
88.5	0.1041	0.0980	0.0891
89.0	0.1094	0.1030	0.0937
89.5	0.1144	0.1078	0.0980
90.0	0.1192	0.1123	0.1022
90.5	0.1237	0.1166	0.1061
91.0	0.1279	0.1205	0.1097
91.5	0.1318	0.1242	0.1130
92.0	0.1354	0.1276	0.1161
92.5	0.1386	0.1306	0.1189
93.0	0.1416	0.1334	0.1214
93.5	0.1442	0.1358	0.1237

$m_t = 150$ GeV			
$\sqrt{s}$	Higgs mass in GeV		
(GeV)	10	100	1000
88.5	0.1154	0.1094	0.1005
89.0	0.1213	0.1149	0.1056
89.5	0.1269	0.1202	0.1104
90.0	0.1321	0.1252	0.1151
90.5	0.1371	0.1299	0.1194
91.0	0.1418	0.1343	0.1235
91.5	0.1460	0.1384	0.1272
92.0	0.1500	0.1421	0.1307
92.5	0.1536	0.1455	0.1338
93.0	0.1568	0.1486	0.1366
93.5	0.1596	0.1513	0.1391

$m_t = 230$ GeV			
$\sqrt{s}$	Higgs mass in GeV		
(GeV)	10	100	1000
88.5	0.1423	0.1363	0.1273
89.0	0.1494	0.1430	0.1336
89.5	0.1562	0.1495	0.1397
90.0	0.1626	0.1557	0.1455
90.5	0.1686	0.1615	0.1509
91.0	0.1743	0.1669	0.1560
91.5	0.1795	0.1719	0.1607
92.0	0.1843	0.1765	0.1650
92.5	0.1887	0.1807	0.1689
93.0	0.1926	0.1844	0.1724
93.5	0.1962	0.1878	0.1756

Table 5. Weak corrected left-right asymmetry for $M_Z = 91$ GeV

$m_t = 60$ GeV			
$\sqrt{s}$	Higgs mass in GeV		
(GeV)	10	100	1000
88.5	0.0728	0.0683	0.0617
89.0	0.0765	0.0718	0.0648
89.5	0.0801	0.0751	0.0679
90.0	0.0834	0.0783	0.0707
90.5	0.0866	0.0813	0.0734
91.0	0.0896	0.0840	0.0760
91.5	0.0923	0.0866	0.0783
92.0	0.0948	0.0889	0.0804
92.5	0.0971	0.0911	0.0824
93.0	0.0991	0.0930	0.0841
93.5	0.1009	0.0947	0.0856

$m_t = 100$ GeV			
$\sqrt{s}$	Higgs mass in GeV		
(GeV)	10	100	1000
88.5	0.0780	0.0735	0.0668
89.0	0.0820	0.0773	0.0703
89.5	0.0858	0.0808	0.0735
90.0	0.0894	0.0842	0.0766
90.5	0.0928	0.0874	0.0795
91.0	0.0960	0.0904	0.0823
91.5	0.0989	0.0931	0.0848
92.0	0.1016	0.0957	0.0871
92.5	0.1040	0.0980	0.0892
93.0	0.1062	0.1000	0.0911
93.5	0.1081	0.1019	0.0928

$m_t = 150$ GeV			
$\sqrt{s}$	Higgs mass in GeV		
(GeV)	10	100	1000
88.5	0.0866	0.0820	0.0753
89.0	0.0910	0.0862	0.0792
89.5	0.0951	0.0902	0.0828
90.0	0.0991	0.0939	0.0863
90.5	0.1028	0.0975	0.0896
91.0	0.1063	0.1007	0.0926
91.5	0.1095	0.1038	0.0954
92.0	0.1125	0.1066	0.0980
92.5	0.1152	0.1091	0.1003
93.0	0.1176	0.1114	0.1025
93.5	0.1197	0.1135	0.1043

$m_t = 230$ GeV			
$\sqrt{s}$	Higgs mass in GeV		
(GeV)	10	100	1000
88.5	0.1067	0.1022	0.0955
89.0	0.1120	0.1073	0.1002
89.5	0.1171	0.1122	0.1048
90.0	0.1219	0.1168	0.1091
90.5	0.1265	0.1211	0.1132
91.0	0.1307	0.1252	0.1170
91.5	0.1346	0.1289	0.1205
92.0	0.1382	0.1324	0.1237
92.5	0.1415	0.1355	0.1267
93.0	0.1445	0.1383	0.1293
93.5	0.1471	0.1409	0.1317

Table 6. Weak corrected polarized forward-backward asymmetry for $M_Z = 91$ GeV

The reason for also considering slightly off-resonance asymmetries ($\sqrt{s} \in [M_Z - \Gamma_Z, M_Z + \Gamma_Z]$) is to be found in the fact that on-resonance especially the forward-backward asymmetry is very small (after inclusion of QED corrections), which is not true anymore when extending $\sqrt{s}$ to off-resonance values. As the sensitivity of A_{FB} to the probing quantity $\sin^2\theta_w$ decreases when A_{FB} gets smaller [23] consequently the off-resonance A_{FB} values become more interesting. Furthermore it offers us the opportunity to investigate near resonance s dependences. In table 4 we present for $M_Z = 91$ GeV the forward-backward asymmetry for $e^+e^- \rightarrow \mu^+\mu^-$ including only weak corrections. For a discussion of the QED corrections and their cut dependence we refer to [24], whereas a second order initial state QED evaluation in the leading log approximation can be found in [25]. It should be noted that these QED corrections at the moment do not contain the full incorporation of second order non-leading logarithmic terms. As the unknown mass parameter dependence is completely contained in the weak corrections we forget about the QED corrections and present the weak corrected results. Because of the large influence of QED corrections, however, a complete calculation including non-leading logarithmic terms is in our opinion indispensible in view of the expected precision of the experiments and should hence be considered in the near future. From table 4 we see that the strongest top mass dependence occurs at the smallest $\sqrt{s}$ values : about 5 times the aimed experimental error $\Delta A_{FB} = \pm 0.002$ when going from $m_t = 60$ GeV to $m_t = 230$ GeV. On-resonance the top mass dependence has been reduced by almost a factor of 2 and at $\sqrt{s} = M_Z + \Gamma_Z$ it does not even exceed the experimental error. The Higgs mass dependence is not very striking : about once or twice the experimental error, staying almost the same over the full range of $\sqrt{s}$ values (decreasing slightly). Now we come to the weak corrected left-right asymmetry A_{LR} the quantity best suited for probing the unknown model parameters. The advantages of this particular quantity are :

- A_{LR} is practically independent of the final state fermions. This has been mentioned in section 2 for the Born approximation but can be extended to the weak corrected left-right asymmetry as well as those weak corrections can be regarded as redefinitions of the couplings between fermions and gauge bosons. Hence A_{LR} allows for an inclusive measurement, which means that we will not lose any statistics by having to identify the specific fermions in the final state. This feature starts to weaken as soon as $\sqrt{s}$ values are considered which are off-resonance as a consequence of the Born $\gamma - Z$ interference term. So in case of A_{LR} the on-resonance value or values very close to it have our preference.

- A_{LR} is very little influenced by QED corrections [26]. This is a very handy feature as it switches off the set of corrections which is normally dominant, opening the way for a close investigation of the weak quantum effects.

It should be noted that in case of light quark final states also the QCD corrections to A_{LR} are of very little influence. Bearing in mind the expected experimental error $\Delta A_{LR} = \pm 0.003$ [2] we can see from table 5 for $M_Z = 91$ GeV that we can speak for the first time of a real M_H dependence exceeding the experimental error by a factor of 5 at $\sqrt{s} = M_Z - \Gamma_Z$ increasing to a factor of 6 on-resonance and almost 7 at $\sqrt{s} = M_Z + \Gamma_Z$. The top mass dependence is about 3 times as large. Finally we show the top and Higgs mass dependences of the weak corrected polarized forward-backward asymmetry for $M_Z = 91$ GeV in table 6. Also A_{FB}^{pol} has been shown to get only very small QED corrections [27], but it does not have that nice inclusive feature that makes A_{LR} so interesting. The dependences on the top and Higgs masses are in magnitude almost precisely a factor 3/4 smaller than those of A_{LR} just as the weak corrected asymmetries themselves. This is not surprising as the final state fermions, which we have taken to be muons, have the same couplings to the gauge bosons as electrons and both electron and muon masses can be neglected with respect to the CM energy. At Born level the factor 3/4 automatically follows from (2.21), (2.26) and (2.27). Just as discussed above in the case of A_{LR} this feature also holds for the weak corrected asymmetries. In order to give an idea about the way the Born asymmetries are changed by weak corrections we will give the following set of on-resonance values for $M_Z = 91$ GeV, $M_H = 100$ GeV and $m_t = 100$ GeV :

	A_{FB}	A_{LR}
Born	0.0159	0.1451
dressed Born	0.0178	0.1451
Born + weak	0.0127	0.1205

The influence of the resummation of the Born propagators is quite small as the leading logarithmic terms will cancel in the asymmetries. A final remark concerns the inclusion or exclusion of the weak boxes as given in subsection 3.4. As those weak boxes are $\mathcal{O}(\alpha)$ corrections and moreover not resonant it is obvious that they will lead to very small contributions to the various near resonance asymmetries or cross sections and hence can be left out. All numbers presented above have been produced by an adapted version of the program ZSHAPE [21].

The next interesting set of calculations involving weak corrected asymmetries deals with the in fig. 16 displayed forward-backward asymmetry near the $t\bar{t}$ production threshold as compared to the $c\bar{c}$ forward-backward asymmetry at the same values of $\sqrt{s}$, hence being far from threshold. This displays the difference in behaviour and magnitude of A_{FB} related to mass effects as both c and t quarks have the same couplings to the gauge bosons. It should be noted that in these cases the weak boxes are not at all negligible. They lead to percentual corrections (compared with Born) increasing with the CM energy.

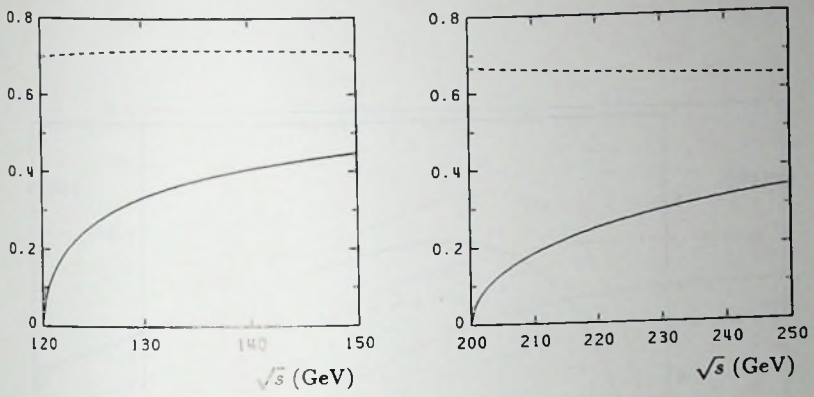

Fig. 16. Forward-backward asymmetry for $M_Z = 91$ GeV and $M_H = 100$ GeV : the dashed line corresponds to $c\bar{c}$ production and the solid line to $t\bar{t}$ production; $m_t = 60$ GeV for the figure on the left and $m_t = 100$ GeV for the figure on the right.

In fig. 17 and fig. 18 the total cross section for top pair production ($m_t = 60$ respectively 100 GeV) from e^+e^- annihilation is displayed. These total cross sections contain besides the weak corrections also the convolution of the weak corrected cross section with the initial state QED corrections up to and including second order with soft photon exponentiation :

$$\sigma(s) = \int_{z_0}^{1} dz\, \sigma_w(sz)\, G(z)\,, \tag{5.1}$$

where the cross section including the weak corrections is denoted by $\sigma_w(sz)$. The invariant mass of the produced top pair is given by

$$s' = sz\,, \tag{5.2}$$

where the invariant mass cut-off z_0 is restricted by

$$\frac{4m_t^2}{s} \leq z_0 \leq z \leq 1\,. \tag{5.3}$$

In both figures we have taken z_0 to be $4m_t^2/s$ in this way reducing the final state QED corrections to the massive version of the QED factor mentioned in subsection 4.4, which hence can be neglected.

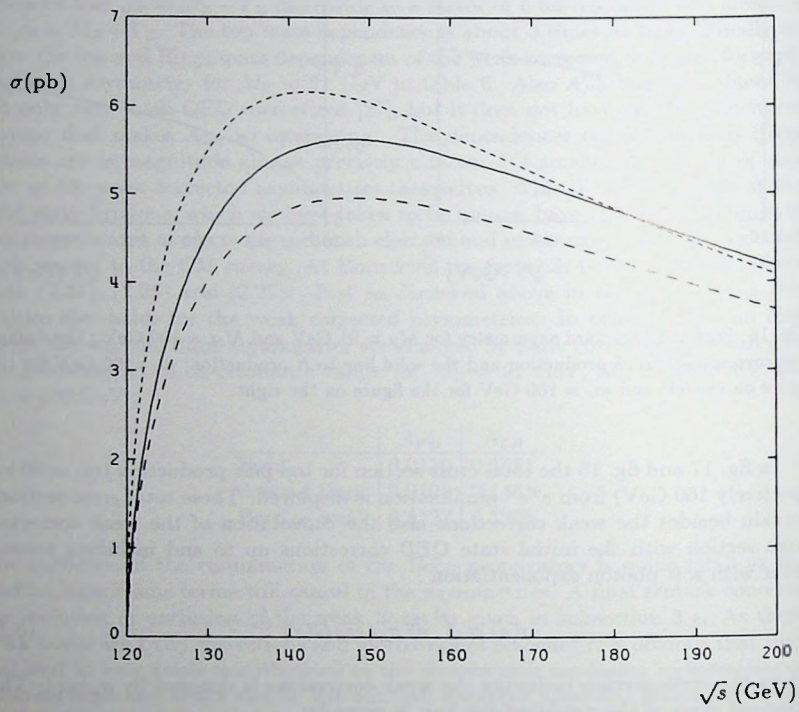

Fig. 17. Total top pair production cross section for $M_Z = 91$ GeV, $M_H = 100$ GeV and $m_t = 60$ GeV : the fine dashed line corresponds to Born + weak, the dashed line to Born + initial state QED convolution and the solid line to Born + weak + initial state QED convolution.

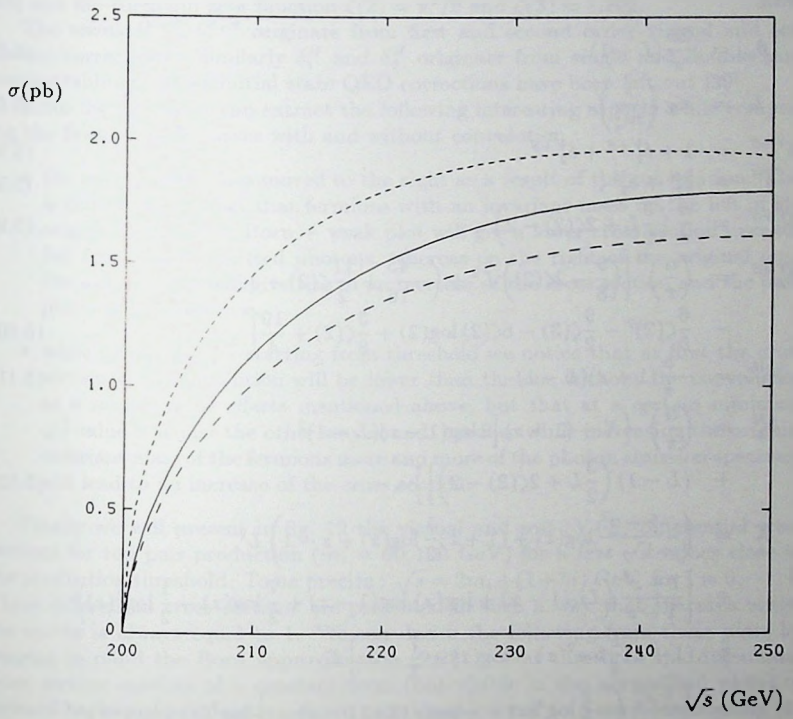

Fig. 18. Total top pair production cross section for $M_Z = 91$ GeV, $M_H = 100$ GeV and $m_t = 100$ GeV : the fine dashed line corresponds to Born + weak, the dashed line to Born + initial state QED convolution and the solid line to Born + weak + initial state QED convolution.

The total flux $G(z)$ is given by

$$G(z) = \beta_e (1-z)^{\beta_e - 1} \delta^{V+S} + \delta^H \,, \tag{5.4}$$

with

$$\beta_e = \frac{2\alpha}{\pi}(L-1)\,, \tag{5.5}$$

$$L = \log\left(\frac{s}{m_e^2}\right) \tag{5.6}$$

$$\delta^{V+S} = 1 + \delta_1^{V+S} + \delta_2^{V+S}\,, \tag{5.7}$$

$$\delta^H = \delta_1^H + \delta_2^H\,, \tag{5.8}$$

$$\delta_1^{V+S} = \frac{\alpha}{\pi}\left(\frac{3}{2}L + 2\zeta(2) - 2\right)\,, \tag{5.9}$$

$$\begin{aligned}\delta_2^{V+S} &= \left(\frac{\alpha}{\pi}\right)^2 \left[\left(\frac{9}{8} - 2\zeta(2)\right)L^2 + \left(-\frac{45}{16} + \frac{11}{2}\zeta(2) + 3\zeta(3)\right)L \right.\\ &- \left. \frac{6}{5}\zeta(2)^2 - \frac{9}{2}\zeta(3) - 6\zeta(2)\log(2) + \frac{3}{8}\zeta(2) + \frac{19}{4}\right]\,,\end{aligned} \tag{5.10}$$

$$\delta_1^H = -\frac{\alpha}{\pi}(1+z)(L-1)\,, \tag{5.11}$$

$$\begin{aligned}\delta_2^H &= \left(\frac{\alpha}{\pi}\right)^2 \left\{X - (1+z)\left[2\log(1-z)(L-1)^2\right.\right.\\ &+ \left.\left.(L-1)\left(\frac{3}{2}L + 2\zeta(2) - 2\right)\right]\right\}\,,\end{aligned} \tag{5.12}$$

$$\begin{aligned}X &= \left(-\frac{1+z^2}{1-z}\log(z) + (1+z)\frac{1}{2}\log(z) + z - 1\right)L^2\\ &+ \left[\frac{1+z^2}{1-z}\left(Li_2(1-z) + \log(z)\,\log(1-z) + \frac{7}{2}\log(z) - \frac{1}{2}\log^2(z)\right)\right.\\ &+ \left.(1+z)\frac{1}{4}\log^2(z) - \log(z) + \frac{7}{2} - 3z\right]L\\ &+ \frac{1+z^2}{1-z}\left(-\frac{1}{6}\log^3(z) + \frac{1}{2}\log(z)\,Li_2(1-z) + \frac{1}{2}\log^2(z)\,\log(1-z)\right.\\ &- \left.\frac{3}{2}\,Li_2(1-z) - \frac{3}{2}\log(z)\,\log(1-z) + \zeta(2)\log(z) - \frac{17}{6}\log(z) - \log^2(z)\right)\\ &+ (1+z)\left(\frac{3}{2}Li_3(1-z) - 2S_{1,2}(1-z) - \log(1-z)\,Li_2(1-z) - \frac{1}{2}\right)\\ &- \frac{1}{4}(1-5z)\log^2(1-z) + \frac{1}{2}(1-7z)\log(z)\,\log(1-z) - \frac{25}{6}z\,Li_2(1-z)\\ &+ (-1 + \frac{13}{3}z)\zeta(2) + (\frac{3}{2} - z)\log(1-z) + \frac{1}{6}(11+10z)\log(z)\\ &+ \frac{2}{(1-z)^2}\log^2(z) - \frac{25}{11}z\log^2(z)\end{aligned}$$

$$- \frac{2}{3}\frac{z}{1-z}\left(1+\frac{2}{1-z}\log(z)+\frac{1}{(1-z)^2}\log^2(z)\right) . \qquad (5.13)$$

In these definitions the polylogarithms $Li_n(x)$ and $S_{n,p}(x)$ have been introduced [28] and the Riemann zeta function $\zeta(2) = \pi^2/6$ and $\zeta(3) \approx 1.202$.

The terms $\delta_1^{V+S}, \delta_2^{V+S}$ originate from first and second order virtual and soft photon corrections. Similarly δ_1^H and δ_2^H originate from single and double hard bremsstrahlung. Other initial state QED corrections have been left out [29].

From the figures we can extract the following interesting aspects while comparing the Born + weak curves with and without convolution :

- the peak position has moved to the right as a result of the convolution. This is caused by the fact that fermions with an invariant mass on the left of the original peak in the Born + weak plot will get a lower cross section over the full spectrum of emitted photons, whereas on the right of the original peak the soft photons will give rise to an increase of the cross section and the hard photons to a decrease.

- while increasing $\sqrt{s}$ starting from threshold we notice that at first the cross section with convolution will be lower than the one without the convolution as a result of the effects mentioned above, but that at a certain minimum $\sqrt{s}$ value it is just the other way round, because while increasing the original invariant mass of the fermions more and more of the photon emission spectrum will lead to an increase of the cross section.

Finally we will present in fig. 19 the virtual and soft (V+S) differential cross sections for top pair production ($m_t = 60, 100$ GeV) for a few $\sqrt{s}$ values close to the production threshold. To be precise : $\sqrt{s} = 2m_t + (1+5i)$ GeV for $i = 0, \cdots, 4$. These differential cross sections are presented in such a way that the area under the curves is always equal to 1. We can derive the following from these plots by keeping in mind the Born approximation (2.22) : near threshold the differential cross section consists of a constant term (not visible in the normalized plots), a forward-backward asymmetry related term proportional to $\beta\cos\theta$ (accounting for the increasing steepness of the curves with increasing $\sqrt{s}$) and a symmetric term proportional to $\beta^2\cos^2\theta$ or $\beta^2\sin^2\theta$ (responsible for the increasing curvature of the curves with increasing $\sqrt{s}$). All this can be seen immediately by investigating the Born differential cross section (2.22) and the functions (2.21). The virtual and soft corrections do not really change this Born picture as they tend to be rather isotropical near threshold.

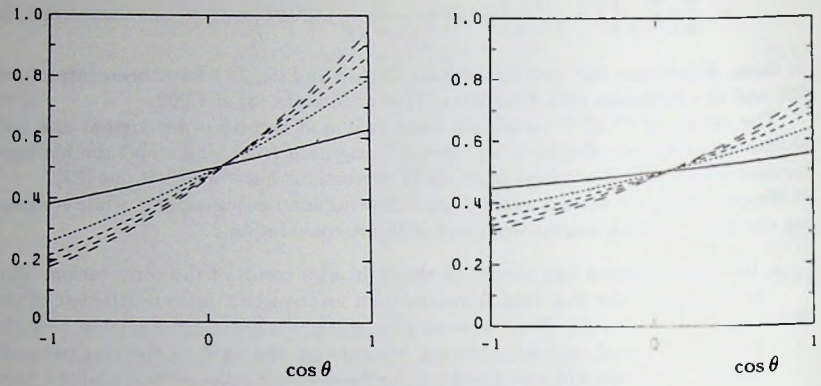

Fig. 19. Differential cross section (V+S) in pb for $M_Z = 91$ GeV and $M_H = 100$ GeV : $m_t = 60$ GeV for the figure on the left and $m_t = 100$ GeV for the figure on the right; the closer to threshold the value of $\sqrt{s}$ gets the finer will be the dash.

References

[1] Yellow CERN Report: "Physics at LEP", eds. J. Ellis and R.D. Peccei, CERN 86-02 (1986).

[2] Yellow CERN Report: "Polarization at LEP", eds. G. Alexander et al., CERN 88-06 (1988).

[3] B.W. Lynn, M. Peskin and R.G. Stuart, in [1];
B.W. Lynn, in [2].

[4] W. Hollik, in [2], and DESY 88-106 (1988).

[5] W. Hollik, DESY 88-188, to be published in Fortschritte der Physik.

[6] M. Böhm, A. Denner and W. Hollik, Nucl. Phys. **B304** (1988) 687.

[7] M. Böhm and T. Sack , Z. Phys. **C35** (1987) 119.

[8] M. Consoli, W. Hollik and F. Jegerlehner, CERN-TH 5395/89 (1989).

[9] W. Beenakker and W. Hollik, in:
Proceedings of the ECFA Workshop on LEP 200, Aachen 1986,
eds. A. Böhm and W. Hoogland, CERN 87-08, ECFA 87/108 (1987).

[10] F.A. Berends and R. Kleiss, Nucl. Phys. **B177** (1981) 237;
F.A. Berends, S. Jadach and R. Kleiss, Nucl. Phys. **B202** (1982) 63.

[11] D. Bardin, W. Beenakker et al., CERN-TH 5468/89 (1989),
to appear in the Proceedings of the Workshop on Z Physics at LEP.

[12] W. Beenakker and W. Hollik, Z. Phys. **C40** (1988) 141.

[13] T.H. Chang, K.J.F. Gaemers and W.L. van Neerven,
Nucl. Phys. B202 (1982). 407.

[14] K.G. Chetyrkin, A.L. Kataev and F.V. Tkachov, Phys. Lett. **85B** (1979) 277;
M. Dine and J. Sapirstein, Phys. Rev. Lett. **43** (1979) 668;
W. Celmaster and R. Gonsalves, Phys. Rev. Lett. **44** (1980) 560.

[15] W. de Boer, SLAC-PUB-4428 (1988):
S.L. Wu, Proceedings of the International Symposium on Lepton
and Photon Interactions, Hamburg 1987, eds. W. Bartel and R. Rückl.

[16] J. Jersak, E. Laerman and P.M. Zerwas, Phys. Rev. **D25** (1980) 1218.

[17] E. Franco, in [1].

[18] F.A. Berends and R. Kleiss, Nucl. Phys. **B260** (1985) 32.

[19] W.J. Marciano and D. Wyler, Z. Phys. **C3** (1979) 81;
D. Albert, W.J. Marciano and D. Wyler, Nucl. Phys. **B166** (1980) 460.

[20] T. Kinoshita, J. Math. Phys. **3** (1962) 650;
T.D. Lee and M. Nauenberg, Phys. Rev. **133** (1964) 1549.

[21] ZSHAPE, authors W. Beenakker, F.A. Berends and S. van der Marck.

[22] M. Veltman, Acta Phys. Pol. **B8** (1977) 475.

[23] G. Altarelli, in [1].

[24] R. Kleiss, in [1].

[25] W. Beenakker, F.A. Berends and W.L van Neerven, Leiden preprint 1989,
to appear in the Proceedings of the Workshop on Electroweak Radiative
Corrections, Ringberg Castle (FRG), 1989.

[26] M. Böhm and W. Hollik, Nucl. Phys. **B204** (1982) 45;
Z. Phys. **C23** (1984) 31;
S. Jadach, J.H. Kühn, R.G. Stuart and Z. Was, Z. Phys. **C38** (1988) 609;
J.H. Kühn and R.G. Stuart, Phys. Lett. **200B** (1988) 360;
D.C. Kennedy, B.W. Lynn, C.J.C. Im and R.G. Stuart,
SLAC-PUB-4128 (1988).

[27] A. Blondel, B.W. Lynn, F.M. Renard and C. Verzegnassi,
Nucl. Phys. **B304** (1988) 438.

[28] R. Barbieri, J.A. Mignaco and E. Remiddi, Nuovo Cim. **11A** (1972) 824,865;
A. Devoto and D.W. Duke, Riv. Nuovo Cim. **7**, No. 6 (1984).

[29] F.A. Berends, G. Burgers and W.L van Neerven,
Nucl. Phys. **B297** (1988) 429; Nucl. Phys. **B304** (1988) 921.

Appendices

Appendix A: Bjorken-Drell metric and summation convention

Any calculation performed in the 4 dimensional Minkowski space in the preceding chapters involves the application of the Bjorken-Drell metric characterized by the metric tensor

$$(g_{\mu\nu}) = \begin{pmatrix} 1 & 0 & 0 & 0 \\ 0 & -1 & 0 & 0 \\ 0 & 0 & -1 & 0 \\ 0 & 0 & 0 & -1 \end{pmatrix} \quad , \quad \mu, \nu = 0, 1, 2, 3 \, . \tag{A.1}$$

A contravariant 4-vector (a^μ) will be denoted by 4 real components as follows :

$$(a^\mu) = (a^0, a^1, a^2, a^3) \, .$$

The corresponding covariant 4-vector (a_μ) can be derived by application of the metric tensor according to the coordinate relation

$$a_\mu = g_{\mu\nu} \, a^\nu \, ,$$

where we have adopted the summation convention that repeated indices are to be summed unless stated otherwise a concept that has been and will be maintained throughout the preceding and forthcoming calculations. Using this convention the contraction between two vectors a and b takes the form :

$$a.b = a^\mu \, b_\mu = a_\mu \, b^\mu = a^\mu \, g_{\mu\nu} \, b^\nu \, . \tag{A.2}$$

In case of dimensional regularization the corresponding Minkowski space will cover n degrees of freedom described by an n-dimensional version of the above given metric tensor (A.1), containing $n - 1$ diagonal elements of the form -1.

Appendix B: Box angular integral for $n = 4$

While applying the Cutkosky cutting rule to a scalar 4-point integral in 4 dimensions, like the one discussed in section 4 of chapter III, one encounters the following

most general angular integral after having performed the l_0 and $|\vec{l}|$ integrals :

$$J = \int d\Omega \, \{ (a + b\cos\theta)(A + B\cos\theta + C\sin\theta\,\cos\phi) \}^{-1} \quad . \tag{B.1}$$

The restrictions on the various cut invariants appearing in the coefficients a, b and A, B, C will lead to the absence of any singularity. So, we can leave out the infinitesimal imaginary offsets $i\epsilon$ and the evaluation below will be restricted by the conditions

$$|b| < |a| \quad \text{and} \quad \sqrt{B^2 + C^2} < |A| \; .$$

The way we have chosen to come to a successful evaluation of J proceeds via Feynman parametrization :

$$J = \int_0^1 dx \int_{-1}^1 d\cos\theta \int_0^{2\pi} d\phi \; \{ \; \alpha(x) + \beta(x)\cos\theta + \gamma(x)\sin\theta\,\cos\phi \; \}^{-2} \quad , \tag{B.2}$$

with

$$\alpha(x) = Ax + a(1-x) \quad , \quad \beta(x) = Bx + b(1-x) \quad , \quad \gamma(x) = Cx \; . \tag{B.3}$$

This can be simplified by realizing that

$$\alpha(x) + \beta(x)\cos\theta + \gamma(x)\sin\theta\,\cos\phi = \alpha(x) + (\,\beta(x), \gamma(x), 0\,) \begin{pmatrix} \cos\theta \\ \sin\theta\,\cos\phi \\ \sin\theta\,\sin\phi \end{pmatrix}$$

is a rotationally invariant expression, which means that a proper rotation can get rid of the ϕ dependence of the integrand of (B.2) and will bring J in the form

$$J = 2\pi \int_0^1 dx \int_{-1}^1 d\cos\theta' \left\{ \alpha(x) + \sqrt{\beta^2(x) + \gamma^2(x)}\,\cos\theta' \right\}^{-2} \quad . \tag{B.4}$$

This results in

$$J = 4\pi \int_0^1 \frac{dx}{\alpha^2(x) - \beta^2(x) - \gamma^2(x)} = \frac{2\pi}{\sqrt{X}} \int_0^1 dx \left[\frac{1}{x - x_+} - \frac{1}{x - x_-} \right] \quad , \tag{B.5}$$

with

$$\begin{aligned} x_\pm &= \left[(A-a)^2 - (B-b)^2 - C^2 \right]^{-1} \left\{ a(a-A) - b(b-B) \pm \sqrt{X} \right\} \\ X &= (aA - bB)^2 - (a^2 - b^2)(A^2 - B^2 - C^2) \end{aligned} \tag{B.6}$$

and hence

$$J = \frac{2\pi}{\sqrt{X}} \log \left(\frac{aA - bB + \sqrt{X}}{aA - bB - \sqrt{X}} \right) \; . \tag{B.7}$$

Appendix C: A special logarithmic integral

Consider the following integral :

$$I = \int_0^t dz \, \frac{\log(z-a)}{z-b} \quad , \quad t \epsilon I\!R \quad \text{and} \quad \begin{cases} a \epsilon \mathbb{C} \setminus \{ x \epsilon I\!R \ : \ x > \min(0,t) \} \\ b \epsilon \mathbb{C} \setminus \{ x \epsilon I\!R \ : \ x \geq \min(0,t) \} \end{cases} . \quad \text{(C.1)}$$

The excluded real b values outside the integration region can be covered by using $-z$ as integration variable. At the moment we will assume b not to be situated on the logarithmic cut or to coincide with the corresponding branching point. Because of the fact that the integrand has a logarithmic cut as well as a pole we will first eliminate the pole by adding a term in such a way that the residue of the pole becomes zero :

$$J \equiv \int_0^t dz \, \frac{1}{z-b} \{ \log(z-a) - \log(b-a) \} . \quad \text{(C.2)}$$

Shift the integration variable according to $y = z - a$, resulting in

$$J = \int_{-a}^{t-a} \frac{dy}{y+a-b} \{ \log(y) - \log(b-a) \} . \quad \text{(C.3)}$$

Now we can make the following replacement :

$$\int_{-a}^{t-a} dy \rightarrow - \int_0^{-a} dy + \int_0^{t-a} dy ,$$

because there are (by construction) no poles or cuts to be found inside the triangle denoted by the points $-a, t-a, 0$ (see fig. 1). Now transform the first of the so

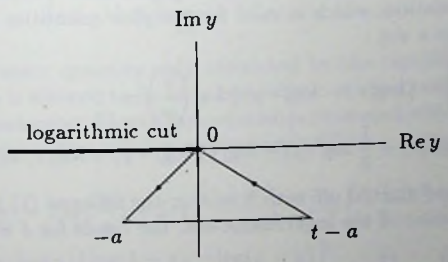

Fig. 1. Triangular integration contour

acquired integrals using $y = -ay'$ and the second integral using $y = (t-a)y'$ resulting in

$$\begin{aligned} J &= -\int_0^1 \frac{dy'}{y' - \frac{a-b}{a}} \{ \log(-ay') - \log(b-a) \} \\ &\quad + \int_0^1 \frac{dy'}{y' + \frac{a-b}{t-a}} \{ \log([t-a]\,y') - \log(b-a) \} \\ &= -\int_0^1 dy' \left[\frac{d}{dy'} \log\left(1 - \frac{ay'}{a-b}\right) \right] \{ \log(-ay') - \log(b-a) \} \\ &\quad + \int_0^1 dy' \left[\frac{d}{dy'} \log\left(1 - \frac{(a-t)y'}{a-b}\right) \right] \{ \log([t-a]\,y') - \log(b-a) \} \\ &= \left[\{ \log(y'-a) - \log(b-a) \} \log\left(\frac{y'-b}{a-b}\right) + Li_2\left(\frac{a-y'}{a-b}\right) \right]_{y'=0}^{y'=t} . \end{aligned} \tag{C.4}$$

This can be rewritten by making use of the dilogarithm relation (D.4) leading to :

$$J = \left[-Li_2\left(\frac{y'-a}{y'-b}\right) - \frac{1}{2}\log^2\left(\frac{y'-b}{a-b}\right) + \{ \log(y'-a) - \log(b-a) \} \log\left(\frac{y'-b}{a-b}\right) \right]_{y'=0}^{y'=t} . \tag{C.5}$$

Now we can complete the determination of I by adding to J the term

$$J' = \int_0^t dz\, \frac{\log(b-a)}{z-b} = \Big[\log(b-a)\, \log(z-b) \Big]_{z=0}^{z=t} , \tag{C.6}$$

yielding

$$I = \left[-Li_2\left(\frac{z-a}{z-b}\right) + \frac{1}{2}\log^2(z-b) + \{ \log(z-b) - \log(z-a) \} \log\left(\frac{a-b}{z-b}\right) \right]_{z=0}^{z=t} , \tag{C.7}$$

which involves a careful handling of the various logarithms. To this end we mention a useful logarithm relation, which is valid for complex quantities provided none of the arguments lies on a cut :

$$\begin{aligned} &\frac{1}{2}\log^2\left(\frac{x}{y}\right) - [\log(x) - \log(-y)] \log\left(\frac{x}{y}\right) = \\ &\quad -\frac{1}{2}\log^2(x) + \frac{1}{2}\log^2(y) - \log(y)\log(-y) + \log(x)\log(-y) . \end{aligned} \tag{C.8}$$

In case we would have started off with $b = a$ in the integral (C.1), so b coincides with the branching point of the logarithmic cut, the result for I would have been :

$$I = \int_0^t dz\, \frac{\log(z-a)}{z-a} = \left[\frac{1}{2}\log^2(z-a) \right]_{z=0}^{z=t} , \quad a \in \mathbb{C} \setminus \{ x \in \mathbb{R} \,:\, x \geq \min(0,t) \} , \tag{C.9}$$

which is consistent with (C.7). Using $b = a - x$ with $x \epsilon I\!R^+$ as starting point in (C.1), so b is situated on the logarithmic cut, an unsubtracted version of the above reasoning can be applied. By unsubtracted we mean that no subtraction of the form (C.2) is needed as the pole $z = b$ being part of the logarithmic cut can not sneak into the triangular contour of fig. 1. The result for I will also in this case be given by (C.7).

Appendix D: Dilogarithm relations

The dilogarithm is defined by means of the integral representation

$$Li_2(z) = -\int_0^z dt\, \frac{\log(1-tz)}{t} \quad , \quad z \epsilon \mathbb{C} \setminus \{ x \epsilon I\!R \ : \ x > 1 \} \, . \tag{D.1}$$

The following set of one parameter dilogarithm relations can come in very handy :

$$Li_2(z) + Li_2(1/z) = -\frac{\pi^2}{6} - \frac{1}{2}\log^2(-z) \tag{D.2}$$

$$Li_2(z) + Li_2(1-z) = \frac{\pi^2}{6} - \log(z)\log(1-z) \tag{D.3}$$

$$Li_2(z) + Li_2\left(\frac{1}{1-1/z}\right) = -\frac{1}{2}\log^2(1-z) \tag{D.4}$$

$$Li_2(1-z) + Li_2(1-1/z) = -\frac{1}{2}\log^2(z) \tag{D.5}$$

$$Li_2(z) + Li_2(-z) = \frac{1}{2}Li_2(z^2) \tag{D.6}$$

$$Li_2(1) = \frac{\pi^2}{6} \tag{D.7}$$

$$Li_2(-1) = -\frac{\pi^2}{12} \, , \tag{D.8}$$

where z is a complex quantity only restricted by the condition that none of the above arguments is allowed to lie on a logarithmic or dilogarithmic cut. For special purposes a two parameter dilogarithm relation is presented which is just the complex version of a corresponding relation appearing in [1] :

$$\begin{aligned} -Li_2(x) + Li_2(y) = {} & Li_2\left(\frac{y}{x}\right) + Li_2\left(\frac{1-x}{1-y}\right) - Li_2\left(\frac{y}{x}\frac{1-x}{1-y}\right) - \frac{\pi^2}{6} \\ & + \log(x)\left[\log(1-x) - \log(1-y)\right] \\ & + \log\left(\frac{1-x}{1-y}\right)\left[\log\left(\frac{x-y}{1-y}\right) - \log(x) - \log\left(\frac{x-y}{x}\right) + \log(1-y)\right] \end{aligned}$$

$$- \log\left(\frac{y}{x}\frac{1-x}{1-y}\right)\left[\log\left(\frac{x-y}{x(1-y)}\right) - \log\left(\frac{x-y}{x}\right) + \log(1-y)\right] , \tag{D.9}$$

where x, y are complex quantities such that none of the arguments lies on a cut.

Appendix E: Continuation procedure

As can be seen from the intermediate result (*III*.4.20) for the IR-divergent scalar 4-point integral (*III*.4.1) the continuation of terms of the form $\log(x_1 x_2 \cdots x_n)$ and $Li_2(1 - x_1 x_2 \cdots x_n)$ is needed to extend its range of validity beyond all possible thresholds. These thresholds will coincide with the crossing of the logarithmic and dilogarithmic cuts originating from the above logarithms and dilogarithms and corresponding to the transition from one Riemann sheet to another. The continuation procedure is just the translation of the exact position on the various Riemann surfaces, in general beyond the first sheet, in terms of expressions defined on the first sheet (the one we started off with) in this way removing any cut structure of D_0 for the full range of real cut invariant values.

- Continuation prescription for $\log(x_1 x_2 \cdots x_n)$:

$$\log\left(\prod_{i=1}^{n} x_i\right) \to \sum_{i=1}^{n} \log(x_i) . \tag{E.1}$$

  As the x_i are situated on the first Riemann sheet the property of absence of any cut becomes obvious.

- As usual the continuation prescription for $Li_2(1 - x_1 x_2 \cdots x_n)$ is somewhat more involved :

$$\begin{aligned} Li_2\left(1 - \prod_{i=1}^{n} x_i\right) \to Li_2\left(1 - \prod_{i=1}^{n} x_i\right) + \left[\log\left(\prod_{i=1}^{n} x_i\right)\right. \\ \left. - \sum_{i=1}^{n} \log(x_i)\right]\left[\log\left(1 - \prod_{i=1}^{n} x_i\right) - \theta\left(|\prod_{i=1}^{n} x_i| - 1\right)\left\{\log\left(-\prod_{i=1}^{n} x_i\right)\right.\right. \\ \left.\left. - \frac{1}{2}\log\left(\prod_{i=1}^{n} x_i\right) - \frac{1}{2}\sum_{i=1}^{n} \log(x_i)\right\}\right] . \end{aligned} \tag{E.2}$$

  This more complicated structure is caused by the double cut structure of the dilogarithm as can be seen from the fact that the discontinuity function (*III*.4.6) across the dilogarithmic cut has itself a cut structure.

In this way one arrives at an expression for D_0 which will contain all possible normal thresholds, as given by the Cutkosky cutting rule, as well as the anomalous ones,

which correspond to the extension of the normal cuts caused by the possibility of the discontinuity function across the normal cut having a branching point that crosses the normal cut while continuating in some of the other cut invariants.

Appendix F: Special scalar integrals for $e^+e^- \to f\bar{f}$

In this appendix the various IR-divergent scalar 3- and 4-point integrals and a scalar 3-point integral containing a 'mass singular' double pole are listed which will enter the specific calculation of the EWRC effects to the process $e^+e^- \to f\bar{f}$. To this end we will adopt the notations used in chapter IV which might involve a definition of the Mandelstam variables s,t which is different from the one used in chapter III (e.g. s and t interchanged). Whenever possible the electron mass m_e will be neglected compared to combinations of the process invariants (like s,t) and other masses (like M_W, M_Z and m_{f_H}). In case of light final state fermions, for instance muons, the same applies to m_{f_L}. The forthcoming integrals will be indicated by specifying the mass parameters appearing in (*III*.4.1) or (*III*.4.26). First we will list some 4-point integrals :

1. $m_1 = m_2 = m_e$, $m_3 = m_4 = m_f$, $m_0 = \lambda$ with supplementary conditions $|t - m_f^2| \gg m_e m_f$, m_e^2 $\Rightarrow$

$$D_0 = \frac{2}{s\,(t - m_f^2)} \log\left(\frac{m_e m_f}{m_f^2 - t - i\epsilon}\right) \log\left(\frac{\lambda^2}{-s - i\epsilon}\right) . \qquad \text{(F.1)}$$

   To be applied to $e^+e^- \to f_H\bar{f}_H$, whereas in the case of $e^+e^- \to f_L\bar{f}_L$ the m_f^2 term can be neglected with respect to t.

2. $m_1 = m_2 = m_e$, $m_3 = m_4 = m_f$, $m_0 = M_Z$ with supplementary conditions $|t - m_f^2| \gg m_e m_f$, m_e^2 $\Rightarrow$

$$\begin{aligned} D_0 \;=\; & \frac{1}{(t - m_f^2)(M_Z^2 - s)} \left\{ \log\left(\frac{m_e m_f}{m_f^2 - t - i\epsilon}\right) \left[-\log\left(\frac{m_e m_f}{m_f^2 - t - i\epsilon}\right) \right.\right. \\ & \left. - \log\left(\frac{\lambda^2}{m_e^2}\right) - 2\log\left(\frac{M_Z^2}{M_Z^2 - s - i\epsilon}\right) \right] + \frac{\pi^2}{6} - Li_2\left(1 - \frac{m_f^2 - t}{m_f^2} z_1\right) \\ & \left. - Li_2\left(1 - \frac{m_f^2 - t}{m_f^2} z_2\right) - 2\pi i\, \theta(t - m_f^2) \log\left(1 - \frac{m_f^2 - t}{m_f^2} z_1\right) \right\} , \end{aligned} \qquad \text{(F.2)}$$

with

$$z_{1,2} = \frac{1}{2} \left\{ 1 \pm \sqrt{1 - \frac{4m_f^2}{M_Z^2 - i\epsilon}} \right\} . \qquad \text{(F.3)}$$

To be applied to $e^+e^- \to f_H\bar{f}_H$, whereas in the case of $e^+e^- \to f_L\bar{f}_L$ the supplementary conditions $|t| \gg m_f^2$, $|M_Z^2| \gg m_f^2$ have to be added and (F.2) consequently takes on the form :

$$D_0 = \frac{1}{t(M_Z^2-s)}\left\{-2\log\left(\frac{m_e m_f}{-t-i\epsilon}\right)\log\left(\frac{M_Z\lambda}{M_Z^2-s-i\epsilon}\right)+\log^2\left(\frac{m_e}{M_Z}\right)\right.$$
$$\left.+\log^2\left(\frac{m_f}{M_Z}\right)+\frac{\pi^2}{3}+Li_2\left(1+\frac{M_Z^2}{t+i\epsilon}\right)\right\} . \qquad \text{(F.4)}$$

Extending the above results to the case of a complex Z gauge boson mass related to a resonant Z-propagator corresponds to the mere replacement $M_Z^2 \to M_Z^2 - iM_Z\Gamma_Z$.

This completes the set of special 4-point scalar integrals. Now we present a few special scalar 3-point integrals entering the calculation of EWRC effects to the fermion production processes $e^+e^- \to f\bar{f}$:

3. $m_1 = m_4 = m_f \Rightarrow$

$$C_0 = \frac{x_s}{m_f^2(1-x_s^2)}\left\{\log(x_s)\left[-\frac{1}{2}\log(x_s)+2\log(1+x_s)-\log\left(\frac{\lambda^2}{m_f^2}\right)\right]\right.$$
$$\left.+\frac{\pi^2}{6}+2Li_2(-x_s)\right\} , \qquad \text{(F.5)}$$

with

$$x_s = -K(s+i\epsilon, m_f, m_f) . \qquad \text{(F.6)}$$

To be used in the case of heavy final state fermions. When light final state fermions are considered, hence $|s| \gg m_f^2$, this reduces to

$$C_0 = \frac{1}{s}\left\{\log\left(\frac{m_f^2}{-s-i\epsilon}\right)\log\left(\frac{\lambda^2}{m_f^2}\right)-\frac{\pi^2}{6}+\frac{1}{2}\log^2\left(\frac{m_f^2}{-s-i\epsilon}\right)\right\} . \qquad \text{(F.7)}$$

4. $m_1 = m_v$, $m_4 = m_f$ with the supplementary conditions $|t-m_f^2| \gg m_e m_f$, $m_e^2 \Rightarrow$

$$C_0 = \frac{1}{m_f^2-t}\left\{-\log\left(\frac{m_e m_f}{m_f^2-t-i\epsilon}\right)\log\left(\frac{\lambda^2}{m_e m_f}\right)+Li_2\left(1-\frac{m_f^2}{m_f^2-t-i\epsilon}\right)\right.$$
$$\left.-\frac{1}{2}\log\left(\frac{m_e^2}{m_f^2-t-i\epsilon}\right)\log\left(\frac{m_f^2}{m_f^2-t-i\epsilon}\right)\right\} . \qquad \text{(F.8)}$$

Which covers once again the massive case, whereas the light final state fermion case corresponds to the replacements $m_f^2 - t \to -t$ and the dilogarithmic term $\to \pi^2/6$.

5. In order to wrap things up a 'mass singular' though IR-finite scalar 3-point integral containing the in the end vanishing double poles $\log^2(\frac{m_e^2}{s})$ is listed :

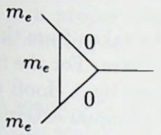

$$: \quad C_0 = \frac{1}{s}\left\{\frac{1}{2}\log^2\left(-\frac{m_e^2}{s+i\epsilon}\right)+\frac{2\pi^2}{3}\right\} . \tag{F.9}$$

Appendix G: Reduction of 2-,3- and 4-point tensor integrals

In this appendix we will present a listing of the expressions for the coefficients appearing in (*III*.5.3) corresponding to the reduction of the 2-,3- and 4-point tensor integrals (*III*.5.1), which has been performed in n dimensions. As these expressions will finally contain just scalar integrals we will first discuss these scalar integrals defined in (*III*.5.1).

The scalar 1-point integral $A_0(M_1)$ is given by

$$A_0(M_1) = M_1^2\,[1+\Delta_{M_1}] , \tag{G.1}$$

where Δ_{M_1} is a shorthand notation for the UV-divergent term

$$\Delta_M = -\frac{2}{n-4} - \gamma_E + \log\left(\frac{4\pi\mu^2}{M^2}\right) . \tag{G.2}$$

The constant γ_E denotes the Euler constant.

The scalar 2-point integral $B_0(p_1, M_1, M_2)$, which is symmetric in the masses M_1 and M_2, is for $M_1 \neq 0$ given by

$$B_0(p_1^2, M_1, M_2) = \Delta_{M_1} + 2 - x_+ \log\left(\frac{x_+}{x_+-1}\right) - x_- \log\left(\frac{x_-}{x_--1}\right) , \tag{G.3}$$

with

$$x_\pm = \frac{1}{2}\left\{1+\frac{M_2^2-M_1^2}{p_1^2+i\epsilon} \pm \sqrt{\left(1+\frac{M_2^2-M_1^2}{p_1^2+i\epsilon}\right)^2 - \frac{4M_2^2}{p_1^2+i\epsilon}}\right\} . \tag{G.4}$$

In case $M_1 = M_2 = 0$ the following expression should be used :

$$B_0(p_1^2, 0, 0) = \Delta_M + 2 - \log\left(-\frac{p_1^2+i\epsilon}{M^2}\right) , \tag{G.5}$$

where for M any non-zero mass can be inserted. The reason for using p_1^2 instead of p_1 as function argument of B_0 is that the only possible invariant (scalar) which can

be constructed from the momentum p_1 is this very p_1^2. The same holds of course for all 2-point reduction coefficients, which will hence appear in explicit calculations with p_1^2 as first argument. For asymptotic forms and special mass configurations we refer to appendix I.

The scalar 3-point integral $C_0(p_1, p_2, M_1, M_2, M_3)$ can be taken from the last appendix in case of IR divergences or 'mass singular' double poles. For the remaining scalar 3-point integrals the general 1-loop integral formalism by 't Hooft and Veltman [2] can be used. In case of real internal masses M_i and equal external masses ($p_1^2 = p_2^2 = m_f^2$), as will be the case in appendix J where final state vertex corrections to $e^+e^- \to f\bar{f}$ are considered, we can also mention an adapted version of the general formula given by 't Hooft and Veltman. After Feynman parametrization we find for the scalar 3-point integral in this case : $s \equiv (p_1 + p_2)$

$$C_0(p_1, p_2, M_1, M_2, M_3) = -\int_0^1 dy \int_0^y dx \, (ay^2 + bx^2 + cxy + dy + ex + f)^{-1} \, , \quad \text{(G.6)}$$

with

$$a = m_f^2 \; , \; b = -c = s \; , \; d = M_3^2 - M_2^2 - m_f^2 \; , \; e = M_1^2 - M_3^2 \; , \; f = M_2^2 - i\epsilon \, . \quad \text{(G.7)}$$

This can be casted in the pure dilogarithmic form

$$C_0(p_1, p_2, M_1, M_2, M_3) = \frac{1}{c + 2\alpha b} \sum_{l=1}^{3} \sum_{j=1}^{2} (-1)^l \left\{ Li_2\left(\frac{x_l}{x_l - y_{lj}}\right) - Li_2\left(\frac{x_l - 1}{x_l - y_{lj}}\right) \right\} \, , \quad \text{(G.8)}$$

with

$$\alpha \equiv \frac{1 - \beta}{2} \quad , \quad \beta \equiv \sqrt{1 - \frac{4m_f^2}{s}} \quad \Rightarrow \quad c + 2\alpha b = -s\beta \quad \text{(G.9)}$$

and

$$\begin{aligned}
x_1 &= -\frac{d + e\alpha}{c + 2\alpha b} + \alpha \qquad , \qquad y_{1j} = \frac{-c - e \pm \sqrt{(c+e)^2 - 4b(a+d+f)}}{2b} \\
x_2 &= -\frac{d + e\alpha}{(1-\alpha)(c + 2\alpha b)} \qquad , \qquad y_{2j} = \frac{-d - e \pm \sqrt{(d+e)^2 - 4f(a+b+c)}}{2(a+b+c)} \\
x_3 &= \frac{d + e\alpha}{\alpha(c + 2\alpha b)} \qquad , \qquad y_{3j} = \frac{-d \pm \sqrt{d^2 - 4af}}{2a} \, .
\end{aligned} \quad \text{(G.10)}$$

The scalar 4-point integral $D_0(p_1, p_2, p_3, M_1, M_2, M_3, M_4)$ can be taken from the last appendix in case of IR divergences. For the remaining (weak) scalar 4-point integrals the scalar 3-point integral expressions can be used as appearing in the general 1-loop integral formalism by 't Hooft and Veltman. The reason for this is that at least one of the internal masses is zero or negligibly small as compared to

combinations of process invariants and the other internal masses (as a consequence of the absence of 'mass singular' terms). This offers us the opportunity to leave out this small mass in one of the propagators which after shifting the integration variable in a proper way takes on the form $1/l^2$. Transforming the integration variable according to

$$(r^\mu) = (l^\mu)/l^2$$

renders a scalar 3-point integral, see for instance [3].

After this scalar introduction we can shift our attention to the tensor integral reductions starting with the 2-point one. Introduce to this end

$$f_1 = M_2^2 - M_1^2 - Q_2^2 \ ,$$

where we have used the shorthand notation Q_i as defined in chapter III. Then the reduction coefficients can be expressed as follows :

$$\begin{aligned} B_1 &= \frac{1}{2p_1^2}\left[f_1 B_0 + A_0(M_1) - A_0(M_2) \right] \\ B_{22} &= \frac{1}{n-1}\left\{ M_1^2 B_0 - \frac{1}{2}\left[f_1 B_1 - A_0(M_2) \right] \right\} \\ B_{21} &= \frac{1}{p_1^2}\left\{ \frac{1}{2}\left[f_1 B_1 + A_0(M_2) \right] - B_{22} \right\} \ . \end{aligned} \tag{G.11}$$

Now we will give an overview on the reduction of 3-point tensor integrals using the definitions for the 2-point integrals as given by (*III*.5.6) and the 2-point reduction coefficients as given above. Introduce to this end :

$$X = \begin{pmatrix} p_1^2 & p_1.p_2 \\ p_1.p_2 & p_2^2 \end{pmatrix} \quad : \text{considered to be an invertable matrix}$$

$$f_1 = M_2^2 - M_1^2 - Q_2^2 \ \text{ and } \ f_2 = M_3^2 - M_2^2 - Q_3^2 + Q_2^2 \ .$$

Then the reduction coefficients can be expressed as follows :

$$\begin{aligned} R_1 &= \frac{1}{2}\left[f_1 C_0 + B_0(1,3) - B_0(2,3) \right] \\ R_2 &= \frac{1}{2}\left[f_2 C_0 + B_0(1,2) - B_0(1,3) \right] \end{aligned}$$

matrix relation : $\begin{pmatrix} C_{11} \\ C_{12} \end{pmatrix} = X^{-1} \begin{pmatrix} R_1 \\ R_2 \end{pmatrix}$

$$C_{24} = \frac{1}{n-2}\left\{ M_1^2 C_0 - \frac{1}{2}\left[f_1 C_{11} + f_2 C_{12} - B_0(2,3) \right] \right\}$$

$$
\begin{aligned}
R_3 &= \frac{1}{2}[f_1 C_{11} + B_1(1,3) + B_0(2,3)] \\
R_4 &= \frac{1}{2}[f_2 C_{11} + B_1(1,2) - B_1(1,3)] \\
R_5 &= \frac{1}{2}[f_1 C_{12} + B_1(1,3) - B_1(2,3)] \\
R_6 &= \frac{1}{2}[f_2 C_{12} - B_1(1,3)]
\end{aligned}
$$

$$
\text{matrix relations} \quad : \quad \begin{pmatrix} C_{21} \\ C_{23} \end{pmatrix} = X^{-1} \begin{pmatrix} R_3 - C_{24} \\ R_4 \end{pmatrix}, \begin{pmatrix} C_{23} \\ C_{22} \end{pmatrix} = X^{-1} \begin{pmatrix} R_5 \\ R_6 - C_{24} \end{pmatrix}
$$

$$
\begin{aligned}
R_{10} &= \frac{1}{2}[f_1 C_{24} + B_{22}(1,3) - B_{22}(2,3)] \\
R_{11} &= \frac{1}{2}[f_2 C_{24} + B_{22}(1,2) - B_{22}(1,3)]
\end{aligned}
$$

$$
\text{matrix relation} \quad : \quad \begin{pmatrix} C_{35} \\ C_{36} \end{pmatrix} = X^{-1} \begin{pmatrix} R_{10} \\ R_{11} \end{pmatrix}
$$

$$
\begin{aligned}
R_{12} &= \frac{1}{2}[f_1 C_{21} + B_{21}(1,3) - B_0(2,3)] \\
R_{13} &= \frac{1}{2}[f_2 C_{21} + B_{21}(1,2) - B_{21}(1,3)] \\
R_{14} &= \frac{1}{2}[f_1 C_{22} + B_{21}(1,3) - B_{21}(2,3)] \\
R_{15} &= \frac{1}{2}[f_2 C_{22} - B_{21}(1,3)] \\
R_{16} &= \frac{1}{2}[f_1 C_{23} + B_{21}(1,3) + B_1(2,3)] \\
R_{17} &= \frac{1}{2}[f_2 C_{23} - B_{21}(1,3)]
\end{aligned}
$$

$$
\begin{aligned}
\text{matrix relations} \quad : \quad & \begin{pmatrix} C_{31} \\ C_{33} \end{pmatrix} = X^{-1} \begin{pmatrix} R_{12} - 2C_{35} \\ R_{13} \end{pmatrix}, \begin{pmatrix} C_{34} \\ C_{32} \end{pmatrix} = X^{-1} \begin{pmatrix} R_{14} \\ R_{15} - 2C_{36} \end{pmatrix}, \\
& \begin{pmatrix} C_{33} \\ C_{34} \end{pmatrix} = X^{-1} \begin{pmatrix} R_{16} - C_{36} \\ R_{17} - C_{35} \end{pmatrix} . \qquad \text{(G.12)}
\end{aligned}
$$

Now we list the reduction of the 4-point tensor integrals in the same way using the definitions for the 3-point integrals as given by (*III*.5.7) and the 3-point

reduction coefficients as given above. Introduce to this end :

$$X = \begin{pmatrix} p_1^2 & p_1 \cdot p_2 & p_1 \cdot p_3 \\ p_1 \cdot p_2 & p_2^2 & p_2 \cdot p_3 \\ p_1 \cdot p_3 & p_2 \cdot p_3 & p_3^2 \end{pmatrix} \quad : \text{considered to be an invertable matrix}$$

$f_1 = M_2^2 - M_1^2 - Q_2^2$, $f_2 = M_3^2 - M_2^2 - Q_3^2 + Q_2^2$ and $f_3 = M_4^2 - M_3^2 - Q_4^2 + Q_3^2$.
Then the reduction coefficients can be expressed as follows :

$$\begin{aligned} R_{20} &= \frac{1}{2}[f_1 D_0 + C_0(1,3,4) - C_0(2,3,4)] \\ R_{21} &= \frac{1}{2}[f_2 D_0 + C_0(1,2,4) - C_0(1,3,4)] \\ R_{22} &= \frac{1}{2}[f_3 D_0 + C_0(1,2,3) - C_0(1,2,4)] \end{aligned}$$

matrix relation : $\begin{pmatrix} D_{11} \\ D_{12} \\ D_{13} \end{pmatrix} = X^{-1} \begin{pmatrix} R_{20} \\ R_{21} \\ R_{22} \end{pmatrix}$

$$D_{27} = \frac{1}{n-3}\left\{ M_1^2 D_0 - \frac{1}{2}[f_1 D_{11} + f_2 D_{12} + f_3 D_{13} - C_0(2,3,4)] \right\}$$

$$\begin{aligned} R_{30} &= \frac{1}{2}[f_1 D_{11} + C_{11}(1,3,4) + C_0(2,3,4)] \\ R_{31} &= \frac{1}{2}[f_2 D_{11} + C_{11}(1,2,4) - C_{11}(1,3,4)] \\ R_{32} &= \frac{1}{2}[f_3 D_{11} + C_{11}(1,2,3) - C_{11}(1,2,4)] \\ R_{33} &= \frac{1}{2}[f_1 D_{12} + C_{11}(1,3,4) - C_{11}(2,3,4)] \\ R_{34} &= \frac{1}{2}[f_2 D_{12} + C_{12}(1,2,4) - C_{11}(1,3,4)] \\ R_{35} &= \frac{1}{2}[f_3 D_{12} + C_{12}(1,2,3) - C_{12}(1,2,4)] \\ R_{36} &= \frac{1}{2}[f_1 D_{13} + C_{12}(1,3,4) - C_{12}(2,3,4)] \\ R_{37} &= \frac{1}{2}[f_2 D_{13} + C_{12}(1,2,4) - C_{12}(1,3,4)] \\ R_{38} &= \frac{1}{2}[f_3 D_{13} - C_{12}(1,2,4)] \end{aligned}$$

matrix relations : $\begin{pmatrix} D_{21} \\ D_{24} \\ D_{25} \end{pmatrix} = X^{-1} \begin{pmatrix} R_{30} - D_{27} \\ R_{31} \\ R_{32} \end{pmatrix}$, $\begin{pmatrix} D_{24} \\ D_{22} \\ D_{26} \end{pmatrix} = X^{-1} \begin{pmatrix} R_{33} \\ R_{34} - D_{27} \\ R_{35} \end{pmatrix}$,

$$\begin{pmatrix} D_{25} \\ D_{26} \\ D_{23} \end{pmatrix} = X^{-1} \begin{pmatrix} R_{36} \\ R_{37} \\ R_{38} - D_{27} \end{pmatrix}$$

$$\begin{aligned}
R_{40} &= \frac{1}{2}[f_1 D_{27} + C_{24}(1,3,4) - C_{24}(2,3,4)] \\
R_{41} &= \frac{1}{2}[f_2 D_{27} + C_{24}(1,2,4) - C_{24}(1,3,4)] \\
R_{42} &= \frac{1}{2}[f_3 D_{27} + C_{24}(1,2,3) - C_{24}(1,2,4)]
\end{aligned}$$

matrix relation : $\begin{pmatrix} D_{311} \\ D_{312} \\ D_{313} \end{pmatrix} = X^{-1} \begin{pmatrix} R_{40} \\ R_{41} \\ R_{42} \end{pmatrix}$

$$\begin{aligned}
R_{43} &= \frac{1}{2}[f_1 D_{21} + C_{21}(1,3,4) - C_0(2,3,4)] \\
R_{44} &= \frac{1}{2}[f_2 D_{21} + C_{21}(1,2,4) - C_{21}(1,3,4)] \\
R_{45} &= \frac{1}{2}[f_3 D_{21} + C_{21}(1,2,3) - C_{21}(1,2,4)] \\
R_{46} &= \frac{1}{2}[f_1 D_{22} + C_{21}(1,3,4) - C_{21}(2,3,4)] \\
R_{47} &= \frac{1}{2}[f_2 D_{22} + C_{22}(1,2,4) - C_{21}(1,3,4)] \\
R_{48} &= \frac{1}{2}[f_3 D_{22} + C_{22}(1,2,3) - C_{22}(1,2,4)] \\
R_{49} &= \frac{1}{2}[f_1 D_{23} + C_{22}(1,3,4) - C_{22}(2,3,4)] \\
R_{50} &= \frac{1}{2}[f_2 D_{23} + C_{22}(1,2,4) - C_{22}(1,3,4)] \\
R_{51} &= \frac{1}{2}[f_3 D_{23} - C_{22}(1,2,4)] \\
R_{52} &= \frac{1}{2}[f_1 D_{24} + C_{21}(1,3,4) + C_{11}(2,3,4)] \\
R_{53} &= \frac{1}{2}[f_2 D_{24} + C_{23}(1,2,4) - C_{21}(1,3,4)] \\
R_{54} &= \frac{1}{2}[f_3 D_{24} + C_{23}(1,2,3) - C_{23}(1,2,4)]
\end{aligned}$$

matrix relations : $\begin{pmatrix} D_{31} \\ D_{34} \\ D_{35} \end{pmatrix} = X^{-1} \begin{pmatrix} R_{43} - 2D_{311} \\ R_{44} \\ R_{45} \end{pmatrix}$, $\begin{pmatrix} D_{36} \\ D_{32} \\ D_{38} \end{pmatrix} = X^{-1} \begin{pmatrix} R_{46} \\ R_{47} - 2D_{312} \\ R_{48} \end{pmatrix}$,

$$\begin{pmatrix} D_{37} \\ D_{39} \\ D_{33} \end{pmatrix} = X^{-1} \begin{pmatrix} R_{49} \\ R_{50} \\ R_{51} - 2D_{313} \end{pmatrix}, \begin{pmatrix} D_{34} \\ D_{36} \\ D_{310} \end{pmatrix} = X^{-1} \begin{pmatrix} R_{52} - D_{312} \\ R_{53} - D_{311} \\ R_{54} \end{pmatrix}. \tag{G.13}$$

In order to complete this scalar and tensor integral appendix we will explicitly mention the UV-divergent content of the above given scalar functions in terms of the UV-divergent quantity Δ which is just (G.2) without the mass M :

	B_0	B_1	B_{21}	B_{22}	C_{24}	C_{35}	C_{36}
UV-div. ($\times\Delta$)	1	$-1/2$	$1/3$	$[3M_1^2 + 3M_2^2 - p_1^2]/12$	$1/4$	$-1/6$	$-1/12$

.

Appendix H: Basic spin summed contractions

The interference of the set of basic helicity amplitudes (*IV*.2.9) with the Born one yields the following expressions : (in case of repeated indices no summation is intended)

$$\begin{aligned}
\sum_{\eta,\bar{\eta}} M_1^{\rho\kappa} \left(M_1^{\rho'\kappa}\right)^* &= 4\,\delta^{\rho}_{\rho'} \left\{\delta^{\rho}_{\kappa}(u - m_f^2)^2 + \delta^{\rho}_{-\kappa}(t - m_f^2)^2\right\} + 4\,\delta^{\rho}_{-\rho'} m_f^2 s \\
\sum_{\eta,\bar{\eta}} M_2^{\rho\kappa} \left(M_1^{\rho'\kappa}\right)^* &= 2(ut - m_f^4)\,\delta^{\rho}_{\rho'} \left\{\delta^{\rho}_{\kappa}(u - m_f^2) - \delta^{\rho}_{-\kappa}(t - m_f^2)\right\} \\
\sum_{\eta,\bar{\eta}} M_3^{\rho\kappa} \left(M_1^{\rho'\kappa}\right)^* &= -2m_f(ut - m_f^4) \\
\sum_{\eta,\bar{\eta}} M_4^{\rho\kappa} \left(M_1^{\rho'\kappa}\right)^* &= 4m_f s\,\delta^{\rho}_{-\kappa} \left\{\delta^{\rho'}_{-\kappa}(t - m_f^2) + \delta^{\rho'}_{\kappa}(u - m_f^2)\right\}.
\end{aligned} \tag{H.1}$$

In the light fermion limit only the first two interferences are present for $\rho = \rho'$ as a consequence of final state chiral symmetry in that case, while at the same time they are related by

$$\sum_{\eta,\bar{\eta}} M_2^{\rho\kappa} \left(M_1^{\rho\kappa}\right)^* = \frac{1}{4} \left\{t(1 + \rho\kappa) - u(1 - \rho\kappa)\right\} \sum_{\eta,\bar{\eta}} M_1^{\rho\kappa} \left(M_1^{\rho\kappa}\right)^*. \tag{H.2}$$

Appendix I: Renormalized transverse gauge boson self energies

After adding all the renormalization constants as prescribed by the 'on-shell' renormalization scheme the following result is obtained for the renormalized transverse gauge boson self energies :

$$\hat{\Sigma}^T(s) = \Sigma^T(s) - s\,\Pi^T(0)$$

$$
\begin{aligned}
\hat{\Sigma}^{\gamma Z}(s) &= \Sigma^{\gamma Z}(s) - \Sigma^{\gamma Z}(0) + s\left\{2\frac{\Sigma^{\gamma Z}(0)}{M_Z^2} - \frac{c_w}{s_w}\left[\frac{\mathrm{Re}\,\Sigma^Z(M_Z^2)}{M_Z^2} - \frac{\mathrm{Re}\,\Sigma^W(M_W^2)}{M_W^2}\right]\right\} \\
\hat{\Sigma}^Z(s) &= \Sigma^Z(s) - \mathrm{Re}\,\Sigma^Z(M_Z^2) - (s - M_Z^2)\,\Pi^\gamma(0) \\
&\quad - (s - M_Z^2)\frac{c_w^2 - s_w^2}{c_w s_w}\left\{2\frac{\Sigma^{\gamma Z}(0)}{M_Z^2} - \frac{c_w}{s_w}\left[\frac{\mathrm{Re}\,\Sigma^Z(M_Z^2)}{M_Z^2} - \frac{\mathrm{Re}\,\Sigma^W(M_W^2)}{M_W^2}\right]\right\} \\
\hat{\Sigma}^W(s) &= \Sigma^W(s) - \mathrm{Re}\,\Sigma^W(M_W^2) - (s - M_W^2)\,\Pi^\gamma(0) \\
&\quad - (s - M_W^2)\frac{c_w}{s_w}\left\{2\frac{\Sigma^{\gamma Z}(0)}{M_Z^2} - \frac{c_w}{s_w}\left[\frac{\mathrm{Re}\,\Sigma^Z(M_Z^2)}{M_Z^2} - \frac{\mathrm{Re}\,\Sigma^W(M_W^2)}{M_W^2}\right]\right\},
\end{aligned}
\tag{I.1}
$$

where we have introduced the shorthand notation

$$
\Pi^\gamma(0) \equiv \left.\frac{\Sigma^\gamma(k^2)}{k^2}\right|_{k^2=0} = \frac{\partial \Sigma^\gamma}{\partial k^2}(0)\,. \tag{I.2}
$$

In order to be able to present the forthcoming self energy expressions as compact as possible, without loosing any transparancy, we are led to introduce a few more shorthand notations (only to be used in this appendix) :

$$
z = M_Z \quad , \quad w = M_W \quad , \quad h = M_H \quad , \quad \Delta_i = \Delta_{M_i}\,, \tag{I.3}
$$

where Δ_M has been defined in appendix G. By decomposing the scalar 2-point function in appendix G according to

$$
B_0(s, M_1, M_2) = \frac{1}{2}(\Delta_1 + \Delta_2) + 1 - \frac{M_1^2 + M_2^2}{M_1^2 - M_2^2}\log\left(\frac{M_1}{M_2}\right) + F(s, M_1, M_2)\,, \tag{I.4}
$$

where the function $F(s, M_1, M_2)$ is symmetric in the masses, the unrenormalized transverse gauge boson self energies $\Sigma(s)$ occuring in the above expressions can be brought in the form : (the fermion summation also extends over the quark colours)

$$
\begin{aligned}
\Sigma^\gamma(s) &= \frac{\alpha}{4\pi}\left\{\frac{4}{3}\sum_f Q_f^2\left[s\Delta_f + (s + 2m_f^2)\,F(s, m_f, m_f) - \frac{s}{3}\right]\right. \\
&\quad \left. - \left[3s\Delta_W + (3s + 4w^2)\,F(s, w, w)\right]\right\} \\
\Sigma^{\gamma Z}(s) &= \frac{\alpha}{4\pi}\left\{-\frac{4}{3}\sum_f Q_f v_f\left[s\Delta_f + (s + 2m_f^2)\,F(s, m_f, m_f) - \frac{s}{3}\right]\right. \\
&\quad + \frac{1}{c_w s_w}\left[\left((3c_w^2 + \frac{1}{6})\,s + 2w^2\right)\Delta_W\right. \\
&\quad \left.\left. + \left((3c_w^2 + \frac{1}{6})\,s + (4c_w^2 + \frac{4}{3})\,w^2\right)F(s, w, w) + \frac{s}{9}\right]\right\}
\end{aligned}
$$

$$
\begin{aligned}
\Sigma^Z(s) \;=\; & \frac{\alpha}{4\pi}\left\{\frac{4}{3}\sum_{l=e,\mu,\tau} 2a_l^2 s\left[\Delta_l+\frac{5}{3}-\log\left(-\frac{s+i\epsilon}{m_l^2}\right)\right]\right. \\
& +\frac{4}{3}\sum_{f\neq\nu_l}\left[(v_f^2+a_f^2)\left(s\Delta_f+(s+2m_f^2)\,F(s,m_f,m_f)-\frac{s}{3}\right)\right. \\
& \qquad \left.-\,6a_f^2 m_f^2\,(\Delta_f+F(s,m_f,m_f))\right] \\
& +\left[(3-\frac{19}{6s_w^2}+\frac{1}{6c_w^2})\,s+(4+\frac{1}{c_w^2}-\frac{1}{s_w^2})\,z^2\right]\Delta w \\
& +\left[\left(-c_w^4(40s+80w^2)+(c_w^2-s_w^2)^2(8w^2+s)+12w^2\right)F(s,w,w)\right. \\
& +\left(10z^2-2h^2+s+\frac{(h^2-z^2)^2}{s}\right)F(s,h,z) \\
& -2h^2\log\left(\frac{h^2}{w^2}\right)-2z^2\log\left(\frac{z^2}{w^2}\right) \\
& +(10z^2-2h^2+s)\left(1-\frac{h^2+z^2}{h^2-z^2}\log\left(\frac{h}{z}\right)-\log\left(\frac{hz}{w^2}\right)\right) \\
& \left.\left.+\frac{2}{3}s(1+(c_w^2-s_w^2)^2-4c_w^4)\right]\frac{1}{12c_w^2s_w^2}\right\}
\end{aligned}
$$

$$
\begin{aligned}
\Sigma^W(s) \;=\; & \frac{\alpha}{4\pi}\frac{1}{3s_w^2}\left\{\sum_{l=e,\mu,\tau}\left[(s-\frac{3}{2}m_l^2)\,\Delta_l+(s-\frac{m_l^2}{2}-\frac{m_l^4}{2s})\,F(s,0,m_l)+\frac{2}{3}s-\frac{1}{2}m_l^2\right]\right. \\
& +\sum_{j\,(quark)}\left[\frac{\Delta_{j+}}{2}(s-\frac{5}{2}m_{j+}^2-\frac{1}{2}m_{j-}^2)+\frac{\Delta_{j-}}{2}(s-\frac{5}{2}m_{j-}^2-\frac{1}{2}m_{j+}^2)\right. \\
& \qquad +\left(s-\frac{m_{j+}^2+m_{j-}^2}{2}-\frac{(m_{j+}^2-m_{j-}^2)^2}{2s}\right)F(s,m_{j+},m_{j-}) \\
& \qquad \left.+\left(s-\frac{m_{j+}^2+m_{j-}^2}{2}\right)\left(1-\frac{m_{j+}^2+m_{j-}^2}{m_{j+}^2-m_{j-}^2}\log\left(\frac{m_{j+}}{m_{j-}}\right)\right)-\frac{s}{3}\right] \\
& -\left[\frac{19}{2}s+3w^2\left(1-\frac{s_w^2}{c_w^2}\right)\right]\Delta w \\
& +\left[3s_w^4z^2-c_w^2\left(7z^2+7w^2+10s-2\frac{(z^2-w^2)^2}{s}\right)\right. \\
& \qquad \left.-\frac{1}{2}\left(w^2+z^2-\frac{s}{2}-\frac{(z^2-w^2)^2}{2s}\right)\right]F(s,z,w) \\
& +s_w^2\left[-4w^2-10s+\frac{2w^4}{s}\right]F(s,0,w)
\end{aligned}
$$

$$+\frac{1}{2}\left[5w^2-h^2+\frac{s}{2}+\frac{(h^2-w^2)^2}{2s}\right]F(s,h,w)$$
$$+\left[c_w^2\,(3z^2+11w^2+10s)-3s_w^4z^2+\frac{1}{2}(2w^2-\frac{s}{2})\right]\frac{z^2}{z^2-w^2}\log\left(\frac{z^2}{w^2}\right)$$
$$-(2w^2+\frac{s}{4})\frac{h^2}{h^2-w^2}\log\left(\frac{h^2}{w^2}\right)-c_W^2\,(7z^2+7w^2+\frac{32}{3}s)$$
$$+3s_w^4z^2+\frac{1}{2}(\frac{5}{3}s+4w^2-z^2-h^2)-s_W^2\,(4w^2+\frac{32}{3}s)\Big\}\ . \tag{I.5}$$

In the last expression the notation given in section 4 of chapter II has been used. The above given unrenormalized self energies do not contain any Higgs vacuum expectation value related tadpole contributions, as the tadpole renormalization causes them to disappear from the renormalized self energies anyhow. Concerning the function $F(s,M_1,M_2)$ as defined above we can consider the following interesting special cases or asymptotic forms in view of the way they appear in the expressions of both renormalized and unrenormalized transverse gauge boson self energies :

- $M_1=0$:
$$F(s,0,M_2)=1+\left[\frac{M_2^2}{s}-1\right]\log\left(1-\frac{s+i\epsilon}{M_2^2}\right) \tag{I.6}$$
- $s\ll M_1^2,M_2^2$ and $M_1\neq M_2$:
$$F(s,M_1,M_2)\approx\frac{s}{(M_1^2-M_2^2)^2}\left[\frac{M_1^2+M_2^2}{2}-\frac{M_1^2M_2^2}{M_1^2-M_2^2}\log\left(\frac{M_1^2}{M_2^2}\right)\right] \tag{I.7}$$
$s\ll M_1^2=M_2^2$:
$$F(s,M_1,M_1)\approx\frac{s}{6M_1^2}\left[1+\frac{s}{10M_1^2}\right] \tag{I.8}$$
$s\ll M_1^2\ll M_2^2$:
$$F(s,M_1,M_2)\approx\frac{s}{2M_2^2} \tag{I.9}$$
and hence $F(0,M_1,M_2)=0$ provided M_1 and M_2 are not both equal to zero.
- $s\gg M_1^2,M_2^2$:
$$F(s,M_1,M_2)\approx 1-\log\left(-\frac{s+i\epsilon}{M_1M_2}\right)+\frac{M_1^2+M_2^2}{M_1^2-M_2^2}\log\left(\frac{M_1}{M_2}\right) \tag{I.10}$$
- $M_1^2\ll s\ll M_2^2$:
$$F(s,M_1,M_2)\approx\frac{s}{2M_2^2}\left[1+\frac{s}{3M_2^2}\right]\ . \tag{I.11}$$

Using the above given renormalized and unrenormalized transverse gauge boson self energies combined with the asymptotic forms of the function $F(s, M_1, M_2)$ we can derive a few interesting features concerning the gauge invariant fermion sector of these self energies. First of all we can discuss the large top mass limit ($m_t^2 \gg s \gg m_b^2$) which hence means a large mass plitting in the (t, b) doublet. The interactions which are sensitive to these mass splitting effects consequently involve an isospin changing character. This results in the fact that the largest top mass dependence is to be found in the unrenormalized W self energy and consequently in all renormalized self energies containing this W self energy (direct or indirect as part of the counter terms). The coupling of heavy fermions to the photon however leads to a decoupling which is maintained in the renormalized photon self energy as a result of the fact that the W self energy does not enter its counter terms in contrast to for instance the γZ mixing self energy. We can summarize this by showing the leading top mass term (Lt) for all four renormalized self energies :

$$\begin{aligned}
\hat{\Sigma}^{\gamma}_{Lt}(s) &= s\frac{\alpha}{3\pi}N_c^t Q_t^2 \frac{s}{5m_t^2} \\
\hat{\Sigma}^{\gamma Z}_{Lt}(s) &= -s\frac{c_w}{s_w}\left[\frac{\alpha}{4\pi}N_c^t \mu_t^2\right] \\
\hat{\Sigma}^{Z}_{Lt}(s) &= (s-M_Z^2)\frac{c_w^2-s_w^2}{s_w^2}\left[\frac{\alpha}{4\pi}N_c^t \mu_t^2\right] \\
\hat{\Sigma}^{W}_{Lt}(s) &= (s-M_W^2)\frac{c_w^2}{s_w^2}\left[\frac{\alpha}{4\pi}N_c^t \mu_t^2\right] ,
\end{aligned} \tag{I.12}$$

where we have used the shorthand notation (IV.3.31). A consequence of this leading top mass behaviour is that the quantity Δr linking M_Z, M_W and $\sin^2\theta_w$ according to (II.7.3) has a leading top mass behaviour of the form [4]

$$(\Delta r)_{Lt} = \frac{\hat{\Sigma}^W_{Lt}(0)}{M_W^2} = -\frac{c_w^2}{s_w^2}\left[\frac{\alpha}{4\pi}N_c^t \mu_t^2\right] . \tag{I.13}$$

From the above leading top mass discussion we see that the top mass enters the radiative corrections in a quadratic way. This results in a top mass dependence of several measurable quantities which exceeds the experimental accuracy and hence allows for an indirect top mass determination. This in contrast to the screening of the Higgs mass leading to 1-loop radiative corrections which only have a logarithmic large Higgs mass dependence [5]. Because of this screening the Higgs mass in general manages to escape indirect detection. The contributions originating from light fermion loops constitute the dominating part of the renormalized self energies. This is not caused by the unrenormalized self energies but a direct consequence of the $\Pi^{\gamma}(0)$ counterterm involving the charge renormalization mass scale $q^2 = 0$ which is quite extreme compared to the other renormalization mass scales and the scale s at which the self energies are evaluated. Besides being responsible

for the large light fermion contributions (called leading logarithms), $\Pi^\gamma(0)$ introduces the problem of evaluating the light quark loops including QCD corrections at a non-perturbative scale. This problem can be overcome by realizing that the renormalized hadronic vacuum polarization $\hat{\Pi}^\gamma_{had}(s)$, containing $\Pi^\gamma_{had}(0)$, satisfies the once subtracted dipersion relation

$$\mathrm{Re}\,\hat{\Pi}^\gamma_{had}(s) = \frac{\alpha}{3\pi}\, s \int_{4m_\pi^2}^{\infty} ds' \frac{R^\gamma(s')}{s'(s'-s-i\epsilon)}\,, \tag{I.14}$$

with the quite well known experimental quantity

$$R^\gamma(s) = \frac{\sigma(e^+e^- \to \gamma^* \to hadrons)}{\sigma(e^+e^- \to \gamma^* \to \mu^+\mu^-)}\,. \tag{I.15}$$

In this way all large hadronic non-perturbative contributions are covered by this dispersion integral [6]. Explicit calculations show that the above dispersion integral can be approximated by evaluating the renormalized hadronic vacuum polarization in a perturbative way using a set of effective quark masses. This mass parameter fit, incorporating the real non-perturbative QCD corrections, describes the hadronic content of all renormalized self energies for our purposes in an adequate way. We finish this discussion of the light fermion (lf) contributions to the renormalized self energies by presenting the explicit expressions including the newly acquired effective light quark masses :

$$\begin{aligned}
\hat{\Sigma}^\gamma_{lf}(s) &= s\frac{\alpha}{3\pi}\sum_{f_L} Q^2_{f_L}\left[\frac{5}{3} - \log\left(-\frac{s+i\epsilon}{m^2_{f_L}}\right)\right] \\
\hat{\Sigma}^{\gamma Z}_{lf}(s) &= s\frac{\alpha}{3\pi}\sum_{f_L}\left\{Q_{f_L}v_{f_L}\log\left(-\frac{s+i\epsilon}{M_Z^2}\right) - \frac{c_w}{8s_w^3}\log(c_w^2)\right\} \\
\hat{\Sigma}^{Z}_{lf}(s) &= (s-M_Z^2)\frac{\alpha}{3\pi}\sum_{f_L}\left\{Q^2_{f_L}\left[\frac{5}{3} - \log\left(\frac{M_Z^2}{m^2_{f_L}}\right)\right] + \frac{c_w^2-s_w^2}{8s_w^4}\log(c_w^2)\right. \\
&\qquad \left. - (v^2_{f_L}+a^2_{f_L})\frac{s}{s-M_Z^2}\log\left(-\frac{s+i\epsilon}{M_Z^2}\right)\right\} \\
\hat{\Sigma}^{W}_{lf}(s) &= (s-M_W^2)\frac{\alpha}{3\pi}\sum_{f_L}\left\{Q^2_{f_L}\left[\frac{5}{3} - \log\left(\frac{M_Z^2}{m^2_{f_L}}\right)\right] + \frac{c_w^2-s_w^2}{8s_w^4}\log(c_w^2)\right. \\
&\qquad \left. - \frac{1}{8s_w^2}\frac{s}{s-M_W^2}\log\left(-\frac{s+i\epsilon}{M_W^2}\right)\right\}\,.
\end{aligned} \tag{I.16}$$

A consequence of this light fermion behaviour is that the quantity Δr linking M_Z, M_W and $\sin^2\theta_w$ according to (*II*.7.3) has itself a light fermion behaviour of the form

$$(\Delta r)_{lf} = -\frac{\alpha}{3\pi}\sum_{f_L}\left\{Q^2_{f_L}\left[\frac{5}{3} - \log\left(\frac{M_Z^2}{m^2_{f_L}}\right)\right] + \frac{c_w^2-s_w^2}{8s_w^4}\log(c_w^2)\right\}\,. \tag{I.17}$$

Appendix J: Special orthogonal 3-point tensor integral reduction

Consider the following tensor integral , slightly deviating from the one given in (*III*.5.1) :

$$\bar{C}_{\{\mu,\mu\nu\}}(p_1,p_2,M_1,M_2,M_3) \equiv (2\pi\mu)^{4-n} \int \frac{d^n l}{i\pi^2} \frac{\{l_\mu,\, l_\mu l_\nu\}}{D_1 D_2 D_3} \,, \tag{J.1}$$

with

$$\begin{aligned} D_1 &= (l-p_1)^2 - M_1^2 + i\epsilon \\ D_2 &= (l-p_2)^2 - M_2^2 + i\epsilon \\ D_3 &= l^2 - M_3^2 + i\epsilon \,. \end{aligned} \tag{J.2}$$

From fig. 2 the parameter specifications wll become clear. The reason for intro-

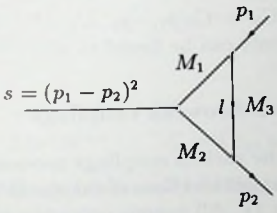

Fig. 2.

ducing these types of tensor integrals is to be found in the fact that we are dealing with equal mass final state particles $p_1^2 = p_2^2 = m_f^2$, so the above integral is invariant under the combined replacements $p_1 \leftrightarrow p_2$ and $M_1 \leftrightarrow M_2$. In the case $M_1 = M_2$, which occurs quite frequently, this leads to a symmetry under $p_1 \leftrightarrow p_2$ yielding a couple of zero coefficients in the following orthogonal reduction : $(k_\pm = p_1 \pm p_2)$

$$\begin{aligned} \bar{C}_\mu &= C_1^+ k_{+\mu} + C_1^- k_{-\mu} \\ \bar{C}_{\mu\nu} &= C_2^+ k_{+\mu} k_{+\nu} + C_2^- k_{-\mu} k_{-\nu} + C_2^{+-} [\, k_{+\mu} k_{-\nu} + k_{+\nu} k_{-\mu}\,] + C_2^0 g_{\mu\nu} \,. \end{aligned} \tag{J.3}$$

So, the case $M_1 = M_2$ automatically yields $C_1^- = C_2^{+-} = 0$. After applying the projective operator method described in chapter III the following expressions can be found for the coefficients :

$$(4m_f^2 - s)\, C_1^+ = B_0(s, M_1, M_2) - \frac{1}{2} \left[B_0(m_f^2, M_3, M_1) + B_0(m_f^2, M_3, M_2) \right]$$

$$
\begin{aligned}
&+ \frac{1}{2}\left(2M_3^2 + 2m_f^2 - M_1^2 - M_2^2\right) C_0 \\
s\,C_1^- &= \frac{1}{2}\left[B_0(m_f^2, M_3, M_1) - B_0(m_f^2, M_3, M_2)\right] + \frac{1}{2}\left(M_2^2 - M_1^2\right) C_0 \\
C_2^0 &= \frac{1}{2} M_3^2\, C_0 + \frac{1}{4} + \frac{1}{4}\left[\left(M_1^2 + M_2^2 - 2M_3^2 - 2m_f^2\right) C_1^+ + \left(M_1^2 - M_2^2\right) C_1^-\right. \\
&\qquad \left. + \; B_0(s, M_1, M_2)\right] \\
\left(4m_f^2 - s\right) C_2^+ &= -C_2^0 + \frac{1}{2}\left(2M_3^2 + 2m_f^2 - M_1^2 - M_2^2\right) C_1^+ + \frac{1}{2} B_0(s, M_1, M_2) \\
&\qquad + \frac{1}{4}\left[B_1(m_f^2, M_3, M_1) + B_1(m_f^2, M_3, M_2)\right] \\
s\,C_2^- &= -C_2^0 + \frac{1}{2}\left(M_2^2 - M_1^2\right) C_1^- - \frac{1}{4}\left[B_1(m_f^2, M_3, M_1) + B_1(m_f^2, M_3, M_2)\right] \\
4s\,C_2^{+-} &= 2\left(M_2^2 - M_1^2\right) C_1^+ + B_1(m_f^2, M_3, M_2) - B_1(m_f^2, M_3, M_1)
\end{aligned}
\tag{J.4}
$$

The scalar 3-point integral $C_0 = C_0(p_1, -p_2, M_1, M_3, M_2)$ as well as the various 2-point integrals and coefficients can be found in appendix G.

Appendix K: A few electroweak couplings

In this appendix we will list the various couplings necessary for deriving the vertex correction expressions and box contributions of chapter IV. To this end we will adopt the notations used in chapter IV. All bosons occurring in the couplings below are defined to be incoming.

- Couplings between gauge bosons and fermions $(G_1 f \bar{f})$:

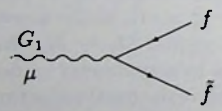

$$\equiv\; ie\,\gamma_\mu\left(V - A\,\gamma_5\right), \tag{K.1}$$

with specifications

$$
\begin{aligned}
\gamma f f \quad &: \quad V = -Q_f \;,\; A = 0 \\
Z f f \quad &: \quad V = v_f \;,\; A = a_f \\
W f f' \quad &: \quad V = A = \frac{1}{2\sqrt{2}\, s_w} \,.
\end{aligned}
\tag{K.2}
$$

- Couplings between Higgs bosons and fermions $(H_1 f \bar{f})$:

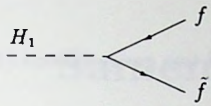

$$\equiv ie\,(S - P\gamma_5)\,, \tag{K.3}$$

with specifications

$$\begin{aligned} Hff &: \quad S = -\mu_f \;,\quad P = 0 \\ \chi ff &: \quad S = 0 \;,\quad P = -2i\,I_3^f\,\mu_f \\ \phi ff' &: \quad S = \sqrt{2}\,I_3^f\,[\,\mu_f - \mu_{f'}\,] \;,\quad P = -\sqrt{2}\,I_3^f\,[\,\mu_f + \mu_{f'}\,]\,. \end{aligned} \tag{K.4}$$

Thereby we have used the definition (*IV*.3.31) of μ_f.

- Couplings between 3 gauge bosons ($NW^{\lambda}W^{-\lambda}$) :

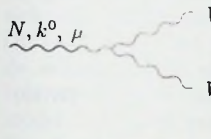

$$\equiv ie\,G\,\left\{g_{\mu\nu}(k^{\lambda} - k^0)_{\rho} + g_{\nu\rho}(k^{-\lambda} - k^{\lambda})_{\mu} + g_{\rho\mu}(k^0 - k^{-\lambda})_{\nu}\right\}\,, \tag{K.5}$$

with specifications

$$\begin{aligned} \gamma W^{\lambda}W^{-\lambda} &: \quad G = -\lambda \\ Z W^{\lambda}W^{-\lambda} &: \quad G = \lambda\, c_w/s_w\,. \end{aligned} \tag{K.6}$$

- Couplings between one gauge boson and two Higgs bosons ($G_1 H_1 H_2$) :

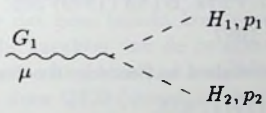

$$\equiv ie\,G\,(p_1 - p_2)_{\mu}\,, \tag{K.7}$$

with specifications

$$\begin{aligned} \gamma\phi^{\lambda}\phi^{-\lambda} &: \quad G = -\lambda \\ Z\phi^{\lambda}\phi^{-\lambda} &: \quad G = \lambda\,\frac{c_w^2 - s_w^2}{2 s_w c_w} \\ Z\chi H &: \quad G = -\frac{i}{2 s_w c_w} \\ W^{\lambda}\phi^{-\lambda}H &: \quad G = -\frac{\lambda}{2 s_w} \\ W^{\lambda}\phi^{-\lambda}\chi &: \quad G = -\frac{i}{2 s_w}\,. \end{aligned} \tag{K.8}$$

Interchanging the two Higgs bosons H_1 and H_2 causes the coupling constant G to change sign.

- Couplings between one Higgs boson and two gauge bosons ($H_1 G_1 G_2$) :

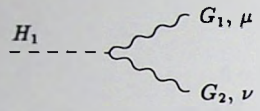

$$\equiv ie\,G\,g_{\mu\nu}\,, \tag{K.9}$$

with specifications

$$\begin{aligned} HZZ &: G = \frac{M_W}{s_w c_w^2} \\ HWW &: G = \frac{M_W}{s_w} \\ \phi W\gamma &: G = -M_W \\ \phi WZ &: G = -\frac{M_W s_w}{c_w}\,. \end{aligned} \tag{K.10}$$

Interchanging the two gauge bosons G_1 and G_2 makes no difference to G.

References

[1] R. Lewin, "Dilogarithms and associated functions", London 1958.

[2] G. 't Hooft and M. Veltman, Nucl. Phys. **B153** (1979) 365.

[3] T. Sack, Ph.D. Thesis, Würzburg 1987.

[4] W. Hollik, DESY 88-188, to be published in Fortschritte der Physik.

[5] M. Veltman, Acta Phys. Pol. **B8** (1977) 475.

[6] F. Jegerlehner, Z. Phys. **C32** (1986) 195.

Samenvatting

stralingscorrecties : technieken en toepassingen

Ten gevolge van de verwachte hoge precisie experimenten die plaats zullen vinden op CERN (nabij Genève) en SLAC (Stanford) zal het onderzoek naar de eigenschappen van de zwakke interacties een nieuw tijdperk ingaan. Tot voor kort beperkte de informatie die gewonnen kon worden via met name hoog energetische electron-positron en proton-antiproton botsings experimenten zich voornamelijk tot de klassieke eigenschappen van de zwakke interacties. Dit resulteerde eind jaren 60 in een theoretisch beschrijvingskader dat naast de zwakke ook de electromagnetische interacties omvatte. Men pleegt dit beschrijvingskader aan te duiden als het Glashow-Salam-Weinberg (GSW) model. De basis van dit model wordt gevormd door een quantum velden theorie gepaard gaande met naast een massaloos ijkboson als drager van de electromagnetische interacties ook 2 massieve ijkbosonen als dragers van de zwakke interacties. De experimentele bevestiging in 1983 van het bestaan van deze massieve ijkbosonen, W en Z deeltjes genaamd, als voorspeld door het GSW model, leidde tot de definitieve doorbraak van dit model als zijnde het standaard model ter beschrijving van electromagnetische en zwakke fenomenen. De stand van zaken voor wat betreft de experimenten was op dat moment echter zodanig dat geen inzicht kon worden verkregen aangaande het quantummechanische karakter van de zwakke interacties. Dit in tegenstelling tot de electromagnetische interacties waarvan het quantummechanische karakter, als beschreven door QED (quantum electrodynamica), tot zeer hoge precisie is getest op grond van de extreem nauwkeurige metingen van het anomaal magnetisch moment van het electron en het muon. Het vooruitzicht van bovenvernoemde hoge precisie experimenten biedt de mogelijkheid om ook de zwakke quantum effecten te bestuderen. De theoretische berekeningen dienen echter hiermee gelijke tred te houden, hetgeen inhoudt dat het onontbeerlijk is hogere orde correcties gerelateerd aan de zwakke quantum effecten hierin te betrekken. Dit om uitsluitsel te kunnen geven of de gemeten zwakke quantum effecten de deur openen naar buiten het GSW model gelegen concepten. Deze hogere orde correcties, stralingscorrecties genaamd, maken het verder ook mogelijk om het bestaan van een tweetal tot op heden nog niet ontdekte in het GSW model aanwezige deeltjes aan te tonen. Het gaat hierbij om het top quark en het Higgs boson, deeltjes waarvan de massa's via de zwakke quantum effecten tot de meetbare grootheden in met name electron-positron botsings processen kunnen bijdragen. Dit is derhalve te zien als een indi-

recte detectie methode in tegenstelling tot detectie via directe productie in electron-positron botsingen, iets wat ook tot de mogelijkheden behoort tenzij de te detecteren deeltjes te zwaar zijn.

In hoofdstuk II wordt het GSW model beschreven zoals dat zal worden gebruikt in expliciete berekeningen. In hoofdstuk III worden enkele speciale technieken geintroduceerd die in belangrijke mate tot hulp kunnen zijn om numerieke en algebraische problemen het hoofd te bieden. Het gaat hierbij om projectie methodes teneinde de lijvige algebra in te tomen, die inherent is aan de zwakke stralingscorrecties, en om een combinatie van de snijregel van Cutkosky en dispersie integraal technieken ter bepaling van die integralen die de oorzaak zijn van numerieke instabiliteiten ten gevolge van grote tegen elkaar wegvallende termen. In hoofdstuk IV worden verschillende aspecten belicht die te maken hebben met de zwakke quantum effecten, met name de afhankelijkheid van de onbekende model parameters m_t (de massa van het top quark) en M_H (de massa van het Higgs boson). De processen die hiertoe bekeken zullen worden zijn die van fermion paar productie (o.a. top quarks) uit electron-positron annihilatie en die van het fermionische verval van het Z ijkboson.

Curriculum Vitae

van

Wilhelmus Johannes Petrus Beenakker

geboren op 15 januari 1962 te Eindhoven

Aan het Mencia de Mendoza Lyceum te Breda behaalde ik in 1980 het VWO diploma. Daarna vervolgde ik mijn studie aan de Rijksuniversiteit te Leiden. Het kandidaatsexamen natuurkunde met bijvakken wiskunde en sterrenkunde werd afgelegd in februari 1983. Gedurende mijn experimentele stage heb ik gewerkt in de groep Quantumvloeistoffen o.l.v. Prof. Dr. R. de Bruyn Ouboter. In oktober 1985 volgde het doctoraalexamen theoretische natuurkunde met bijvak wiskunde. Het doctoraal onderzoek is verricht onder begeleiding van Prof. Dr. F.A. Berends aan het onderwerp "De renormalisatie van het electrozwakke standaard model". Direct na het doctoraalexamen begon ik aan mijn promotie onderzoek. Dit stond onder leiding van Prof. Dr. F.A. Berends en vond plaats binnen de werkgroep H-th-L van de Stichting voor Fundamenteel Onderzoek der Materie.

List of Publications

[1] Electroweak radiative corrections at LEP energies,
A. Barroso, W. Beenakker et al., in:
Proceedings of the ECFA Workshop on LEP 200, Aachen 1986, p. 157.

[2] Electroweak one-loop corrections to heavy-fermion pair production,
W. Beenakker and W. Hollik, in:
Proceedings of the ECFA Workshop on LEP 200, Aachen 1986, p. 185.

[3] Electroweak radiative corrections to $e^+e^- \to W^+W^-$,
M. Böhm, A. Denner, T. Sack, W. Beenakker, F. Berends and H. Kuijf,
Nucl. Phys. **B304** (1988) 463.

[4] The width of the Z boson,
W. Beenakker and W. Hollik,
Z. Phys. **C40** (1988) 141.

[5] Infrared divergent scalar box integrals with applications in the electroweak standard model,
W. Beenakker and A. Denner,
Leiden Preprint, Dec. 1988.

[6] QCD corrections to heavy-quark production in $p\bar{p}$ collisions,
W. Beenakker, H. Kuijf, W.L. van Neerven and J. Smith,
Phys. Rev. **D40** (1989) 54.

[7] Applications of renormalization group methods to radiative corrections,
W. Beenakker, F.A. Berends and W.L van Neerven,
Leiden preprint 1989, to appear in the Proceedings of the Workshop on Electroweak Radiative Corrections, Ringberg Castle (FRG), 1989.

[8] Z line shape,
D. Bardin, W. Beenakker et al.,
CERN-TH 5468/89 (1989), to appear in the Proceedings of the Workshop on Z Physics at LEP.

Tot de promotie wordt met oog op de beperkte ruimte in de Senaatskamer, uitsluitend toegang verleend op vertoon van een uitnodigingskaart.

RECEPTIE NA AFLOOP VAN DE PROMOTIE
IN HET ACADEMIEGEBOUW
RAPENBURG 73, LEIDEN

N.B. Met tijdrovende parkeermoeilijkheden bij het Academiegebouw moet rekening worden gehouden.

Stellingen

1. Gebruik makende van de projectieve impulsen K_l^μ voor $l = 1, \cdots, d-1$ gegeven in (*III*.5.23) en de projectieve tensoren

$$K^{\mu_1 \cdots \mu_{2a}} = \left[\prod_{i=0}^{a-1} \frac{(n-d+1)^2}{n+2i-d+1} \right] K^{\mu_1 \mu_2} \cdots K^{\mu_{2a-1} \mu_{2a}} \quad \text{voor } a \geq 1$$

kan geprojecteerd worden op elke willekeurige term voorkomend in de reductie van d-punts tensor-integralen ($d = 2, 3, 4$) naar de orthogonale impulsen $k_1, \cdots, k_{d-1}$ en de projectieve tensor $K^{\mu\nu}$ gegeven in (*III*.5.24).

Hoofdstuk III van dit proefschrift.

2. In het kader van de huidige generatie grootschalige fenomenologische projecten in de hoge-energiefysica is het onontbeerlijk dat er samenwerking is tussen onafhankelijk werkende groepen dan wel personen.

3. In tegenstelling tot wat in het algemeen wordt aangenomen zijn de totale en 'voorwaarts-achterwaartse' flux voor de reactie $e^+e^- \to \mu^+\mu^-$, corresponderend met QED beginstralings-correcties in de zogenaamde 'leading log' benadering, niet aan elkaar gelijk. De verschillen treden pas op wanneer $\mathcal{O}(\alpha^2)$ correcties worden beschouwd.

W. Beenakker, F.A. Berends and W.L. van Neerven,
Workshop on Electroweak Radiative Corrections,
Ringberg Castle (FRG), 1989.

4. Goede benaderingen voor de voor zwakke interacties gecorrigeerde asymmetrieën, te weten de 'voorwaarts-achterwaarts'- (A_{FB}), de 'links-rechts'- (A_{LR}) en de polarisatie-asymmetrie (A_{FB}^{pol}), worden op de Z resonantie gegeven door

$$A_{LR} = -\frac{\sum_{\kappa=\pm} \kappa \Gamma_Z(e^-, \kappa; e^+, -\kappa)}{\sum_{\kappa=\pm} \Gamma_Z(e^-, \kappa; e^+, -\kappa)} \quad , \quad A_{FB}^{pol} = -\frac{3}{4} \frac{\sum_{\eta,\bar{\eta}=\pm} \eta \Gamma_Z(f, \eta; \bar{f}, \bar{\eta})}{\sum_{\eta,\bar{\eta}=\pm} \Gamma_Z(f, \eta; \bar{f}, \bar{\eta})}$$

en $A_{FB} = A_{LR} A_{FB}^{pol}$. Hierbij geeft $\Gamma_Z(f, \eta; \bar{f}, \bar{\eta})$ de voor zwakke interacties gecorrigeerde vervalsbreedte per heliciteit aan van het neutrale Z vectorboson.

5. Snijtechnieken voor scalaire integralen komen het best tot hun recht als er sprake is van een uitwisseling van een massaloos vectorboson.

6. Om iedere atleet gelijke kansen te bieden wordt het de hoogste tijd de bochten van indoor atletiekbanen aan te passen aan de snelheid waarmee de atleten er met name op de 200 meter doorheen komen.

7. In het proces $e^+e^- \to W^+W^-$ geeft de aanwezige ijksymmetrie voor grote zwaartepunts-energie aanleiding tot een $1/s$ afhankelijkheid van de differentiële werkzame doorsnede, terwijl de afzonderlijke termen een afhankelijkheid evenredig met s hebben. Met het oog op de betrouwbaarheid van numerieke evaluaties in dat regime is het derhalve aan te bevelen het virtueel gecorrigeerde matrix element samen te trekken met het matrix element in de Born-benadering alvorens de tensor-integraal reductie uit te voeren.

M. Böhm et al., Nucl. Phys. B304 (1988) 463.

8. Ter bepaling van scalaire 4- en 5-puntsintegralen in massaloze theorieën met n-dimensionale regularisatie, verdient het gebruik van dubbele snijtechnieken met bijbehorende dispersie-integralen in twee van de invarianten de voorkeur boven het gebruik van enkelvoudige snijtechnieken met bijbehorende dispersie-integraal in één van de invarianten.

9. Een goede benadering voor de halfwaarde posities $\sqrt{s_\pm}$ van de electrozwak-gecorrigeerde resonantie van het neutrale Z vectorboson wordt gegeven door

$$\sqrt{s_\pm} = M_Z \left\{1 - \frac{1}{8}\gamma^2 + \frac{1}{4}\pi\beta_e\gamma(1+\beta_e) - \frac{5}{16}\pi\beta_e\gamma^2 + \frac{1}{8}\beta_e\gamma\log(2)(\pi\beta_e+\gamma)\right\}$$
$$\pm\frac{\Gamma_Z}{2}\left\{1 + [\frac{1}{4}\pi\beta_e + \frac{1}{2}\beta_e\log(2)][1+\beta_e+\frac{1}{4}\pi\beta_e] - \frac{1}{2}\pi\beta_e\gamma - \frac{5}{8}\gamma^2\right\},$$

met

$$\gamma \equiv \Gamma_Z/M_Z \qquad \text{en} \qquad \beta_e \equiv \frac{2\alpha}{\pi}\left\{\log\left(\frac{M_Z^2}{m_e^2}\right) - 1\right\}.$$

Hierbij staan M_Z en Γ_Z voor de massa en de vervalsbreedte van het neutrale Z vectorboson.

10. Voor het bepalen van de topmassa-afhankelijkheid van werkzame doorsneden, asymmetrieën en vervalsbreedtes dient terdege rekening te worden gehouden met de topmassa-afhankelijke bijdragen afkomstig van de Yukawa koppelingen tussen fermionen en Higgs bosonen.

11. Tot nu toe is het gebleken dat hogere orde QCD correcties slechts de normalisatie van distributies veranderen en niet de vorm. Als nu ook nog blijkt dat het gecorrigeerde resultaat beschreven kan worden door in de Born-benadering de factorisatie- en renormalisatieschaal te veranderen, dan heeft het geen zin om QCD correcties te berekenen.

12. Aan de uitspraken en meningen van fysici kan slechts zoveel waarde worden gehecht als men er zelf aan wenst toe te kennen.

W.J.P. Beenakker
Leiden, 19 oktober 1989